The Role of Genomic Integrity in Mn-Induced Neurotoxicity

Mechanistic investigations of Mn-induced oxidative stress, DNA damage, DNA repair, and neurodegeneration in two different model systems

Dissertation

Zur Erlangung des Doktorgrades
der Naturwissenschaften (Dr. rer. nat.) im Fachbereich Chemie und Biologie
der Mathematisch-Naturwissenschaftlichen Fakultät
der Bergischen Universität Wuppertal

vorgelegt von
Merle Marie Nicolai
aus Berlin
– 2021 –

Dekan:in: ..... Prof. Dr. Stefan F. Kirsch

Erste:r Gutachter:in: ..... Prof. Dr. Julia Bornhorst

Zweite:r Gutachter:in: ..... Prof. Dr. Tanja Schwerdtle

Tag der mündlichen Prüfung: 04.01.2022

Tag der Promotion: ..... __.__.____

“Biology is the best chemist.”

Francis Arnold

The PhD thesis can be quoted as follows:

urn:nbn:de:hbz:468-urn:nbn:de:hbz:468-20220124-113612-9
[http://nbn-resolving.de/urn/resolver.pl?urn=urn%3Anbn%3Ade%3Ahbz%3A468-20220124-113612-9]

DOI: 10.25926/fy3d-jn84
[https://doi.org/10.25926/fy3d-jn84]

Für meine Familie

Preliminary remarks to the structure of the dissertation

This semi-cumulative dissertation consists of 7 chapters, whereby chapters 3 – 6 are based on first-author publications published or submitted to peer-reviewed journals. These chapters include suggestions of co-authors, reviewers, and journal editors as an outcome of the peer-review process. Within chapter 2 (Background Information), the most relevant fundamentals for understanding the publications are described. Chapter 7 contains a general conclusion and outlook of the entirety of the project. Each isolated publication offers a more specific introduction, conclusion, and outlook of the respective topic.

Despite the studies being published in different journals and publication styles, it was chosen to combine the bibliographies, figure and table legends for reasons of clarity and comprehensibility. The original layouts of the publications were therefore altered, and some editorial changes have been made. If applicable, the sources of the original publications are marked clearly at the beginning of each chapter. Due to the different publication styles of each journal, inconsistency in abbreviations, nomenclature, and spelling (British and American English) might be noticeable.

The nomenclature for human/ mammalian genes and proteins was chosen as the following: *GENE* names are written in italicized and upper case letters, while PROTEIN names are written in non-italicized upper case letters. Whereas the nomenclature for *C. elegans* genes and proteins was chosen as the following: *gene* names are written in italicized and lower case letters, while protein names are written in non-italicized lower case letters.

Table of Contents

Figure and Table Legends

Figures

Tables

List of Abbreviations

Note: Abbreviations based on chemical elements are not given.

2D	two-dimensional
2D-LC	two-dimensional liquid chromatography
8OHdG	8-hydroxy deoxyguanine
8oxodG	8-oxo-7,8-dihydroguanine
ACN	acetonitrile
AP sites	apurinic/ apyrimidinic sites
ATP	adenosine triphosphate
AU	alkaline unwinding
BER	base excision repair
BHT	butylhydroxy toluol
BLM	bleomycin
C. elegans	*Caenorhabditis elegans*
cAMP	cyclic AMP
CAT	catalase
CL	cardiolipin(s)
CLox	cardiolipin oxidation products(s)
COMET	single cell gel electrophoresis assay
cyt c	cytochrome c
DAT-1	dopamine transporter 1
DCFH-DA	2´-7´-dichlorodihydrofluorescein diacetate
dePARylation	degradation of PAR chains
DFG	German Research Foundation
DMT1	divalent metal transporter 1
DNPH	2,4-dinitrophenylhydrazine
DSB	double-strand break
dsDNA	double-stranded DNA
EC	effective concentration

E. coli	*Escherichia coli*
EFSA	European Food Security Association
EIC	extracted ion current
ER	endoplasmic reticulum
ESI	electrospray ionization
EtOH	ethanol
FA	fatty acid
FPN	Fe exporter ferroportin
FPG	formamidopyrimidine-DNA glycosylase
GNDF	glial-derived neurotrophic factor
GPX	glutathione peroxidase
GSH	glutathione
GSSG	glutathione disulphides
HILIC	hydrophilic interaction liquid chromatography
HPLC	high-performance liquid chromatography
HRMS	high-resolution mass spectrometry
ICP-OES	inductively coupled plasma-optical emission spectrometry
IPA	2-propanol
LC	liquid chromatography
LD	lethal doses
LUHMES	Lund human mesencephalic neuronal cell line
m/z	mass-to-charge ratio
MDA	malondialdehyde
MeOH	methanol
MRM	multiple reaction monitoring
MS/MS	tandem mass spectrometry
MTBE	methyl *tert*-butyl ether
NAC	N-acetyl cysteine
NAD^+	nicotinamide adenine dinucleotide

NP	nucleotide pool
OECD	Organisation for Economic Co-operation and Development
PARG	poly(ADP-ribose) glycohydrolases
PARP	poly(ADP-ribose) polymerases
PARylation	poly(ADP-ribosyl)ation
PARi	PAR inhibitor
RNAi	RNA interference
RONS, ROS, RNS, RO(N)S	reactive oxygen and/ or nitrogen species
RT-qPCR	real-time quantitative polymerase chain reaction
SD	standard deviation
SEM	standard error of the mean
SOD	superoxide dismutase
SPE	solid-phase extraction
SSB	single-strand breaks
ssDNA	single-stranded DNA
*t*BOOH	*tert*-butyl hydroperoxide
TET-off	tetracycline-responsive v-myc oncogene
TG	test guideline
ToF	time-of-flight
WHO	World Health Organization
WT	wild type

Summary

Manganese (Mn) is an essential trace element needed as a cofactor for many cellular processes, but (chronic) overexposure of the transition metal has been associated with various adverse neurological effects. Mn is omnipresent in food and drinking water; a deficiency is therefore not of concern. However, due to the rising industrial use of Mn as a transition metal and the resulting environmental pollution, Mn uptake is constantly increasing, and overexposure has become more relevant, not only in an occupational setting but also for the general population, leading to a rapidly evolving research interest in Mn-induced neurotoxicity. Oxidative stress, meaning the imbalance of reactive oxygen and nitrogen species (RONS) formation and degradation, has been identified as one of the main pathways in Mn toxicity. Mn-induced oxidative stress can affect many diverse cellular mechanisms, which eventually may cause Mn-induced neurotoxicity. Despite the ongoing research, the underlying mechanisms of Mn-induced neurotoxicity, key targets of the Mn-induced oxidative stress and the neurodegeneration itself are not yet fully understood.

This work was conducted to investigate the link between oxidative stress and neurotoxicity after Mn overexposure further, focussing hereby on RONS-induced DNA damage, DNA damage response, and DNA repair. For this, the multicellular model organism *Caenorhabditis elegans* (*C. elegans*) was used for studying genomic integrity in an entire organism, and dopaminergic-like differentiated Lund human mesencephalic neuronal (LUHMES) cells were used to focus the research on the genomic integrity in neuronal cells.

The first part of this work consisted of developing novel methods for assessing oxidative stress and genomic integrity in *C. elegans*. The nematode has gained increasing recognition in research regarding oxidative stress, DNA damage and DNA repair, but methods for measuring specifically genotoxicity in *C. elegans* are still scarce.

Cardiolipins (CLs) are exclusively located in mitochondria and therefore offer a unique relevance regarding oxidative stress, mitochondria dysfunction, and related diseases. Due to their location and the high level of unsaturation of these lipids, CL oxidation products (CLox) can be an early and sensitive biomarker for oxidative stress.

Utilising online two-dimensional liquid chromatography hyphenated with high-resolution mass spectrometry (2D-LC-HRMS), the CL and CLox distributions in *C. elegans*

were determined. The method was then tested on its applicability as an oxidative stress marker by provoking RONS formation in *C. elegans* using *tert*-butyl hydroperoxide (*t*BOOH). The results proved a concentration-dependent formation of oxidised CL after *t*BOOH treatment and confirmed the great potential of this method for CLox analysis as a feasible and sensitive marker of oxidative stress.

For genotoxicity assessment in *C. elegans*, we developed a reliable and practicable lysis method and adapted the alkaline unwinding (AU) assay to the nematode matrix. This allows investigations of DNA damage by measuring the percentage of double-stranded DNA (dsDNA) and calculating the DNA strand breaks as a marker for genomic integrity. Utilising *C. elegans* for genotoxicity assessment allows working within the niche of less transferable *in vitro* and costlier rodent experiments. This novel approach of the established *in vitro* AU assay was validated using the genotoxic substances bleomycin (BLM) and *t*BOOH as positive controls, and the method proved to be highly meaningful and reproducible. Therefore, the AU assay in *C. elegans* is a reliable genotoxicity test within the 3R concept (reduction, refinement, and replacement of animal experiments) and can be used to complement the classic genotoxicity bacterial, cell culture, or rodent experiments by a multicellular model organism.

After method development, the effects of Mn on oxidative stress, DNA damage, and DNA repair were analysed in *C. elegans* to elucidate the mode of action of Mn-induced neurodegeneration. For this, worms were exposed to $MnCl_2$ and bioavailability and lethality were assessed for optimal concentration finding for genotoxicity testing. DNA damage induction was analysed by measuring DNA strand breaks using the AU assay and measuring the formation of 8-oxo-7,8-dihydroguanine (8oxodG). Different deletion mutants were then used to investigate the role of DNA damage response induction (via analysis of poly(ADP-ribosyl)ation (PARylation)) and the oxidative DNA damage-specific DNA repair (base excision repair) in Mn-induced toxicity. The results illustrate a Mn uptake that is dose- and time-dependent and correlates directly with the lethality rate of exposed *C. elegans*. Measuring the DNA damage and gene expression of BER-involved enzymes revealed a decrease in genomic integrity and induction of DNA repair after excessive Mn exposure. Additionally, we were able to show that the poly(ADP-ribose) glycohydrolase 1 (*parg-1*) accounts for most of the glycohydrolase activity in *C. elegans*. Collectively, these results highlight the vital role of genomic integrity in Mn-induced neurotoxicity and broaden the molecular understanding of the underlying pathways.

The last part of this work consisted of similar investigations as those described above, but by changing the model system, we were able to focus the research specifically on neurotoxicity instead of global effects. Previous *in vivo* studies observed that Mn accumulation in the brain occurs mainly in dopamine-rich regions, indicating that dopaminergic neurons are a primary target for Mn-induced neurotoxicity. Using LUHMES cells, assessment of Mn bioavailability, cytotoxicity, DNA damage induction, DNA repair, and consequences of Mn overexposure on the neurite network in dopaminergic-like neurons was possible. Thus, conclusions about the neurotoxicity of Mn can be drawn. Measurements of bioavailability and cytotoxicity indicated a concentration-dependent uptake and cytotoxic effect again. The formation of DNA damage (8oxodG and DNA strand breaks) showed, likewise to *C. elegans* investigations, a significant dose- and time-dependent increase after Mn exposure. Analysing PARylation and DNA repair gene expression implies induction of the DNA damage response that is not regulated on a transcriptional level. The neuronal outgrowth is also adversely affected by Mn overexposure, as this was shown by a significant degradation of the neuronal network.

Altogether, these results confirm the important role of adverse effects of Mn and Mn-induced oxidative stress on the genomic integrity, globally in an entire organism, but also specifically in post-mitotic dopaminergic-like neurons.

Chapter 1

Motivation and Scope of the Thesis

1.1 Introduction

Manganese (Mn) is an essential trace element that is needed as a cofactor for a large number of cellular processes. Exposure to this metal is omnipresent in food and drinking water; a deficiency is therefore not of concern for the general population. In contrast to this, chronic overexposure is of higher importance [1]. High levels of Mn exposure have been associated with various adverse neurological effects and possible occurring symptoms resembling those of Parkinson´s disease [2]. The association of chronic Mn overexposure and neurodegenerative diseases has been discussed extensively. Considering the increasing exposure due to the rising industrial use of Mn as a transition metal, research in the field of Mn-induced neurotoxicity is rapidly evolving [3]. Possible underlying mechanisms for neurodegeneration are being discussed, and investigations are ongoing, for example, regarding neuro-inflammation, dysregulation of mitochondrial function, redox homeostasis, and altered neurotransmitter metabolism [4]. Induction of oxidative stress, so the imbalance of reactive oxygen and nitrogen species (RONS) formation and degradation, by Mn has been identified as a main intermediate mechanism of Mn-induced neurotoxicity, which then affects many diverse cellular mechanisms [3, 5, 6]. However, the underlying mechanisms and the role of Mn-induced oxidative stress in the pathophysiology of those key targets and, ultimately, neurological diseases are not yet fully understood.

Utilising two different model organisms/ systems, this research work was conducted to investigate in depth the link between Mn-induced oxidative stress and neurotoxicity, focussing hereby on genomic integrity. Interactions of RONS with DNA is a constant cellular event that is under physiological conditions balanced by the DNA damage response and DNA repair. However, excessive production of RONS or insufficient DNA repair after Mn exposure might increase the formation and persistence of oxidative DNA damage, putting the genomic integrity in jeopardy [7]. This, in turn, could promote the neurological dysfunction after Mn exposure observed in humans and experimental *in vivo* studies [4].

While some published *in vitro* and *in vivo* studies of Mn toxicity started to address endpoints of genomic integrity [8-11], their results are not well comparable and are often incomprehensive. Moreover, classical rodent experiments are often cost- and time-intensive. Taking advantage of the simple but multicellular model organism *Caenorhabditis elegans* (*C. elegans*), this work aimed to establish a “complete” model for

meaningful *in vivo* genotoxicity testing, from oxidative stress endpoints, quantifying the DNA damage and analysing the activation of the DNA damage response and DNA repair. Additionally, utilising *C. elegans* allows less expensive, less time-consuming and higher reproducible *in vivo* experiments within the ethics of the 3R principle (reduction, refinement, and replacement of animal experiments), and still conduct experiments that are easier transferrable to animal experiments than classical cell culture systems [12]. Thus, creating a modern approach for genotoxicity testing that is then applicable for mechanistic studies of Mn-induced neurotoxicity.

Further research was then conducted, focussing less on adverse outcomes of Mn exposure globally on a complete organism but more intensively on the aspect of the neurotoxicity itself. Based on the location of Mn brain accumulation and decrease of dopamine release, dopaminergic neurons are identified to be one of the main targets of Mn toxicity [13-15]. Additionally, altered neurotransmitter (γ-aminobutyric acid, glutamate, and dopamine) release, mediated by effects of Mn on the neurotransmitter systems and their convoluted interplay, has been associated with Mn overexposure [3]. By utilising the differentiated Lund Human Mesencephalic (LUHMES) neuronal cell line, investigations on the effects of Mn on cellular mechanisms in post-mitotic cells, like Mn uptake, cytotoxicity, genomic integrity, and neurite outgrowth, were analysed. After differentiation of these cells, they become dopaminergic-like neurons, showing many properties of dopaminergic neurons, and are therefore highly relevant for Mn-induced neurotoxicity research [16].

In combination, the two model organism/ systems provide a well-rounded basis for research on the role of genomic integrity and the associated pathways in Mn-induced neurotoxicity.

1.2 Scope of the Thesis

This work was focused on the following key points

- Development of new markers for the assessment of oxidative stress and genotoxicity in the multicellular model organism *C. elegans.*
- Investigations of bioavailability, oxidative stress, DNA damage, DNA repair and survival after Mn exposure in *C. elegans.*
- Analysis of Mn-induced neurodegeneration by utilising LUHMES cells for mechanistic studies of bioavailability, cytotoxicity, genomic integrity, and tubulin expression after Mn exposure in a dopaminergic-like neuron.

Chapter 2
Background Information

2.1 Oxidative Stress

The balance of generation and depletion of RONS is a crucial objective for biological systems. At low and moderate levels, the formation and presence of RONS are needed for various cellular processes and signalling pathways, like the immune response, protein phosphorylation, activation of transcription factors, and apoptosis [17-21]. In addition to intrinsic RONS scavengers (e.g. glutathione, ascorbic acid, carotenoids), cells contain several different antioxidant systems that are used to lower the number of free radicals. These defence systems mainly rely on enzymatic activity, like the glutathione peroxidase (GPX) or the superoxide dismutase (SOD), to protect cells from RONS-induced damage [22-24]. If the balance is shifted towards the induction of RONS and physiological levels are exceeded, increasing interactions of RONS with important cellular structures will occur, causing harmful modifications of proteins, lipids, and nucleic acid [25]. This phenomenon of excess RONS is commonly referred to as oxidative stress and has, with varying degrees of importance, been associated with the onset and progression of several diseases and accelerated ageing processes. Examples of RONS are superoxide radicals ($O_2^{\cdot -}$), hydrogen peroxide (H_2O_2), hydroxyl radicals ($^{\cdot}OH$), and nitric oxide (NO) [17]. Endogenously, they are mainly formed as metabolic by-products under physiological and pathological conditions in mitochondria (cellular respiration, arachidonic acid metabolism), endothelial cells, and inflammatory cells [26]. In addition, metals, like iron(II) (Fe^{2+}) and Mn^{2+}, can act as cofactors for the formation of the most reactive free radical species, ·OH, by the reaction of $O_2^{\cdot -}$ with water, namely Fenton(-like) reactions [27, 28]. Exogenously caused free radical production is stimulated by the degradation and metabolising of environmental pollutions, heavy metals (e.g. mercury, cadmium, arsenic, Fe and Mn), certain drugs (e.g. bleomycin, cyclosporine), chemical solvents, and “lifestyle” pollutions (e.g. alcohol, cigarette smoke, smoked meat). Irradiation is also known to induce RONS-formation [17, 23, 29-34]. DNA is prone to oxidative damage, causing loss of epigenetic information and increasing the risk of mutagenicity. Oxidative base damage is a prevalent occurrence under excessive RONS, with 8-oxo-7,8-dihydroguanine (8oxodG) being the most invested modification of DNA bases [25]. Aside from DNA damage, RONS-induced excessive lipid peroxidation (and subsequent radical chain reactions) result in cell membrane and lipoprotein damage and can affect large quantities of lipid molecules [35]. Upon oxidative stress, also conformational modifications of proteins occur, which are causal to loss or impairment of the enzymatic activity [25].

2.1.1 Biomarkers of oxidative stress

Oxidative stress has been linked to many (neurological) diseases and is considered to be either a primary or secondary cause of many multifactorial syndromes. This makes a quantitative assessment of oxidative stress indispensable for many research fields within toxicology, pharmacology, and clinical settings. The most direct estimation of oxidative stress is likely the measurement of RONS itself. Different dyes, mostly 2´-7´-dichlorodihydrofluorescein diacetate (DCFH-DA), MitoTracker®red, or MitoSOX™, are used to quantify RONS via fluorescent or chemiluminescent signals [36-39]. Analytical or biochemical measurements of glutathione levels provide another approach towards the assessment of the redox balance in cells and organisms. Glutathione is likely the most important intracellular redox buffer [40]. Under physiological conditions, most of the redox-active glutathione molecules are present in the reduced form (GSH). In the presence of RONS, GSH is oxidised to glutathione disulphides (GSSG), causing a reduction of the reactive species and reducing its oxidative capacity. Quantification of the GSH/GSSG ratio can therefore be used as an indicator of the redox status of an organism [41-43].

Analysing the expression and activity of antioxidant enzymes is an indirect measure of oxidative stress and the redox status of an organism. Gene expression is classically measured by reverse transcription combined with quantitative polymerase chain reaction (RT-qPCR) [44, 45]. From relative-fold changes in transcription levels, information on the regulation of specific signalling cascades and protein levels can be drawn, while it does not allow the assessment of enzyme activity. An example of enzyme activity determination is the analysis of the inhibition of the superoxide-induced lucigenin chemiluminescence by superoxide dismutase (SOD) activity [46]. A second large approach of indirect investigations of oxidative stress is the measurement of oxidative damage on proteins, lipids, or DNA. Here it is very important to understand the nature of the present reactive species, as they target different, and in some cases very specific, endpoints. For example, protein carbonylation is highly inducible by HOCl, whereas DNA and lipids are no likely targets for this specific radical. Protein oxidation is often investigated using 2,4-dinitrophenylhydrazine (DNPH) [47], which reacts specifically with the carbonyl groups of aldehydes and ketones, causing a spectrophotometric change. Analytical and biochemical quantification of isoprostanes and malondialdehyde (MDA) are common examples of lipid peroxidation endpoints [48, 49]. Directly resulting from

RONS attack, oxidative DNA damage levels can be assessed to conclude on the redox status. Oxidative damage of the guanine base is likely the most investigated oxidative DNA damage [50-52] and will be discussed in more detail in Section 2.2.2. An overview of some recognized oxidative stress markers is given in Table 1. It is important to notice that each biomarker has its advantages and disadvantages. Dye methods are usually fast and easy to perform, but their binding might be relatively unspecific and radicals are often short-lived. Analytical methods are far more specific but the stability of molecules of interest might not always be given. Additionally, RONS have various diverse endpoints that might be site-specific and exhibit different sensitivities towards oxidative stress [53-55]. Finding and developing an optimal combination of oxidative stress biomarkers is therefore of essential importance.

Table 1 Overview of some selected examples of frequently used oxidative stress biomarkers.

Endpoint	Possible method
Cellular and mitochondrial RONS	
RONS	Chemiluminescent/ fluorescent measurements: MitoTracker, MitoSOX, DCFH-DA, Amplex Red, Lucigen [56-59] High-performance liquid chromatography-mass spectrometry (HPLC-MS) analytical measurements: 2,3-Dihydroxybenzoic acid [60]
Glutathione	Fluorescent/ spectrophotometric measurement: redox-cycling assay for quantification of GSH/ GSSG [61] HPLC-MS/MS or HPLC-qTOF measurements: GSH/ GSSG simultaneously [41, 52]
Antioxidant enzymes	
Enzyme activity	Chemiluminescent/ fluorescent measurements: SOD, catalase (CAT), GPX [62]
Gene expression	Quantitative measurement of changes in gene expression levels via RT-qPCR [45, 63]
Oxidative damage endpoints	
Carbonylated proteins	Immunoblotting: OxyBlot [64] Chemiluminescent/ fluorescent measurements: DNPH, fluorescein-5-thiosemicarbazide (FTC) [47, 65]
Lipid oxidation products	Fluorescence measurements: lipofuscin [66] HPLC-MS/MS: Isoprostanes [48, 67] HPLC-FLD: MDA [68]
Oxidative DNA damage	Immunofluorescence: (8-hydroxy deoxy-guanine) 8OHdG [52, 69] HPLC-MS/MS: (8-oxo-7,8-dihydroguanine 8oxodG) [50, 70] qPCR: non-polymerase blocking DNA damage [51] general oxidative DNA damage: Fpg-modified alkaline COMET assay [71]

2.2 Genotoxicity as a Consequence of RONS

Genotoxicity describes the potential of a substance to cause genetic alterations, which can lead to several negative outcomes, like impaired transcription, replication, and apoptosis. Affecting somatic cells, genotoxicity will potentially result in cancer (if proto-oncogenes or tumour suppressor genes are affected) and non-cancerous genetic diseases. Arising in germ cells, those genetic alterations can cause infertility, heritable DNA damage (= mutations) and intergenerational genetic diseases [30, 72-74]. Concerningly, DNA damage that occurs in single cells at only low exposures and might only manifest after unusually long periods following the exposure can be causal to the adverse outcomes [75]. Mutations include changes in single base pairs and genes, chromosomal alterations (breaks, stable deletions, duplications, or rearrangements), and changes of chromosomal number (loss or gain), which are changes that are persistent and heritable. Mutations can either be caused by mutagens or via mitotic recombination. Genotoxicity includes mutagenicity but also non-heritable DNA damage caused by processes such as unscheduled DNA synthesis, DNA strand breaks, DNA base modifications and DNA adduct formations [76]. RONS-mediated genotoxicity is well recognized. Free radicals have the potential to directly cause DNA strand breaks or damage the DNA by forming oxidative base modifications. Accumulation of RONS under oxidative stress is also associated with the induction of mitochondrial DNA lesions, strand breaks and the degradation of mitochondrial DNA [77-79].

2.2.1 Genotoxicity testing

Testing for the genotoxic potential of a substance is part of the mandatory approval procedures within the chemical and pharmaceutical industry and is required for risk assessment of food ingredients and other substances. The procedures for genotoxicity testing are strictly defined by the Organisation for Economic Co-operation and Development (OECD) guidelines [76]. Due to the wide variety of possibly induced/ arising DNA damages, testing batteries are usually applied for a systematic assessment of multiple genotoxicity endpoints. These include assays for 1) measurement of the mutagenic potential as well as 2a) quantification of the DNA damage itself, which may or may not cause permanent genetic alterations, and for 2b) mechanisms involved in the preservation of genome integrity. Therefore, the two latter groups are no direct methods

for measuring mutagenicity but reflect the efficiency of the genomic integrity maintaining machinery [76]. The guidelines recommend a battery, which is adaptable to the nature of the tested substance and is built on bacterial reverse mutation assays (AMES test), *in vitro* evaluations of chromosomal damage, and finally, *in vivo* (mostly rodents) assessment of chromosomal damage [80-82]. Which specific tests should be performed strongly depends on the chemical properties of the test substance and the results assessed previously within the test battery but are usually set up in order of increasing (ethical) complexity. An overview of the genotoxicity tests currently regulated by the OECD test guidelines (TGs) can be seen in Figure 1. Additionally, the TGs include indicator tests, which detect the primary DNA damage but give no information on the resulting physiological outcome of these damages (repair of the DNA, mutation, or cell death). These tests are used for preliminary screening, mechanistic investigations, as an estimate for exposure biomarkers, or as an *in vivo* follow up of positive *in vitro* results [75].

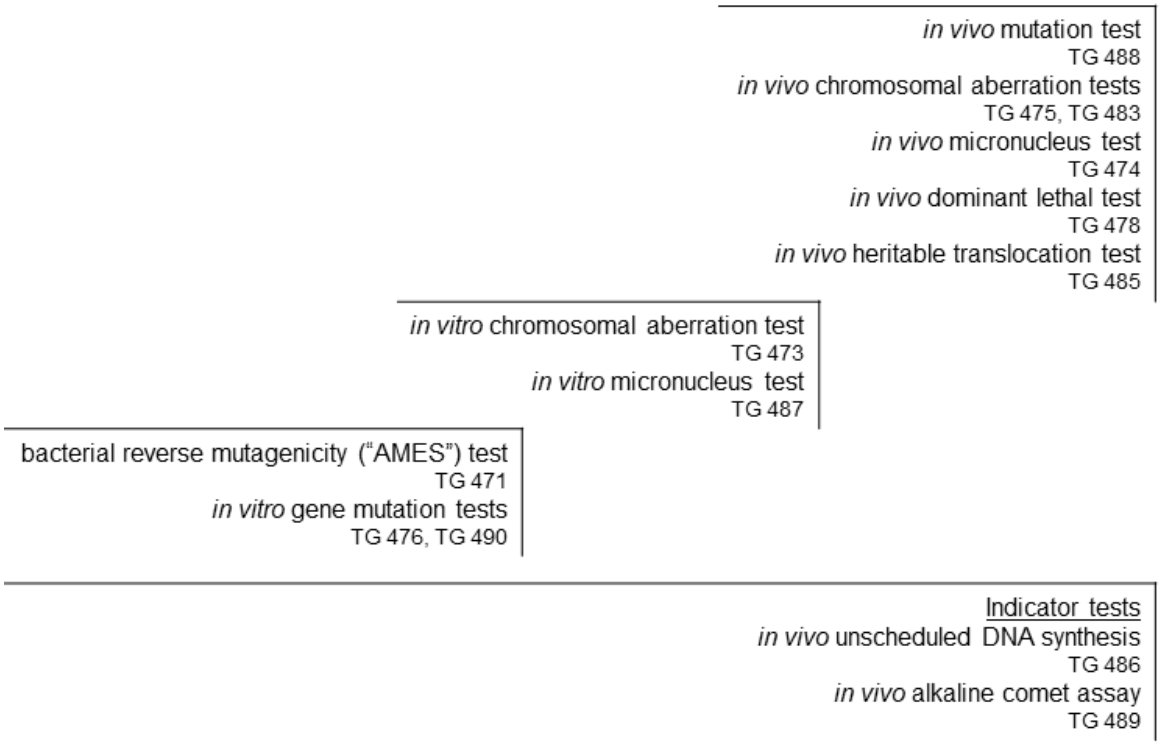

Figure 1 Overview of TGs for genotoxicity testing defined by the OECD guidelines. The scheme shows all currently included tests of the OECD genotoxicity (and indicator) test guidelines. Summarized from [75]. The methods are presented from left to right with increasing (ethical) complexity and indicator test are shown separately.

2.2.2 Oxidative DNA damage

DNA damage caused by RONS is a constant challenge for the genome as reactive species are ubiquitously present within cells. Oxidative DNA lesions are distributed heterogeneously over the genome, and the level of occurrence differs immensely, depending on many factors like mitochondrial activity, DNA repair efficiency, as well as cell- and tissue-type [7, 23, 83]. Oxidative DNA damage is one of the main drivers of mutagenic processes within the germline and has been associated with ageing and age-related diseases like neurodegeneration and cancer. Depending on its genomic location, oxidative DNA damage has also been identified as a site-specific gene regulator and impacts functional genomic features by changing the DNA secondary structure and DNA replication efficiency [84-86], thus acting resembling epigenetic marks.

RONS induce many different modifications of the DNA bases, which occur with different frequencies due to the varying oxidation potential of the initial bases and the stereo-chemical properties of the products. Both genomic bases, as well as bases within the nucleotide pool (NP), can be oxidatively altered. Common oxidised base lesions include formamidoadenine, 8-oxo-adenine, 5-hydroxy-cytosine, 5-hydroxy-uracil, and thymine glycol [87]. Persisting DNA damage can cause loss of information, disruption of cellular functions by altering DNA-protein binding of transcription factors (e.g. SP1, p50, CREB) and changing the DNA secondary structure in the form of changed G-quadruplex folds or stacked guanine groups. Consequently, genomic stability, gene regulation, telomere length, and replication can be affected [86, 88-91]. Under physiological conditions, most base lesions are repaired without loss or change of genetic information within minutes. But if not repaired properly, oxidative DNA damage or its repair intermediates can promote loss of information or even mutation.

Likely, the most intensely studied oxidative DNA base modifications are 8oxodG or its equilibrium partner 8OHdG. Guanine, both within the genome and the NP, is particularly prone to oxidation by singlet oxygen due to its low oxidation potential [92, 93]. It is estimated that every day 8oxodG is generated 100 – 500 times in every human cellular genome [7]. 8oxodG is prone to mispairing with adenine during replication instead of cytosine [94] and, if not recognized and corrected by proofreading and mismatch repair mechanisms, can manifest into C>A mutations [95] (Figure 2). During DNA repair, 8oxodG is converted into AP sites, causing a loss of information. During the following replication, adenines are typically inserted as bases opposite of these gaps, following the

"A rule", which also results in C>A mutations [96, 97]. Lastly, T>G mutations can occur after mismatching adenine with 8oxodG from the NP instead of thymine [98].

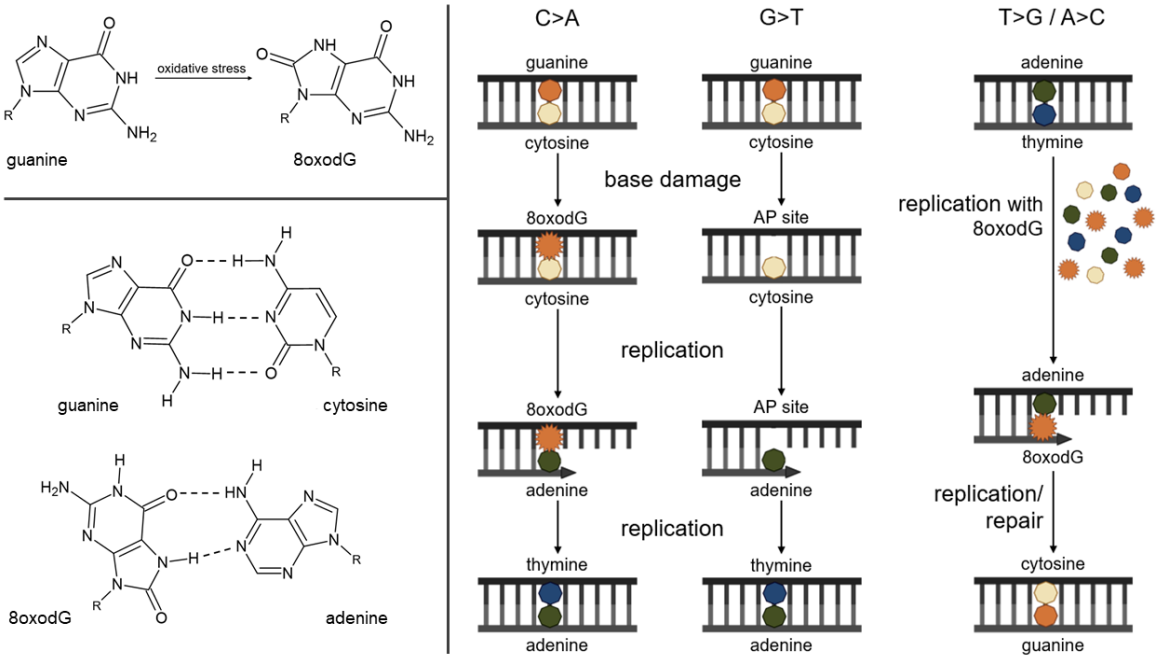

Figure 2 Overview of 8oxodG and resulting mutations. The oxidative modification of guanine causes the formation of 8oxodG, which can cause mispairing with adenine instead of cytosine (C>A). Other transversions can occur during the repair process at AP sites (G>T) or during replication (T>G/ A>C). Adapted from [7].

2.3 DNA Damage Response and DNA Repair

To cope with the constant occurrence of DNA damage, organisms have developed an efficient and far-reaching DNA damage response, which coordinates complex pathways to maintain cell viability, prevents neoplasia, maintain genomic integrity, and, as a last resort, induces controlled cell death. DNA damage response encompasses many mechanisms regulating and affecting DNA damage detection, the cell cycle, chromatin remodelling, metabolism, DNA repair, and apoptosis [99]. Often, these pathways are intertwined and cannot properly function alone. As a result of DNA damage response impairment, genomic instability is promoted by insufficient DNA repair and lack of elimination of cells with damaged DNA via apoptosis [77].

2.3.1 Poly(ADP-ribosyl)ation

A major mechanism of the DNA damage response is the posttranslational modification of proteins via poly(ADP-ribosyl)ation (PARylation), which is associated with DNA repair, protein turnover, and metabolic regulation [100, 101]. Within DNA repair, from at least 17 poly(ADP-ribose) polymerases (PARPs), the highest PARylation activity is exerted by PARP1 and PARP2, whereby PARP1 employs more than 90% of this activity [102-104]. In general, PARPs are a superfamily of multi-domain proteins, which carry (ADP-ribosyl)transferase domains that catalyse the cleavage of nicotinamide adenine dinucleotide (NAD^+) into nicotinamide and ADP-ribose [105]. The ADP-ribose moiety is then transferred to either PARP itself, other acceptor proteins, specific amino acid residues, or other ADP-ribose units [106, 107], resulting in polymeric, linear or branched, ADP-ribose chains [104]. Usually, the ADP-ribose units are transferred to the most distal ADP-ribose terminus, but branching can occur [108]. Some polymerases (PARP1 and PARP2) are able to add multiple ADP-ribose residues to a single acceptor, which can create chains up to hundreds of units long. However, the significance of chain length and severity of branching has not been completely unravelled yet [109].

PARP1 and PARP2 both possess DNA binding domains that facilitate their interaction with the DNA [107]. DNA damage activates the two polymerases, which then bind to the DNA at the damage site and perform PARylation of various target proteins, DNA ends, as well as auto-modification. Thus creating a recruitment platform for downstream repair enzymes, like XRCC1 [102]. Next to protein recruitment, PAR chains enable relaxation of the chromatin condensation, DNA strand dissociation, changes in protein-protein interactions due to the strong electro-negativity of the PAR chains and topographic changes on the acceptor protein [110, 111], as well as stabilization of the DNA replication fork under replication stress [112].

Degradation of PAR chains (dePARylation) is performed by different enzymes, like ADP-ribose hydrolases, ADP-ribosyl lyases, and most importantly, by poly(ADP-ribose) glycohydrolases (PARGs), which are responsible for the rapid removal of the ADP-ribose units from modified proteins [101]. This is achieved partly by endo-glycohydrolase but mostly by exo-glycohydrolase activity, which promotes the removal of mono ADP-ribose units from the most distal ADP-ribose residues of the PAR chains but also cleaving multiple connected units at once [113]. Thus, NAD^+ is recycled back into the cellular system from nicotinamide and the free ADP-ribose unit. Additionally, dePARylation

facilitates the translocation of the recruited XRCC1 directly from PAR to the DNA damage site [114]. The degradation of PAR chains also enables PARPs to move on to further DNA damage sites. Additionally, persisting PARP-DNA complexes might become DNA lesions themselves by acting as replication barriers and collapse of replication forks [115]. Under conditions of hyper-PARP activation, the endo-glycohydrolase activity becomes a major dePARylation pathway, promoting the formation of free PAR chains that are implicated to act as death signals within the apoptosis pathway [116]. Thus, highlighting the importance of a balance between PARylation and dePARylation and a cell´s decision to move into DNA repair or controlled cell death.

2.3.3 Base Excision Repair

There are several repair pathways known in mammalian cells, which are quite specific for distinct DNA lesions. Oxidative DNA damages are largely repaired by base excision repair (BER), as they are mostly small lesions that do not cause changes to the double helix structures of the DNA [117]. This repair pathway acts both in the nuclei and in mitochondria. The BER pathway has been described in detail by Enni Markkanen [118] and is schematically shown in Figure 3. Initiated is BER by lesion-specific DNA glycosylases (e.g. 8-Oxoguanine DNA glycosylase OGG1 and DNA N-glycosylase NTH1), which remove the damaged base. During this process, abasic sites (AP sites) are formed that are in turn cleaved by AP-endonucleases DNA backbone incision. This causes the formation of single-strand breaks (SSB), which triggers the formation of DNA-PARP-complexes. The production of long poly(ADP-ribose) chains promotes recruitment of several transcription factors, DNA polymerase, ligases and flap endonucleases needed for the last steps of BER. The gap-filling and ligation can occur either via short patch or long patch BER, depending on DNA strand orientation [117, 119]. BER is generally well understood, but gaps of knowledge still exist regarding its cell type- and tissue-specific efficiency.

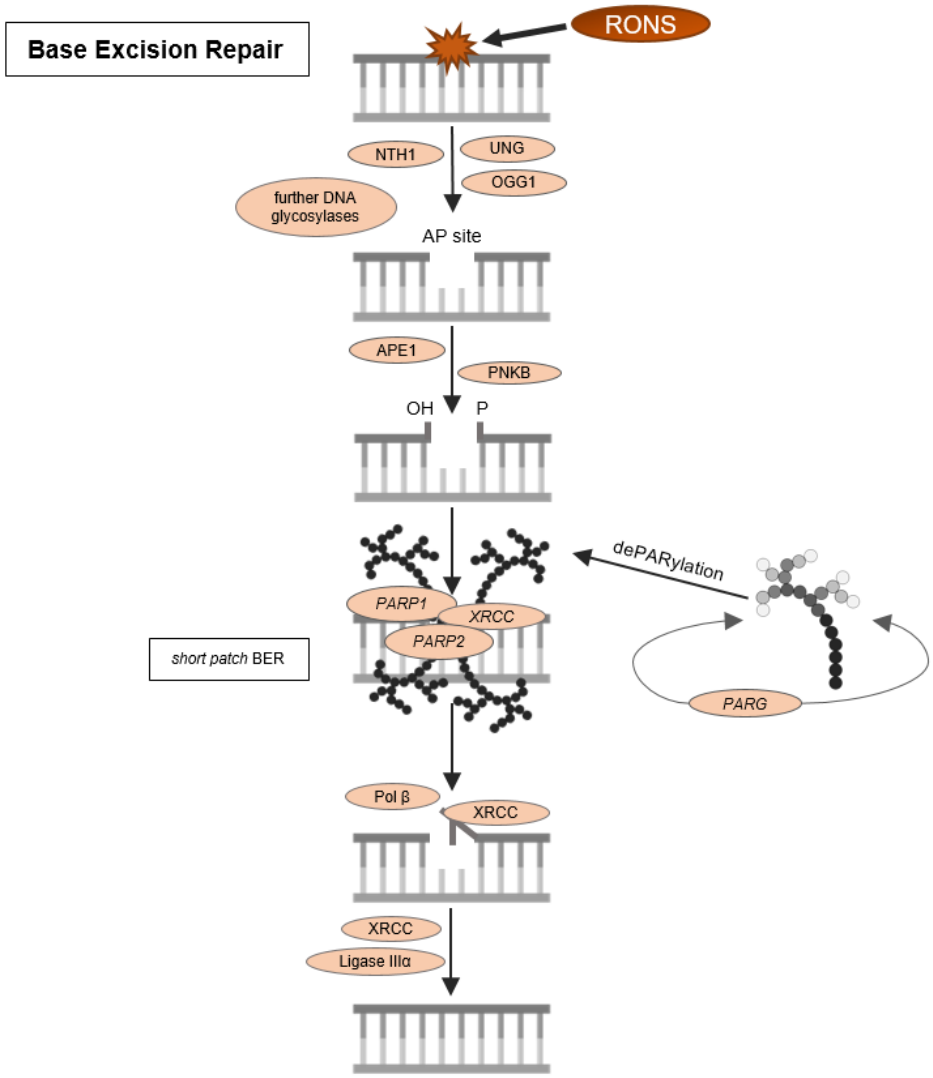

Figure 3 Overview of base excision repair. BER is initiated by DNA N- glycosylases, which cleave the glycosidic bond linking the altered base and the deoxyribose. AP sites are formed. AP-endonucleases will then remove the base-free deoxyribosyl phosphate. The resulting single nucleotide gap induces the formation of DNA-PARP complexes needed for the recruitment of downstream enzymes of short or long patch BER. Adapted from [120].

2.3.2 The role of DNA damage response and DNA repair in neurodegeneration

DNA repair is especially important for long-lived neurons, where keeping the genomic integrity is of high importance for neuronal function. While insufficient DNA repair facilitates an accumulation of DNA damage which in turn may lead to neurodegeneration, excessive DNA repair is also associated with neuronal cell death. Within the DNA damage response, PARylation is activated to initiate further downstream repair processes. PARP1

activity consumes large amounts of $NAD^{+,}$ causing a cellular NAD^+ depletion at high PARylation activity levels, which in combination with ATP loss and deregulated PAR synthesis mediates cell death (namely "parthanatos") [121]. Further, NAD^+ and ATP production are needed for axonal regeneration [122], and an *in vitro* study by Brochier *et al.* in 2015 showed that inhibiting PARylation, by either genetic loss of PARP1 or inhibition of PARP activity, promoted neurite outgrowth [123]. On the other hand, further studies highlight the importance of PARP activity in learning and long-term memory [124, 125], and inhibition of PARP1 caused impaired long-term memory formation [126]. This indicates further that a tightly regulated PARP activity is of great importance to neuronal survival and function.

Additionally, repair intermediates can also be disrupting genomic integrity and genome function. AP sites derive from the repair of oxidatively modified bases via BER and occur in total up to 10,000 times per day in a genome [83]. Similar to oxidative DNA damage, they also have strong effects on DNA secondary structure and protein binding, which can interfere with transcription and replication [88, 127, 128]. Additionally, AP sites harbour reactive aldehyde groups, which may interact with amino groups of proteins, resulting in DNA-protein crosslinks [129], again interfering with genomic integrity at risk. The risk of persisting AP sites as DNA repair intermediates might therefore exceed the danger of the initial DNA damage, and a precise balance of retaining the oxidative DNA damage within the genome and DNA repair is called for. An example of this balance regulation process is the 8oxodG DNA glycosylase OGG1 which becomes enzymatically inactive under conditions of excessive oxidative stress, which results in cell death rather than DNA repair [130].

2.4 Manganese

Despite being toxic at high concentrations, Mn is required as a cofactor for many cellular processes. An understanding of its homeostatic mechanisms, cellular functions, and adverse effects are therefore very important. In the following paragraphs, the chemistry, sources and exposure, physiology and metabolism, health consequences, and the proposed mechanisms of Mn-induced toxicity will be discussed. The European Food Security Association (EFSA) Panel on Dietetic Products, Nutrition and Allergies has published the latest scientific opinion on dietary reference values for Mn in 2013. While

parts of this opinion will be reviewed here, a detailed summary and description of Mn biochemistry would exceed the scope of this work. For further information, the following sources are recommended: EFSA Journal 2013;11(11) [1], Li *et al.* 2018 [5], and Chen *et al.* 2018 [131].

2.4.1 (Bio)chemistry

The transition metal Mn is one of the most abundant naturally occurring elements in the earth´s crust and can be very easily oxidised. Thus, Mn does not usually exist in its elemental form but as silicates, carbonates or oxides [132]. The element can be found in several oxidative states, with Mn(II) and Mn(III) being the most prominent forms in biological systems [133]. Mn is an essential trace element, functioning as a cofactor for several enzyme systems. Mn(II) ions show catalytic and regulatory activity exemplarily required for the Krebs cycle, the maintenance of mitochondria, glutamate synthetase and gluconeogenesis [134, 135]. Due to similarities in structure (crystal structures, electron distribution) and liganding properties between Mn(II) and magnesium(II) (Mg) [136], most enzymatic reactions catalysed by Mn(II) are unspecific, as they can also be activated by Mg(II) [137]. Mn(III) can be found in the manganese-dependent SOD, which primary function is the detoxification of superoxide radicals [137, 138].

2.4.2 Sources and exposure

Large amounts of Mn are released into the air, soil, and waterways by natural erosion and combustion of gas for energy consumption. Adding to this, Mn is used for the manufacturing of steel and iron alloys, batteries, glass, fireworks, unleaded patrol, fertilizers and fungicides (e.g. Mancozeb and Maneb) [134, 139, 140]. Mn can then be absorbed by microorganisms, plants, and animals, causing extensive bioaccumulation. Due to its natural occurrence in soil, water, air and food, as well as industrial pollution, not only occupational workers are exposed to Mn, but also the general population. South Africa, Russia, Gabon, Australia, and Brazil rank among the countries with the richest deposits for Mn [141]. Serving as an essential nutrient, Mn is commonly added in high concentrations to total parenteral nutrition and infant formula [142]. For the general population, the highest exposure is via food with an estimated consumption of

0.7 – 10.9 mg/day according to the World Health Organization (WHO) or 2 – 6 mg/day according to the EFSA [1, 140]. The average daily intake of vegetarians and heavy tea drinkers might be higher compared to the general population, since leafy greens, rice, nuts, grains, and tea are all foods with high Mn-content. The adequate intake is defined as 3 mg/ day for adults (all genders, including pregnant or lactating women) [1]. Mn is also used for medical applications. Due to its chemical properties (paramagnetism), the transition metal can be used as a contrast agent in magnetic resonance imaging (MRI) [143].

2.4.3 Physiology and metabolism

Exposure to Mn can occur via inhalation, orally or dermally, with oral exposure being most relevant to the general population. Uptake of Mn via food and drinking water is followed by gastrointestinal absorption through active transport and passive diffusion [144, 145]. Intestinal absorption was observed between 1.7 — 10.2% depending on the administration carrier (vegetable source or as manganese chloride ($MnCl_2$)) [146, 147]. Mn is then taken up from the blood by the liver and transported bound to transferrin, albumin, or α-2-macroglobulin to extrahepatic tissues [148, 149]. The liver, kidney, pancreas, and brain are the organs with the highest Mn concentrations [132, 150]. The cellular uptake of Mn has not been identified conclusively yet, but evidence suggests that the uptake of Mn(II) into the cells takes place via cell type-specific membrane-bound transport mechanisms, including calcium(II) (Ca) channels [151], the Mn citrate transporter [152], and the divalent metal transporter 1 (DMT1) [153]. Results published by Aschner *et al.* [154] indicate that Mn(III) is transported into the cells via transferrin mechanisms similar to iron(II), but the process has to be investigated further [154, 155]. Once in the cells, Mn can be found mainly in nuclear fractions and mitochondria [156] and can also be metallothionein-bound [157]. ZIP14 (SLC39A14), ZnT10 (SLC30A10), and the multiple metal transporter ZIP8 (SLC39A8) are thought to be some of the main Mn transporters regulating the brain Mn homeostasis [3]. Recent studies by Michalke *et al.* showed that passage of transition metals across neural barriers into the cerebrospinal fluid is in general strictly controlled, but less so for Mn [158]. This might be even more problematic for infants due to their immature, leaky blood-brain barrier and insufficient Mn excretion [159]. In the overall human brain, physiological concentrations are estimated to be between 20.0 – 52.8 µM Mn [160], which can increase strongly due to

accumulation. Concentrations vary greatly between different brain regions, whereby the accumulation is especially high in the mitochondria of the dopamine-rich region of the basal ganglia, particularly the *substantia nigra* [13, 161, 162]. The bodily half-life of Mn shows large inter-individual variations between 13 – 17 days. Suggested factors for the strong differences in half-life are gender and iron status, as well as the homeostatic response to Mn dietary levels [147, 163, 164]. The route of elimination is mainly via bile into the small intestine, followed by excretion via faeces [132].

2.4.4 Health consequences

Mn deficiency is associated with poor bone growth, skin alterations, ataxia, skeletal abnormalities, and hypocholesterolaemia [148, 165], but due to the rich exposure, a deficiency is a rare concern. Mn-induced toxicity caused by excessive and chronic overexposure is of higher importance. High levels of inhaled Mn are acutely toxic to the respiratory system. The primary target organ for Mn toxicity after chronic Mn overexposure is the brain. Epidemiological studies link the overexposure of the trace element to various neurological effects in children and adults all over the world [132, 166]. The adverse effects present as impairment of movement, cognition, emotion, and/ or behavioural responses. The variety of psychiatric and motor disturbances are summed up as “Manganism” and are generally not reversible. This disease resembles idiopathic Parkinson´s disease and includes symptoms like compulsive behaviour, emotional liability, movement disorder, and memory loss [140, 167]. In contrast to parkinsonism, manganism cannot be therapeutically treated via stimulation of the D_2 dopamine receptors (e.g. levodopa) [168]. Vulnerable populations include infants and small children due to their high amounts of Mn/ kg body weight, resulting from a higher intestinal Mn-absorption rate and poorer biliary excretion rate compared to adults [132, 169]. Additionally, the still leaky blood-brain barrier and developing brain increase infants' sensitivity to Mn-induced neurotoxicity [151, 159]. A second vulnerable population includes persons on parenteral nutrition. The intravenous administration increases the bioavailability to 100%, and if Mn uptake exceeds the excretion, Mn homeostasis is omitted. Hypermanganesemia is common in patients treated with long-term parenteral nutrition [170]. Polymorphisms also contribute to the formation of vulnerable groups. An epidemiological study by Zheng *et al.* in 2001 identified the *CYP2D6L* (encoding for phase I oxidative bio transforming protein CYP2D6) gene polymorphism as a possible influence

of manganese-induced neurotoxicity, as a homozygote mutation (single nucleotide polymorphism) in that gene caused a 90% decreased risk of developing manganism compared to the wild type gene [171]. Polymorphisms in *PARK2* (encoding for E3 ubiquitin-protein ligase) and *ATP13A2* (encodes for a cationic transporter ATPase) are likewise indicated to have effects on the risk of manganism. Mutations in both genes are also associated with Parkinson's disease, indicating similar underlying mechanisms resulting from the polymorphisms of the two clinically comparative neurological diseases [172-174].

2.4.5 Proposed mechanisms for Mn-induced (neuro)toxicity

While the association between Mn and neurodegeneration is avowed, little is known about the mechanistic pathways of neurotoxicity. Investigations by Kalia *et al.* in 2008 indicate that in brain epithelial and neuronal cells, the nuclei are the primary pool of intracellular Mn [175]. These findings are in line with *in vivo* experiments, but only under physiological Mn conditions. Under high Mn exposure, the subcellular site of highest relative Mn accumulation shifted from the nucleus to mitochondria [162]. This indicates that the metal is indeed able to enter the nucleus, where the Mn ions might form chelation complexes with phosphates oxygens and bases of the DNA strands [176, 177], but Mn-DNA aggregation is due to chemical properties only likely at extremely high Mn ion concentrations [178]. Under conditions of Mn overexposure, it is, therefore, more likely that the genotoxic effect of Mn is caused indirectly via RONS production in mitochondria. Mn, as a transition metal, can cause excessive production of RONS, either directly via Fenton-like reactions or indirectly by disturbing the respiratory chain in mitochondria [179, 180]. Mn-induced mitochondrial RONS generation occurs mainly at the site of complex II of the respiratory chain, promoting the reduction of the mitochondrial membrane potential and formation of mitochondrial permeability pores, which causes the loss of low-molecular-weight antioxidants [181, 182]. The increase of oxidative stress after chronic Mn exposure has been shown by *in vitro* and *in vivo* experimental studies [10, 41, 183, 184]. The oxidative stress, in turn, might increase oxidative DNA damage. Additionally, (Mn-induced) oxidative stress has the potency to interact with proteins of the DNA damage response and DNA repair pathways [185], causing an accumulation of (improperly repaired) DNA damage. This combination might then contribute to neurological dysfunction [41, 186]. Astrocytes and neuronal cells in the dopamine-rich

area of the basal ganglia have been proposed to be the primary target cells in Mn-induced neurotoxicity due to their location in the brain and the high number of mitochondria [186-189], causing especially dopaminergic neurodegeneration [13, 161, 162]. Nevertheless, the genotoxic potential of Mn and the fate of neurotoxic endpoints are still not fully elucidated.

2.5 Alternative Model Organism and Cell Culture System

For the investigations of Mn-induced toxicity, two very different model systems were used. Both can be used, to some degree, for scientific investigations within the 3R principle. The goal of 3R is to conduct research as humane as possible by 1) avoiding animal experiments altogether (Replacement), 2) limiting the number of research animals (Reduction), and 3) reducing the suffering of animals to the absolute minimum (Refinement). By replacing *in vivo* experiments (rodents or animals of a higher tier) for mechanistic studies with cell culture experiments and investigations in multicellular model organisms, one can reduce the number of (unnecessary) animal experiments [12]. Apart from ethical reasons, using cell lines or model organisms has several advantages. *In vitro* experiments are often cheaper and less time-intensive due to shorter live cycles. Additionally, it is often easier to identify specific mechanisms in simplified models, and genetic modifications are less complicated.

2.5.1 *Caenorhabditis elegans*

The invertebrate model organism *C. elegans* can be classified somewhere in the niche between classic *in vivo* animal models and *in vitro* cell culture systems [190]. In the 1960s, Sydney Brenner was the first researcher utilising the nematode for research of genetics and molecular biology, in the hope of creating a model system that is "simple enough" to understand and conserved enough on cellular and molecular level to other animals and humans to be relevant. Today, *C. elegans* is a widely used model organism for research on development, ageing, neurodegeneration and many related fields. The transparency, a lifespan of 2 – 3 weeks, a short generation time of 3.5 days, high growth rates, cell consistency, and the fully sequenced genome are just a few factors contributing to the attractiveness of this model organism for research. *C. elegans* reaches a maximum size of 1 mm and is usually kept on agar plates in large populations, with Escherichia coli (*E. coli*)

bacteria as the food source [190, 191]. Its transparency allows observation of individual cells and subcellular details, as well as *in vivo* fluorescent staining of proteins and subcellular compartments [192]. The worm exists in two sexes, hermaphrodites and males, whereby males are only naturally occurring with a percentage of 0.1 – 0.2%. Under laboratory settings, they are used to isolate, maintain and move mutations between different strains [193]. Self-fertilizing hermaphrodites create homozygous offspring that are genetically identical, and a single worm can sustain an entire population. Thus, *C. elegans* carry cell consistency, meaning an invariant number of somatic cells (hermaphrodites: 959 somatic cells, males: 1031 somatic cells, including the 302/385 neurons). This was exploited to unravel a complete cell lineage; every cell can be tract from fertilization to adulthood [194, 195]. *C. elegans* is the first multicellular organism to be fully sequenced [196], and forward and reverse genetics are routinely used for molecular identification of important key genes in development and cellular processes [190]. Efficient genome-editing methods (TALEN, CRISPR/Cas9) enable the fairly easy creation of targeted mutations, and by utilising RNA interference (RNAi), specific protein knock-downs can be generated [197, 198]. Despite the apparent simplicity of *C. elegans*, many similarities in the cellular and molecular processes exist between the nematode and other metazoans across the evolutionary time. In fact, 60 – 80% of all human genes have orthologues in the worm´s genome [199], and 40% of human disease-associated genes have also distinct orthologues in *C. elegans* [200].

The length of the life cycle of *C. elegans* depends very much on the temperature conditions. The worms can be kept from 12 – 25 °C, and by changing temperature, one can easily control the growth rate. Through self-fertilization, hermaphrodites can produce up to 300 identical offspring, while fertilization by males can induce the production of ~ 1000 progenies. Embryogenesis lasts ~ 16 h after fertilization, whereby the embryos are usually retained within the hermaphrodite until the 24-cell stage. Embryos are protected by virtually impermeable eggshells and are not dependent on the parental worm, neither during *in utero* nor *ex utero* development. After hatching, *C. elegans* will only develop from the first larval stage (L1) into the subsequent larval stages (L2 – L4) if food is present. While the L1 stage lasts about 16 h, the duration of the L2 – L4 larval stages is shorter, approximately 12 h each. As soon as the worms reach adulthood, they begin with egg-laying [190]. Under suboptimal conditions, like food depletion, high temperatures, or overcrowding of the agar plates, nematodes will transit

into a "Dauer" stage. This facultative diapause stage enables *C. elegans* to survive up to 4 months in a sleep-like period of inactivity [201]. The life cycle is schematically shown in Figure 4.

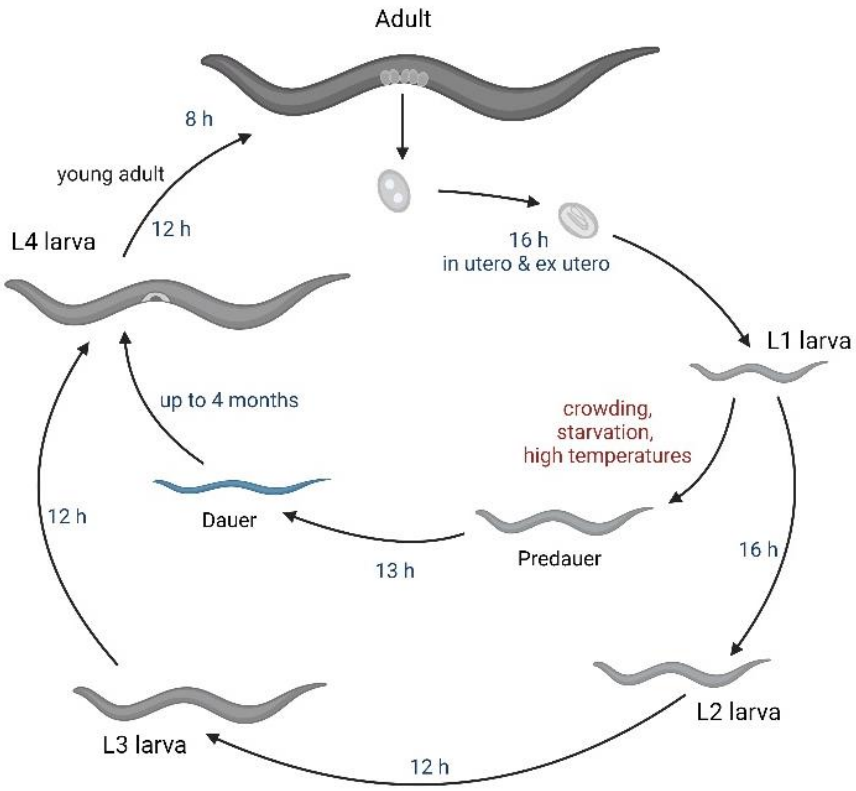

Figure 4 Schematic overview of the *C. elegans* life cycle at ~20 °C. After hatching, *C. elegans* undergo four larval stages before becoming reproducing adults. The length of the life cycle greatly depends on the surrounding temperature.

Oxidative stress and genomic integrity of *C. elegans*

C. elegans offers promising possibilities to study oxidative stress and all aspects of genomic integrity due to many evolutionary maintained processes. For instance, the major oxidative stress pathways, e.g. insulin/IGF-1 signalling pathway, Nrf2/SKN-1 signalling pathway, and the p38 MAP kinase signalling pathway are highly conserved in nematodes and humans [202-204]. Most enzymes involved in the antioxidant system of mammals (like SOD, GPX, CAT) are also present in the worm [205, 206]. Furthermore, several DNA repair mechanisms have been identified in *C. elegans*, including nucleotide excision repair, BER, mismatch repair, non-homologous end-joining, and homologous recombination [207, 208]. In general, most methods for oxidative stress measurements

developed for *in vitro* investigations can also be adapted for use in *C. elegans* and enable a more adequate reflection of the *in vivo* situation. Alongside direct measurements of ROS, oxidative damage endpoints, and gene expression (described in the oxidative stress Section 2.1), mutant worms and transgenic worms containing reporter genes can be used additionally for the identification of mechanistic pathways in the oxidative stress and the DNA damage response. The *gst*-4::gfp strain is a prevalent transgenic strain for the analysis of the oxidative stress defence [209], and mutant worms can exemplarily be used for investigating PARylation in the nematode, as described by Neumann *et al.* [41].

Both *C. elegans* sexes are diploid for five autosomal chromosomes. Differences only exist in the sex chromosomes. While hermaphrodites have 2X, males only have a single X chromosome (X0) [210]. The worm´s genome size encompasses ~100 million bp (including the mitochondrial genome), with ~ 20,000 currently identified protein-coding genes [211].

Neurodegeneration in *C. elegans*

Utilising *C. elegans* enabled research on many aspects of neurobiology, like neuronal generation and specification, synapse formation, neurite regeneration, neuronal degradation, and cell death [190, 212, 213]. The nervous system of the adult hermaphrodite consists of 302 neurons, which are located as a few discrete ganglions in the head, ventral cord, and tail. The male nervous system, however, consists of 383 neuronal cells [194]. In contrast to the human nervous system, most *C. elegans* neurons have a simple structure with only 1 – 2 neurites attached to each cell body. Merely the mechanosensory neurons can form an elaborated neurite network [214]. Distinguishing neurites as either axons or dendrites is mostly not possible, as both provide and receive synaptic signals [215]. The most common neurotransmitters in vertebrates can also be found in the nematode. Several receptors for the detection of dopamine, serotonin, acetylcholine, glutamate, and γ-amino butyric acid (GABA) are present in the worm [216]. Many behaviour patterns of *C. elegans*, e.g. chemotaxis, thermotaxis, response to touch and food, learning, and mating rituals, are strongly linked to very specific neurological events [217-220]. The combination of the study of this behaviour, the microscopic analysis of the neuronal system, quantification of neurotransmitters and the structure of the *C. elegans* nervous systems enables that most problems of cellular and molecular neurobiology can be addressed in the nematode.

Manganese homeostasis in *C. elegans*

In general, *C. elegans* contains highly conserved pathways for metal homeostasis, which have been investigated comprehensively, but the homeostatic regulation of Mn is not fully elucidated yet. Due to the worm's thick cuticle, Mn uptake is mainly via the mouth, and experimental exposure should be well thought out, as many laboratory conditions influence the bioavailability of the metal (detailed reviewed in Taylor *et al.* (2020) [221]). Absorption is then primarily regulated by *C. elegans* homologs (smf-1, smf-2, and smf-3) of the DMT1, which are expressed mainly in the apical gut epithelium but also in sub-apical cell compartments [222]. *C. elegans* does not express any functional homology of the SLC30A10 exporter, Mn cellular clearance is therefore likely done by the basolateral Fe exporter ferroportin (FPN), which is expressed in three *C. elegans* homologs (fpn-1.1, fpn-1.2 and fpn-1.3) [223]. As those mechanisms are also involved in Fe transport, uptake and excretion of Mn might be intertwined with Fe homeostasis [224]. In addition, mRNA studies of the metallothioneins (particularly mtl-1) indicate a prominent role in Mn homeostasis [225]. Summarized, *C. elegans* is a suitable model organism to investigate effects after Mn exposure, as the metal homeostasis is well regulated, even though not all known transporters from mammals have homologues in the nematode.

Advantages and limitations

While many of the worms attributes are highly useful for research, *C. elegans*, like all model organisms, has some limitations. Despite showing a 60 – 80% homology, worms are evolutionary far from humans. The nematodes lack some physiologically relevant systems and organs for vertebrates, like the brain, circulatory systems, or the adaptive immune system [226]. Although the small size is beneficial for cultivation, it can cause great difficulty to obtain enough material for biochemical investigations [227]. For neurobiology, in particular, it might be limiting that some features of vertebrate neurons, like myelination of axons, are not conserved in *C. elegans* [195]. Furthermore, gene silencing via RNAi, which is very efficient for specific knock-downs of most genes, is refractory for many genes of the nervous system. Genetic modifications are relatively easy to conduct in the worm, but only about 30% of *C. elegans* genes can be mutated to visible phenotypes, as the rest results in high levels of lethality [228]. Cultivating strains for long periods (over years) or different laboratory conditions might cause the strains to

develop adaptive mutations, causing the unwanted introduction of additional factors [229]. Although this can easily be avoided by freezing and storing the worms in inactive states at -80 °C and genotyping all strains regularly [230]. Variances in assay conditions have a strong influence on the results, as well as their interpretation. Especially in *C. elegans* research, contradictory results by different authors are frequently published, which might be explained by varying laboratory settings, like substance concentration in the media, time and duration of the incubation, bioavailability, or worm age. Especially the thick cuticle hampers easy drug uptake and reduces the bioavailability of some substances [221]. Up to today, there are no official guidelines present that regulate the laboratory methodology of *C. elegans* nor data interpretation, and the tendency of over-interpretation of phenotypes with little to no evidence of their actual causes can be observed in some publications.

Despite these limitations, *C. elegans* is a highly useful multicellular model organism for various fields of research, including neurodegeneration.

2.5.2 Luhmes

Further investigations regarding specifically the neurodegeneration LUHMES cells were used as a second model system. General cultivation is similar to that of other cell lines, but all cell culture dishes must be pre-coated to enable LUHMES cells to attach and grow. The cell line was first derived from an 8-week old (female) embryonic human mesencephalon at Lund University, Sweden. LUHMES cells are conditional immortalized by a tetracycline-responsive v-myc oncogene (TET-off) [231]. By exposing the cells to tetracycline, cyclic AMP (cAMP), and glial-derived neurotrophic factor (GNDF), LUHMES cells differentiate from mitotic cells into post-mitotic dopaminergic-like neurons. This allows the proliferation of the cells to large scales before transforming them into stable post-mitotic neurons. While tetracycline suppresses the y-myc gene and allows the cells to exit the cell cycle, cAMP and GNDF enable the formation of dopaminergic features [16, 231]. During the differentiation, which takes ~ 6 days to be completed, mRNA levels of specific neuronal and dopaminergic-neuron markers increase at some point during differentiation. Examples include genes for tubulin beta-3 (Tuj1), the potassium inwardly-rectifying channel (KCNJ6), Synapsin I (SYN1), and synaptophysin (SYP) and dopaminergic-specifically: tyrosine hydroxylase (TH), the dopamine transporter (DAT),

and the nuclear receptor-related 1 (Nurr1). On day 6, they express dopaminergic neuron biochemical markers and develop extensive neurite networks, which highly resembles primary neurons [232]. Additionally, LUHMES cells assert spontaneous electrical activities and express functional DAT1 in the membrane for dopamine uptake and release [16]. This all suggests a high relevance of the differentiated LUHMES cells for human dopaminergic neurons.

Genomic integrity in LUHMES cells

DNA damage has been identified as an important initiator of neuronal death and is associated with a variety of (age-related) neurodegenerative diseases [233]. While post-mitotic cells are terminally withdrawn from the cell cycle, they still remain transcriptionally active, and the need to preserve genomic integrity is of high importance for neuronal function. Due to the high metabolic rate of neurons (high mitochondrial RONS formation) and constant exogenous sources of oxidative stress, an adequate DNA damage response is necessary for genomic integrity. Thus, continuous repair of DNA is essential for neuronal survival and normal neuronal function throughout the entirety of an organism´s lifespan. BER is the main repair pathway in neurons, probably due to the fact that most DNA lesions occurring in the brain are oxidative modifications of the bases [234].

Advantages and limitations

One of the main advantages of *in vitro* models, in general, is the consistency and reproducibility of results that can be retrieved from using clonal cells. Moreover, cell culture conditions are strongly regulated and constantly examined so that an influence of the physiochemical environment is kept to an extreme minimum. As LUHMES are an immortalized cell line, they are relatively easy to use and offer the advantage of prior knowledge of their specific culture requirements. They have high physiological relevance, a good batch to batch consistency, and can be cultivated on large scales. This is useful for meaningful high-throughput screening. Compared to other (dopaminergic-) neurodegenerative cell systems, like differentiated SH-SY5Y and PC12 cells, LUHMES cells show a higher relevance for human dopaminergic neurons by expressing dopaminergic markers (tyrosine hydroxylases, dopamine D2 and D3, DAT) more truthful

to human dopamine neurons [235-237]. A practical disadvantage of LUHMES cells is the expense and effort needed for cultivation, which is compared to other cell lines or even *C. elegans* relatively high, but culturing procedures of LUHMES cells are not as complex as culturing primary dopaminergic neurons from rodent embryos. Plus, variation among different primary culture preparations can be avoided. However, the physiological relevance to *in vivo* experiments might be slightly diminished. Another limitation still present today is the lack of a thorough understanding of the differences between differentiated LUHMES cells and neurons. It is still unknown whether the regulatory signalling pathways *in vivo* is captured by this cell system [232]. Follow-up studies in rodent primary neurons and *in vivo* models might therefore be needed to confirm specific research results.

Abstract

The investigation of neurodegenerative and age-related diseases is a highly relevant topic in current research. Especially oxidative stress is thought to be the common underlying mechanism in diseases such as Parkinson's or Alzheimer's disease. The nematode *Caenorhabditis elegans* (*C. elegans*) is a prominent model organism, which is often used for such investigations and has gained extensive recognition in research regarding the linkage of reactive oxygen species (ROS) and neurodegeneration. Not only studies regarding genomics and proteomics have been increasingly conducted, also the number of studies based on the lipidome is rising. The phospholipid class of cardiolipin (CL) is a unique lipid class, which is exclusively located in mitochondria and is therefore of great relevance regarding oxidative stress and associated diseases. CL oxidation products have become a prominent marker for oxidative stress in various species. However, the CL distribution in the nematode *C. elegans* is still scarcely known on the molecular level and oxidation products have not yet been identified. In this work we demonstrate the importance of CL distribution and the applicability of CL oxidation products as a sensitive marker for oxidative stress in *C. elegans.* For this reason, the CL distribution was determined by means of online two-dimensional liquid chromatography hyphenated with high-resolution mass spectrometry (2D-LC-HRMS). Subsequently, worms were treated with *tert*-butyl hydroperoxide (*t*BOOH) in order to provoke oxidative stress and induce the artificial formation of oxidised CL. We were able to detect increasing amounts of CL oxidation products of highly unsaturated CL species in a concentration-dependent manner. This finding emphasizes the great potential of CL oxidation products as a sensitive marker substance of oxidative stress in *C. elegans*, which is not only directly linked to mitochondria function but also favourable to other oxidative stress markers in terms of the needed sample material, relative substance stability, and specificity of the oxidation site.

Chapter 3

Cardiolipin Oxidation Products as a New Endpoint for Oxidative Stress in *C. elegans*

Investigation of cardiolipin oxidation products as a new endpoint for oxidative stress in *C. elegans* by means of online two-dimensional liquid chromatography and high-resolution mass spectrometry

Based on:

Patrick O. Helmer[Δ], **Merle M. Nicolai**[Δ], Vera Schwantes, Julia Bornhorst, Heiko Hayen, Free Radical Biology and Medicine 2020, Jan;162:216-224

DOI: 10.1016/j.freeradbiomed.2020.10.019

[Δ] These authors contributed equally.

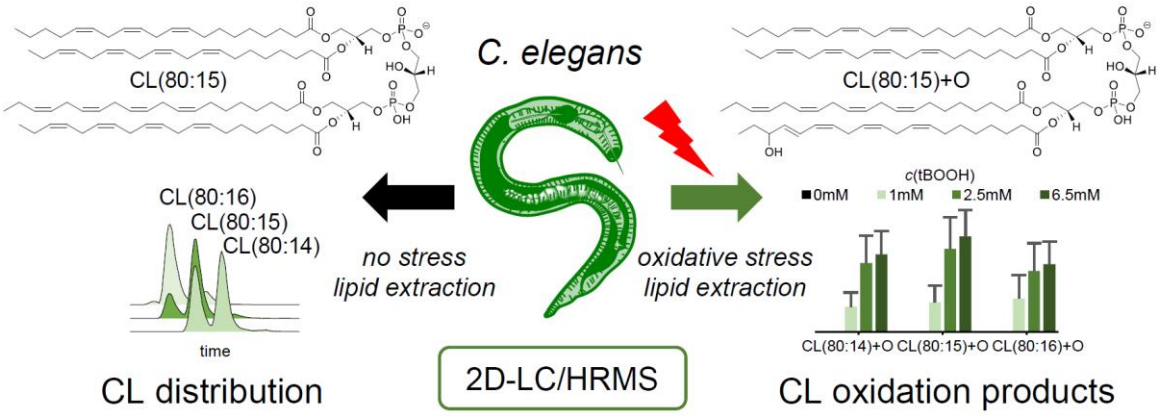

Figure 5 Graphical Abstract: Cardiolipin oxidation products as a new endpoint for oxidative stress in *C. elegans*.

Highlights

- Cardiolipin species distribution in *C. elegans* reveals a high potential as ROS target
- Cardiolipin oxidation products as a new marker for oxidative stress in *C. elegans*
- Increased amount of cardiolipin oxidation products after *t*BOOH treatment
- Tailored analysis for increased sensitivity by heart-cut LC-MS approach

Keywords

Oxidative stress, cardiolipin, *C. elegans*, online two-dimensional liquid chromatography, high-resolution mass spectrometry

3.1 Introduction

Over the last years, the nematode *Caenorhabditis elegans* (*C. elegans*) has become a recognized model organism to study age-related as well as neurodegenerative diseases, such as Parkinson's and Alzheimer's disease. The organism allows extensive investigations regarding genomics, proteomics and lipidomics, but still, defined neurodegenerative pathways are hard to identify [39, 238, 239]. Oxidative stress, defined as the imbalance of antioxidants and oxidants towards an abundance of reactive oxygen species (ROS), and its resulting changes on cellular and organismic level have been believed to be strongly associated to age- and neurodegenerative-related diseases [240-

242]. Typical oxidative stress endpoints, such as decrease of mitochondrial activity [243], decreasing glutathione levels [41], protein modifications [244] and oxidative DNA damage [245] are being studied increasingly in the nematode. However, information on lipid composition and oxidation in *C. elegans* is still limited. Given that the oxidation of polyunsaturated phospholipids is a major outcome of a persistent ROS abundance and the direct involvement of phospholipids in mitochondrial activity and cell death, both linked to neurodegeneration, their systemic identification and quantification is of high interest. [240] Cardiolipin (CL), a mitochondria-specific phospholipid class is highly sensitive to peroxidation of its double bonds by extracellular and intracellular ROS and is directly associated with mitochondrial dysfunction. Furthermore, CL can be target for reactive nitrogen species (RNS) as well [246]. Based on its dimeric structure, the lipid class of CL is paramount for stabilising the protein complexes of the respiratory chain. [247] Decreasing CL levels in the inner mitochondrial membrane, for example due to oxidative processes lead to a destabilization of these complexes. Furthermore, CL oxidation is linked to apoptotic events by the release of cytochrome *c* (cyt *c*). [248-250] CL oxidation products (CLox) can be generated by ROS but also cyt *c* is known to be involved as a catalyst [251-253]. In most cases, CL species with polyunsaturated fatty acyl moieties are targets for oxidation [252]. This makes CL oxidation products an interesting marker for various diseases. CLox have been gaining in importance for Parkinson's disease [253, 254] research in *in vivo* and *in vitro* research, but knowledge of CL in general as well as CLox in nematodes is scarce. Due to its high structural diversity, the analysis of CL itself is very challenging in biological samples and requires powerful analytical methods. Further oxidation increases this diversity even more which necessitate tailored approaches. Liquid chromatography and mass spectrometric detection is in most cases the method of choice. [255] For this reason, we used a selective and sensitive method based on online two-dimensional liquid chromatography to identify, quantify and compare CLox species in wild type *C. elegans*. Using *tert*-butyl hydroperoxide (*t*BOOH) as a prominent ROS inducer, we demonstrate the suitability of CLox as a significant marker of oxidative stress for this model organism.

3.2 Material and Methods

3.2.1 Chemicals and materials

Methanol (MeOH), acetonitrile (ACN) and 2-propanol (IPA) (LC/MS grade) were purchased from VWR International GmbH (Darmstadt, Germany). Methyl *tert*-butyl ether (≥99.99%) was delivered by Fluka (Darmstadt, Germany). Ammonium formate (≥99.995%), ammonium acetate (≥99.99%) and acetic acid (≥99.99%) were obtained from Sigma Aldrich (Steinheim, Germany). Formic acid (99-100% p.a.) was purchased from Th. Geyer (Renningen, Germany). Water was purified by a Milli-Q Academic-System (18.2 MΩcm; 0.2 µm filter; Millipore, Molsheim, France). All chemicals were used as received.

The WT N2 Bristol *C. elegans* strain was provided by the Caenorhabditis Genetic Center (CGC; University of Minnesota).

3.2.2 *C. elegans* culture conditions and *t*BOOH treatment for cardiolipin analysis

For the experimental setting the wild type (N2) Bristol strain was used, which was provided by the Caenorhabditis Genetic Center (CGC; University of Minnesota). The worm culture was handled and maintained as described in Brenner, 1974 [256]. All experiments were performed using synchronized L4 stage populations. For this, L1 stage worms were seeded on OP50- covered NGM plates after hatching and were allowed to develop until L4 without further interference. 6000 L4 stage nematodes per sample were incubated with different concentrations, up to 6.5 mM of *t*BOOH (Sigma-Aldrich, Steinheim, Germany) diluted in 85 mM NaCl for 1 h in siliconized tubes while rotating on low speed to ensure equal substance uptake. After exposure, worms were washed at least three times with 85 mM NaCl containing 0.01% Tween® before shock-freezing the pellets with liquid nitrogen for storage at -80 °C.

3.2.3 Carboxy-DCFH-DA Assay for RO(N)S measurement

The generation of RO(N)S caused by *t*BOOH was measured in L4 stage *C. elegans* likewise, but the experimental set-up did not allow the removal of *t*BOOH during quantification. Hence, worms were incubated with the substance at lower concentrations, only up to 100 µM *t*BOOH, but for longer time periods. The 5(&6)-carboxy-2´,7´-

dichlorodihydrofluorescein-diacetate (Carboxy-DCFH-DA)-based plate reader assay was performed as previously published in Rohn *et al.* 2020 [257]. Briefly, worms were incubated with 500 µM carboxy-DCFH-DA (Invitrogen) diluted in M9 buffer for 2 h in the dark. After washing three times using M9 buffer, 500 worms were transferred to each well of a 96-well plate and worms were exposed to different concentrations of *t*BOOH diluted in dH_2O. Kinetics of the oxidised DCFH-DA were monitored (excitation 485 nm/ emission 535 nm) at various time points (0, 3, 60, 120, 180, 240, 300 and 360 min) using a microplate reader (Tecan Infinite M200 Pro).

3.2.4 Lipid extraction

C. elegans worm pellets of 6000 L4 stage nematodes were extracted according to the lipid extraction protocol of Matyash *et al.*[258]. All extraction steps were carried out utilising ice-cold solvents and on ice. The worm pellet was resuspended in 100 µL of water and 20 µL of 65 mM BHT as antioxidant. Before extraction, three freezing-thawing cycles were carried out followed by addition of 1.5 mL MeOH and 10 min sonication utilising an ultrasonic processor (UP200St, Hielscher Ultrasonics GmbH, Germany). Subsequently, 20 µL of 5 µM d5-CL 72:8 as internal standard (IS) was added before extraction. The extraction was carried out in 10 mL glass vials with teflon caps. 5 mL MtBE were added to the sample and shaken on ice for 1 h at 150 rpm. After that, 1.25 mL water were added to the sample followed by additional incubation on ice for 10 min. Organic and aqueous phases were separated by centrifuging for 10 min at 1000 x g (Centrifuge 5416, Eppendorf AG, Germany). The upper MtBE phase was collected and the aqueous phase was extracted a second time by adding 2 mL of MtBE/MeOH/water (10:3:2.5; v/v/v). The pooled organic supernatants were dried utilising a gentle nitrogen flow. The residue was dissolved in 200 µL IPA, which results in a IS concentration of 0.5 µM and a BHT concentration of 6.5 mM.

3.2.5 Cardiolipin analysis via 2D-LC-HRMS

2D-LC-HRMS was carried out utilising a Thermo Scientific Ultimate 3000 system with dual gradient pump hyphenated with a Q Exactive Plus mass spectrometer. Xcalibur 4.1 software and the SII plugin software for instrument control was utilised. The general instrument and heart-cut setup was described earlier [259]. Phospholipid separation via

HILIC in first dimension (^{1}D) was carried out using a iHILIC Fusion(+) column (20 x 2.1 mm, 1.8 µm, 100 Å). The method was optimized in terms of separation efficiency for CL species of *C elegans*. For this reason an Accucore C30 column (150 x 2.1 mm, 2.6 µm, 80 Å) was used and a new gradient was developed in second dimension (^{2}D). An ammonium acetate buffer (10 mM, 0.01% acetic acid, 5% MeOH) (A) and MeOH/IPA (20:80 (v/v), 10 mM ammonium acetate, 0.01% acetic acid) (B) were used for gradient elution on ^{2}D RP-LC separation. The ^{1}D HILIC gradient was previously described [259]. The ^{2}D RP-LC gradient started at 70% B. Re-equilibration of the RP phase was carried out during the ^{1}D HILIC separation. A transfer window from 5.75 min to 6.30 min was determined for analyte transfer. A detailed gradient overview for the ^{1}D HILIC and ^{2}D RP-LC separation method is shown in Table 2 of the Supporting Information (SI). Due to the high back-pressure of more than 600 bar the six-port valve, which was used for the heart-cut setup (cf. Figure 31), was equipped with a 400 µL sample loop of stainless steel. The analyte transfer was carried out by back-flushing the sample loop onto the ^{2}D RP column. Subsequently, the gradient elution according to Table 2 started. The total run time was 25 minutes including ^{1}D HILIC separation. An injection volume of 5 µL was chosen.

Mass spectrometric detection was carried out in negative electrospray ionization (ESI) mode utilising a HESI-II probe (Thermo Scientific). Probe settings were set as follows: Source voltage -3.5 kV, probe heater 300 °C, sheath gas flow rate 45 arbitrary units, auxiliary gas flow rate 10 arbitrary units, spare gas flow 1 arbitrary units, capillary temperature 325 °C, s-lens rf level 85; *m/z* 600-1800, resolution 140,000 for fragmentation experiments and 280,000 (full width at half maximum peak height at *m/z* 200) for full MS measurements. For structural elucidation, data-dependent MS/MS experiments were performed at a normalized collision energy of 24 eV (based on an *m/z* of 500) by HCD. The resolution was set to 17,500 (at *m/z* 200). For precursor isolation a window of 1.5 Da was chosen to avoid isotopic interferences. A maximum C-trap injection time of 100 ms in full scan and 50 ms for MS/MS experiments was used.

3.2.6 Data processing using MZmine 2

The open source metabolomics software package MZmine 2 (version 2.53) was utilised for orbitrap HRMS data processing and CL species identification based on accurate mass

library matching utilising Lipid search module. The noise level for "exact mass" detection algorithm was set to 2.0E3. Chromatograms were build utilising the ADAP chromatogram builder module (10 ppm m/z tolerance) [260]. Chromatogram deconvolution was carried out using the local minimum search algorithm. The isotopic peaks grouper was set as described earlier. [261] Lipid search module was utilised to identify and annotate CL species and their oxidation products [262]. Subsequently, the created feature lists were aligned and gap filled.

3.2.7 Lipid nomenclature

The lipid nomenclature in this work is based on the recommendations of Liebisch *et al.* [263]. Fatty acyl (FA) composition of CL species are described as CL x:y, where x represents the total carbon number and y the total number of double bonds. CL 80:15 has a total number of 80 carbon atoms and 15 double bonds in total. Individual FA composition is specified using a slash for a specific position and an underscore were *sn*-1 and *sn*-2 position cannot be distinguished.

3.3 Results and Discussion

3.3.1 Cardiolipin composition of the model organism *C. elegans*

In recent years, *C. elegans* has been used as a versatile model organism in many areas of biochemical and aging research [196, 199, 264]. While the genome has been completely decoded and despite numerous studies, there are just few approaches described in the literature with focus on the metabolome or the lipidome. Many studies with regard to the lipid composition of *C. elegans* is based on the genome and proteome. [265, 266] Lipids, for example oxidative modified phospholipids are often used as markers revealing oxidative stress. [252, 253, 267, 268] Especially for mitochondria, cardiolipin (CL) is a prominent phospholipid class for the investigation of oxidative stress and mitochondrial dysfunction. [252, 269] The main fatty acyl composition of *C. elegans*, based on GC-MS studies, was specified by Hou *et al.* [270]. However, the variety of molecular CL species have only been described to track metabolic changes [271] and have not been identified in detail. Especially CL species with polyunsaturated fatty acids are considered as substrates for oxygenation. Due to their specific location in the inner mitochondrial

membrane and their involvement in energy metabolism of the respiratory chain, CL are target of ROS formed in mitochondria. [252]

In order to establish CL oxidation products as marker for oxidative stress in *C. elegans* mitochondria, the investigation of CL molecular species is the first step. Recently, we developed a method of high sensitivity and selectivity for the analysis of CL and their oxidation products in total lipid extracts based on two-dimensional liquid chromatography. In the first dimension (^{1}D), different phospholipid classes (c.f. Figure 6) are separated according to their head group by hydrophilic interaction liquid chromatography (HILIC) and transferred via heart-cut on the second dimension (^{2}D). Due to the highly polyunsaturated character of CL species in *C. elegans*, the separation of CL species based on reversed phase liquid chromatography (RP-LC) in ^{2}D was modified to increase the chromatographic resolution as described in the Supporting Information (Table 2). While a sufficient separation of CL species of *C. elegans* could not be achieved utilising a phenyl-based stationary phase as described in our previous work, the stationary phase and gradient was adjusted [259]. By using a C30 stationary phase, a better resolution was achieved. For the most critical CL species in terms of chain length and degree of saturation (CL 80:14, CL 80:15 and CL 80:16) a resolution R of ≥1.5 was achieved (CL 80:14 vs. CL 80:15 R = 1.5; CL 80:15 vs. CL 80:16 R = 1.7). To guaranty a sufficient elution strength, the amount of IPA in the mobile phase was increased to from 10% to 80% (v/v) in solvent B while solvent A remained the same. In addition to an increased chromatographic resolution, also shorter retention times, which result in an overall shorter method duration of in total 25 minutes were achieved.

Figure 6 shows the total ion chromatogram (TIC) of the pre-separation into different phospholipid classes via HILIC. Due to the high carbon number and degree of unsaturation the co-elution of all CL species, which is required for a quantitative transfer to the second dimension was investigated. The extracted ion chromatograms (EICs) of three CL species with different numbers of carbon atoms and double bonds indicate the pursued co-elution with retention times of approximately 6.05 min. The mass spectrum shows a wide distribution of different CL species. Keeping in mind, that due to the co-elution an identification exclusively by accurate mass is not unequivocally possible. Sodium adducts as one example can lead to false interpretation [261]. For this reason, the characterization was carried out by RP-LC in ^{2}D after HILIC pre-separation and analyte transfer via heart-cut. A C30-based stationary phase was used due to its distinct

selectivity with respect to acyl chains but also to oxidation products as executed by Colombo *et al.* in the analysis of oxidised aminophospholipids [272].

In addition to the most abundant CL species with a total carbon number of the fatty acyl moieties of 80, 78 and 76 also odd numbered CL species with 77 and 79 carbon atoms were observed. Carbon numbers higher than 80 have been indicated as potassium, sodium or sodium acetate adducts (depending on the sample matrix) of the high abundant CL (78:X) (27.6 ± 3.4%) and CL(80:X) (56.5 ± 4.5%) species. Odd numbered CL can be explained by the capability of *C. elegans* of producing and using odd numbered fatty acids. [33] As already mentioned CL species of *C. elegans* consist of polyunsaturated fatty acids with up to five double bonds. The total number of double bonds in the identified CL species varies from 7 to 17 double bonds (see Supporting Information Figure 32). This pronounced degree of unsaturation underlines the high potential of being target of ROS.

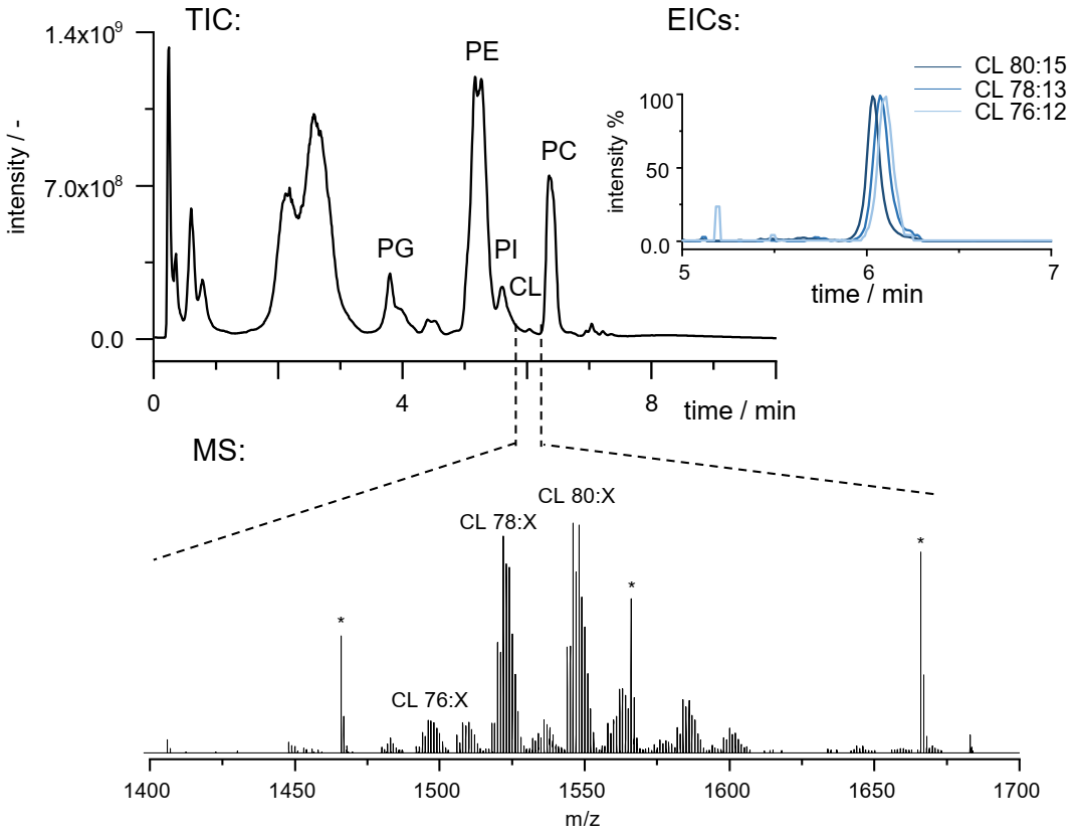

Figure 6 Illustration of the 1D HILIC separation and the pursuit co-elution of CL species. Demonstration of the 1D HILIC separation (total ion chromatogram (TIC)) and the pursuit co-elution of CL species (extracted ion chromatograms (EICs)) which is important for an efficient transfer via the utilised heart-cut setup. The mass spectrum shows the distribution of various CL species with differences in the number of carbon atoms and degree of unsaturation. The asterisks indicate formate clusters based on the modifier salt in the mobile phase used for HILIC separation and the calibration standard (Ultramark).

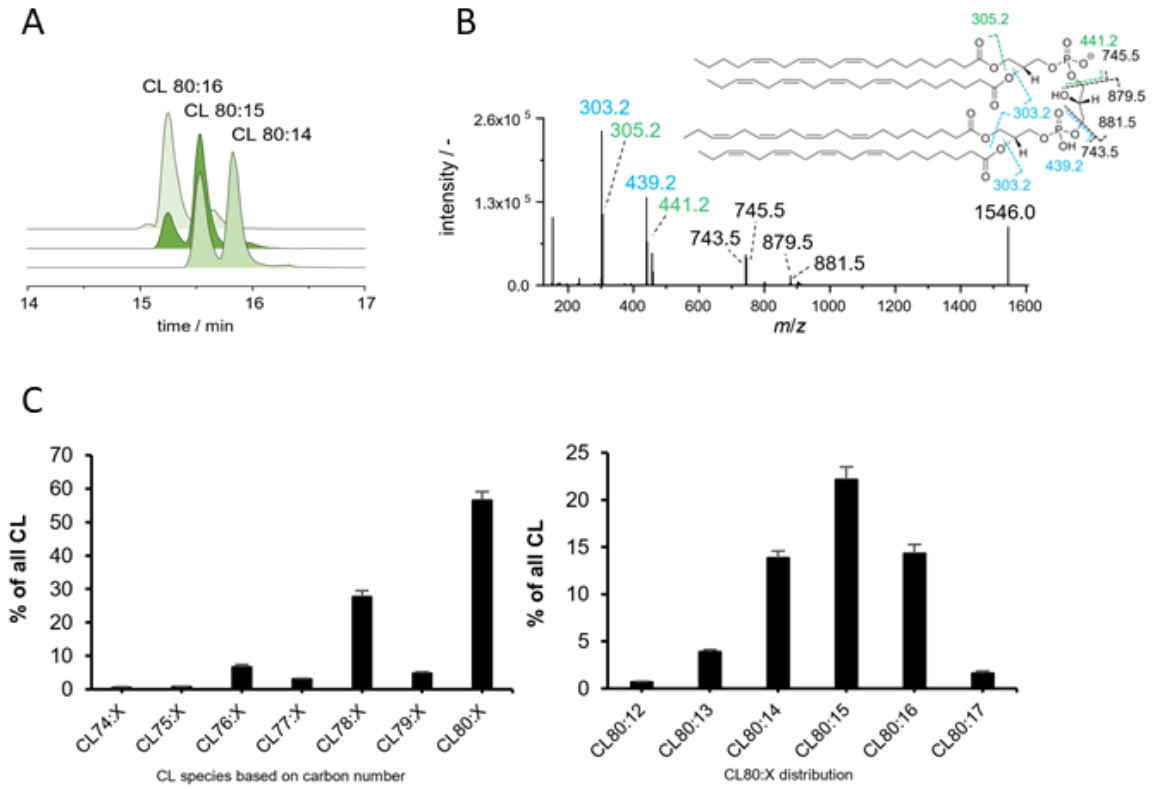

Figure 7 Separation, distribution and fragmentation of main CL species of *C. elegans* by ^{2}D C30 RP-LC. (A) Separation of main CL species of *C. elegans* by ^{2}D C30 RP-LC. Despite the usage of maximum mass spectrometric resolution power, especially $^{13}C_2$ isotopes of abundant CL species have a high potential for false interpretation. (B) Overview of the CL species distribution in *C. elegans*. (C) Exemplary presentation of the fragmentation pattern for structural elucidation of CL(80:15) by MS/MS. Based on the observed fragments, the fatty acyl composition was determined as 20:3_20:4/20:4/20:4. The displayed *m/z* values are rounded to one decimal place for better visualisation.

Figure 7 (A) and (C) show the ^{2}D RP-LC separation of the most abundant species CL(80:14), CL(80:15) and CL(80:16) as well as the distribution of different CL species based on their chain length. The EICs of the chosen CL species with a mass tolerance of 5 ppm. However, a mass tolerance of 5 ppm is not completely sufficient for resolving a species and the $^{13}C_2$ isotope of a species with an additional double bond. Hence, a chromatographic separation of homologous species is required to prevent interferences based on the isotopic overlap. In addition, fragmentation experiments are important for structural elucidation to identify homologous CL species. The fragmentation pattern has been detailed by Hsu and Turk. [273] The combination of HILIC pre-separation with a fast and powerful separation utilising a C30 RP-LC column along with high-resolution

mass spectrometry and fragmentation experiments enables a CL analysis with high confidence and accuracy (Figure 7). Latter, is especially important if we want to analyse oxidised CL species, which are, compared to the main species, of low concentration. CL species which were identified in this work have a relative mass deviation of less than 1.5 ppm with respect to the calculated *m/z* value. A detailed summary of CL species in *C. elegans* based on accurate mass and fragmentation experiments utilising 2D-LC-HRMS is listed in Table 3 and Table 4 of the Supporting Information.

3.3.2 Measurement of ROS levels after *t*BOOH treatment

Following identification of the CL composition, peroxidation of CL caused by oxidative stress was investigated, as ROS was shown to cause mitochondrial dysfunction by impairing the electron transport chain at complex I and III through oxidative damage of CL in other organisms [274, 275]. *t*BOOH is commonly used as an oxidative stress inducer in many different *in vivo* and *in vitro* studies, even though that the exact mechanism of ROS induction is not yet fully understood. The simple lipophilic alkyl hydroperoxide has been reported to induce dose-dependent oxidative stress and damage in various cell lines [276, 277]. The *t*BOOH derived alkoxyl and alkyl radicals induce a cellular redox imbalance, which can cause damage to various intracellular endpoints and may end in apoptosis. [278, 279] To ensure that the tertiary hydroperoxide leads to CL peroxidation via ROS induction as hypothesized, total RO(N)S levels were measured in L4 *C. elegans* using the Carboxy-DCFH-DA assay. Worms were exposed to 25 µM, 50 µM, 100 µM, 150 µM, and 200 µM for up to 6 h. Results indicate an immediate increase of RO(N)S at all *t*BOOH concentrations as can be seen in Figure 8. Concentrations of 50 µM *t*BOOH and above lead to highly significant increases of RO(N)S after 1 h of exposure compared to initial levels, which are only half as high. Over time RO(N)S levels decrease continuously, but levels are still distinctively higher at the last time point of measurement (6 h) compared to control animals. This might indicate an upregulation of various possible antioxidant systems contained in *C. elegans* [280] in response to the oxidative stress. Significant differences between the concentrations are not distinctively detectable, as already low concentration seem to reach the upper limit of RO(N)S induction. Thereby, the assay clearly proves an artificially production of ROS by *t*BOOH exposure in *C. elegans*, which in turn might lead to the lipid peroxidation next to other oxidative stress endpoints.

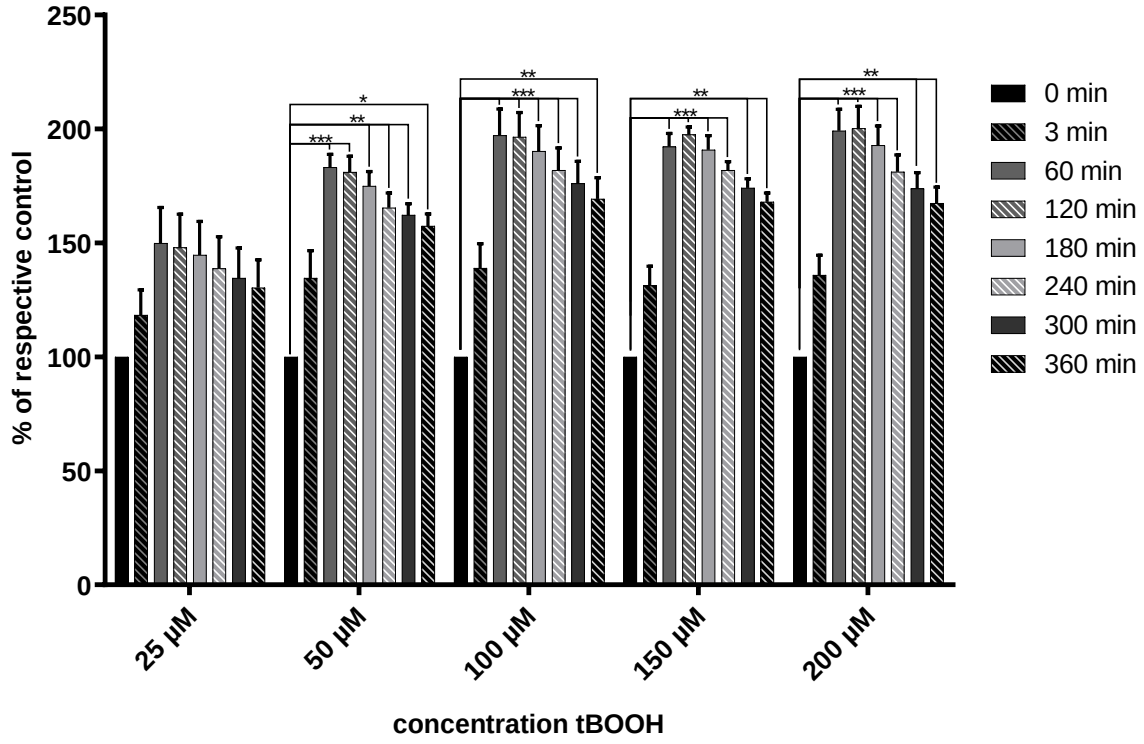

Figure 8 Induction of RO(N)S by *t*BOOH in wild type *C. elegans*. The induction of RO(N)S by *t*BOOH occurs in a concentration- and time-dependent manner. Wild type *C. elegans* were incubated with 25 µM, 50 µM, 100 µM, 150 µM and 200 µM *t*BOOH for up to 6 hours. Significant increases of RO(N)S levels can be seen for 50 µM and above after 1 h or longer incubation. Data are expressed as means ± SEM of at least three independent experiments. Statistical analysis via unpaired t-test. Significance is depicted as *: $p<0.05$, **: $p<0.01$, and ***: $p<0.005$*** vs. control of respective time point 0.

3.3.3 Analysis of cardiolipin oxidation products after treatment with *t*BOOH

After initially examining untreated worms to investigate the CL distribution, *t*BOOH-stressed worms were extracted and analysed. Lipid extraction is a crucial step regarding lipid oxidation. To prevent lipid oxidation during sample preparation, BHT (5 mM) was added as an antioxidant to the sample before extraction. Also all extraction steps were carried out on ice. With this precautionary measures no oxidation products in untreated worms were observed. For this reason, falsification of the results obtained from the sample preparation was avoided. For *t*BOOH treatment three different concentrations (1 mM, 2.5 mM, and 6.5 mM) have been chosen for the experiments, based on previous studies. [41, 67] In contrast to the untreated worms for all three *t*BOOH concentrations, CL oxidation products were identified utilising 2D-LC-HRMS. Based on the shift to lower retention times, the accurate mass and fragmentation experiments oxidation products of

the main CL species CL(80:14), CL(80:15) and CL(80:16) were identified in all treated samples. Besides the main oxidation products, also other oxidation products were observed but not in all replicates. Along with increasing *t*BOOH concentrations we observed higher amounts of oxidation products of CL species containing polyunsaturated fatty acyl moieties. Exclusively mono-oxygenated CL species were detected. While the formation of CL hydroperoxides is often described for artificial oxidation for example by Fenton reaction or cyt c/H_2O_2 [281-283] the finding of mono-oxygenated CL species *in vitro* is usual due to subsequent degradation. [252, 282, 284] However, in order to ensure that BHT does not have any influence of hydroperoxylated CL species we oxidised CL(72:8) of bovine heart by means of Fenton reaction and added 5 mM BHT. After an incubation time of 2 h on ice the samples were analysed. No reduction of the hydroperoxy CL(72:8) species to the corresponding hydroxy species was observed, as for example shown utilising triphenylphosphine. [261]

Figure 9 (A) displays the EICs of the most abundant oxidation products and their origin CL species. By MS/MS fragmentation experiments the structure was confirmed (Figure 9 (B)). In comparison to the fragments shown in Figure 9 (C), fragments based of the oxygenated fatty acid FA (20:4) confirm the oxygenation of the presence of oxidised CL species. Different oxidation products such as hydroxy, hydroperoxy and epoxy species are described in the literature [252, 282]. *t*BOOH triggers the formation of ROS which initially leads to lipid hydroperoxydation. Based on the work of Pope *et al.*, the reduction of hydroperoxides to their corresponding hydroxy species is highly plausible. [252] However, the determination of the location of the hydroxy group was not further pursued. Figure 9 (C) shows the formation of oxidation products depending on the *t*BOOH concentration. With increased concentration an enhanced formation of CL oxidation products was observed. This is especially pronounced in comparison to the non-treated worms. This finding emphasizes the suitability of CL oxidation products as marker for oxidative stress induced by the formation of ROS in the model organism *C. elegans*. In comparison to other oxidative stress markers such as glutathione or isoprostanes, CL oxidation products are specific for oxidation processes in mitochondria. Unintentional oxidation can be avoided utilising BHT or other antioxidants, which also makes it possible to store the samples at for example -70 °C without degradation. Further information with respect to the CL distribution of untreated and *t*BOOH treated worms is provided in Table 3 and Table 4 of the Supporting Information.

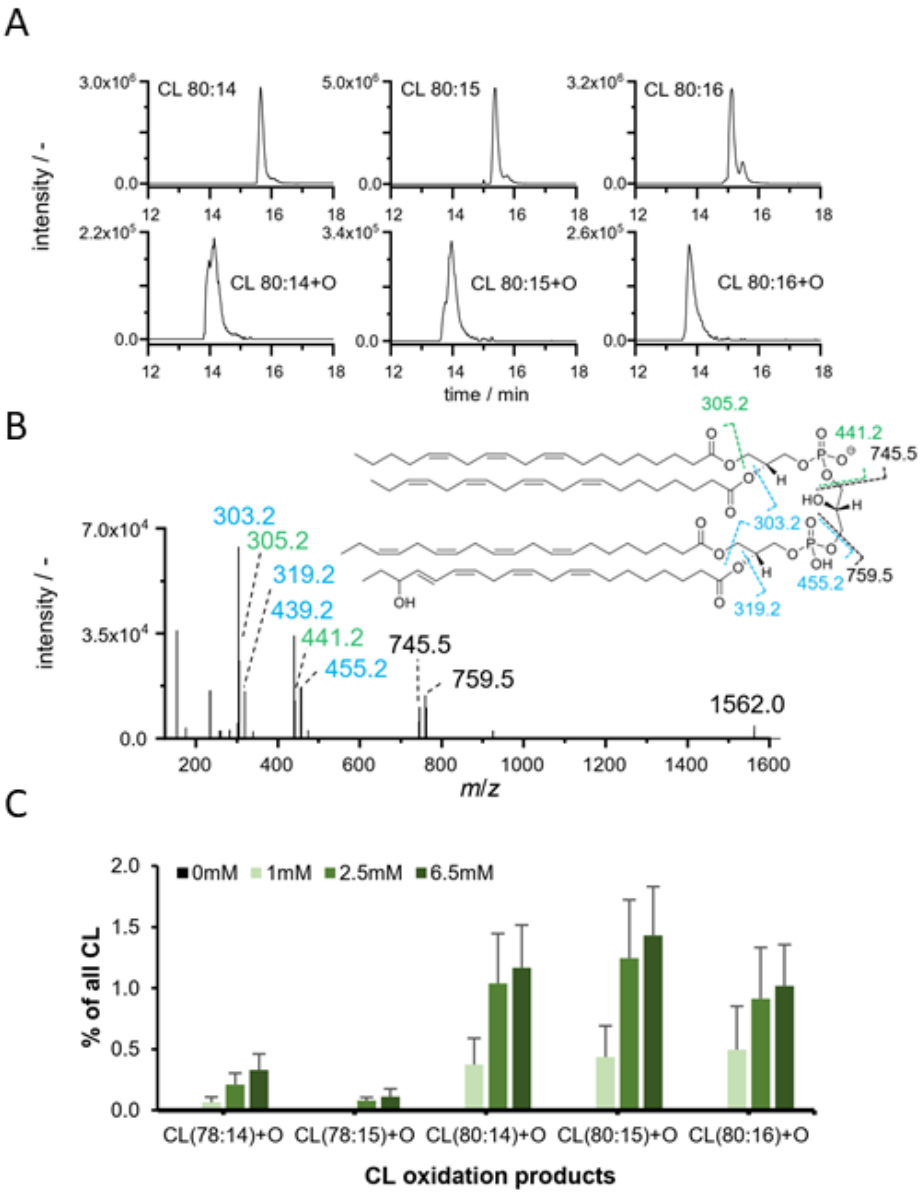

Figure 9: EICs of the main CL species and their oxidation products, fragmentation and distribution exclusively in the *t*BOOH samples. (A) EICs of the main CL species and their oxidation products which were found exclusively in the *t*BOOH samples. The EICs were observed from samples treated with 6.5 mM *t*BOOH. (B) Exemplary presentation of the fragmentation pattern for structural elucidation of CL(80:15)+O by MS/MS. Based on the observed fragments the fatty acyl composition was determined as 20:3_20:4/20:4:1_20:4. The displayed *m/z* values are rounded to one decimal place for better visualisation. (C) Distribution of CL oxidation products based on the total amount of CL in % + SEM, n = 3. For untreated worms no oxidation was observed.

3.3.4 CLox identification as oxidative stress marker in *C. elegans* compared to conventional methods

C. elegans is a multicellular organism and persistent oxidative stress can lead to systemic manifestation of various damaged endpoints. Excessive endogenous and exogenous production of ROS can interfere with macromolecules such as the DNA, proteins, and lipids, which is often associated with ageing-related and neuropathological diseases. [242, 285] It is therefore crucial to ensure reliable measurement of oxidative stress, especially when using a model organism often used for investigations regarding neurodegeneration and aging. Some of the advantages of the described method for use as oxidative stress biomarker have been highlighted in the sections above, but it is crucial to understand the complexity of oxidative stress endpoints when deciding which endpoint is used. In an effort to understand the interaction of ROS, CL peroxidation and mitochondrial disturbance, many studies have been conducted using isolated mitochondria from cell culture experiments, but *in vivo* experiments utilising the model organism *C. elegans* are rare. Various other oxidative stress endpoints can be measured analytically in the nematode, like glutathione levels [41], energy relevant nucleotides [286], or malondialdehyde, being one endpoint used in the worms [287] also involved in the lipid peroxidative chain reaction. To be useful as an oxidative stress indicator, the biomarker must be reasonably stable and present in a quantity that makes reproducible measurements possible and economic. Using the approach of forward genetics it is possible to knock-down/ knock out oxidative stress-relevant genes in the nematode and compare the deletion mutants to wild type worms regarding survival and behaviour [288, 289], but this method does not allow to draw any conclusions regarding the mechanistic pathway. Making use of the transparent body of *C. elegans* it is possible to either stain oxidative stress markers using fluorescent-coupled antibodies or to use transgene nematode strains that show oxidative stress-relevant protein expression by GFP-coupled proteins, such as the gst-4:gfp strain [290]. There are also several other dye methods available, such as DCF or MitoTracker™, which directly or indirectly indicate oxidative stress. All fluorescent-based methods have its advantages in simplicity and visualisation but are lacking in specificity, quantification and reproducibility between different operators as microscopic differences can hardly be overcome. These qualitative methods should always be used in combination with quantitative methods to ensure distinctive measurements between different samples.

Downside to using *C. elegans* as the model organism in analytical approaches is that often large quantities of worms have to be used to ensure sufficient amount of material for measurements. Even though that oxidised CL have a relatively low abundance in the nematodes, the here developed method is sensitive enough to detect small differences in various concentrations of the ROS inducer *t*BOOH. In comparison to a previous published method by Rund *et al.* to measure isoprostanes as oxidative stress marker, 50% less animals can be used (6,000 vs. 12,000) while still ensuring well evaluable results, cutting down cultivation time and costs [67]. Insensitivity of analytical oxidative stress measurement is also often related to a large matrix effects by ion suppression. Using 2D-LC-HRMS based on RP-LC in combination with a pre-separation utilising HILIC in ^{1}D allows the removal of interfering substances and thus avoids co-elution of for example cholesterol-ester and triacylglycerols [259]. The LC-HRMS based analysis of CL oxidation products as marker substances also allows the utilisation of BHT which eliminates artificial ROS production during sample preparation. As can be seen in Section 3.2 control animals do not show any evaluable amounts of CLox pointing to sample preparation that does not artificially produce more oxidative stress. Research during the last years has been increasingly linked to mitochondria disturbance, caused by endogenous and exogenous oxidative stress. CL are crucial for proper mitochondria function, as oxidation leads to the malfunction of complex I and III. CLox identification is therefore a promising endpoint to study in neurodegeneration models. CL are highly sensitive to oxidative damage of its double bonds to the high content of polyunsaturated fatty acids, allowing its identification to be used as an early oxidative stress marker.

3.4 Conclusion

CL are exclusively mitochondrial-bound phospholipids that are highly sensitive to oxidative stress due to their high level of unsaturation. Their activity is directly linked mitochondria activity and oxidation can cause mitochondrial dysfunction and the subsequent failure of additional downstream processes. Still, little is known about the correlation of oxidative stress, CL and neuropathology. Using the nematode *C. elegans*, a recognized model organism for neurodegeneration, we extended the research of CL distribution and its oxidation products to develop a practical method for a sensitive oxidative stress marker, which can be later applied for *C. elegans* research in the field of neurodegeneration. Despite the rising interest in the lipidome of *C. elegans*, so far, the CL

distribution was not precisely described yet. By online two-dimensional liquid chromatography the CL distribution of *C. elegans* was determined on the molecular level. Due to the HILIC pre-separation in the first dimension and the automated transfer of CL and CLox utilising a heart-cut setup, co-eluting lipid species were removed which guaranteed increased sensitivity and selectivity. The identified CL species consist of polyunsaturated fatty acyl moieties with an overall number varying from 7 to 17 double bonds in a CL species. The most abundant species are CL(80:14), CL(80:15) and CL(80:16) consisting fatty acyl moieties of 20 carbon atoms and 3 to 4 double bonds. The high degree of unsaturation correlates with the high potential of CL being targeted by ROS. This in turn leads to the assumption that CL is one of the most sensitive and earliest endpoints of oxidative stress. For this reason, worms were treated with varying concentration of the hydroperoxide *t*BOOH and the presence of CL oxidation products was analysed. Oxidised CL species are of relatively low abundance compared to the main species. However, utilising online 2D-LC-HRMS offers the required selectivity and sensitivity for the analysis and characterization of formed oxidised CL species without the usage of time-consuming sample preparation steps. Further structural elucidation was carried out by means of MS/MS fragmentation experiments. With increasing *t*BOOH concentrations, CL oxidation products increase compared to the non-treated control group. In addition to that, LC-MS based analysis of CL oxidation products might be a new approach for monitoring oxidative stress in the model organism *C. elegans* as demonstrated in this work. As oxidative stress can cause a variety of changes on different endpoints, one must wisely chose which biomarker is useful to monitor and a combination should always be preferred.

3.5 Acknowledgement

The authors thank the Fonds der Chemischen Industrie (FCI, Frankfurt am Main, Germany) for financial support (Ph.D. scholarship for Patrick O. Helmer). We thank the German Research Foundation (DFG) for the financial support (BO 4103/2-1 and INST 211/802-1), as well as the DFG Research Unit TraceAge (FOR 2558). We would also like to thank the *Caenorhabditis* Genetics Center (CGC), which is funded by the NIH Office of Research Infrastructure Programs (P40 OD010440) for providing the *C. elegans* strain used in this work. The authors acknowledge Wen Jiang (HILICON AB, Umeå, Sweden) for providing the iHILIC columns.

3.6 Author Contributions

The results of this chapter are based on a cooperation with Dr. Patrick O. Helmer and Prof. Dr. Heiko Hayen (University of Münster).

Experiments were designed and performed by POH und MMN. VS assisted with experimental execution. Conceptualizing of the study, data analysis and interpretation, and writing of the manuscript were done by POH and MMN. JB and HH contributed to data interpretation, helped with ideas for experimental setup, and revised the manuscript critically for important intellectual content. All authors were involved in compiling the manuscript and approved the final version. J.B and HH rendered this work possible.

Abstract

The identification of genotoxic agents and their potential for genotoxic alterations in an organism is crucial for risk assessment and approval procedures of the chemical and pharmaceutical industry. Classically, testing strategies for DNA or chromosomal damage focus on *in vitro* and *in vivo* (mainly rodent) investigations. In cell culture systems, the alkaline unwinding (AU) assay is one of the well-established methods for detecting the percentage of double-stranded DNA (dsDNA). By establishing a reliable lysis protocol, and further optimization of the AU assay for the model organism *Caenorhabditis elegans (C. elegans),* we provided a new tool for genotoxicity testing in the niche between *in vitro* and rodent experiments. The method is intended to complement existing testing strategies by a multicellular organism, which allows higher predictability of genotoxic potential compared to *in vitro* cell line or bacterial investigations, before utilising *in vivo* (rodent) investigations. This also allows working within the 3R concept (reduction, refinement, and replacement of animal experiments), by reducing and possibly replacing animal testing. Validation with known genotoxic agents (bleomycin (BLM) and *tert*-butyl hydroperoxide (*t*BOOH)) proved the method to be meaningful, reproducible, and feasible for high throughput genotoxicity testing, and especially preliminary screening.

Chapter 4

A Fast and Reliable Method for Monitoring Genomic Instability in the Model Organism *Caenorhabditis elegans*

Based on:

Merle M. Nicolai, Barbara Witt, Andrea Hartwig, Tanja Schwerdtle, Julia Bornhorst, Archives of Toxicology, 2021, Oct;95(10):3417-3424

DOI: 10.1007/s00204-021-03144-7

Highlights

- A fast and reliable method to identify genomic instability in a metabolising organism
- A new tool for genotoxicity testing in the niche between *in vitro* and rodent experiments
- The percentage of double stranded DNA as a marker for genomic stability in *C. elegans*

Keywords

Alkaline unwinding, genomic instability, *Caenorhabditis elegans*

4.1 Introduction

Maintenance of genome integrity is an organism's top priority to ensure a healthy life and successful reproduction of the species [99]. The genomic DNA is under constant attack of extrinsic and intrinsic genotoxic agents which may result in genetic alterations in somatic and/ or germ cells, which in turn might manifest target place-dependent negative outcomes, such as impaired transcription or replication, apoptosis, or necrosis, or fixation to mutation. This potentially will lead to cancer and non-cancer genetic diseases for somatic cells and infertility, heritable damage and intergenerational genetic diseases for germ cells [30, 72-74]. The purpose of genotoxicity testing is to identify such genotoxic agents and their potential for genotoxic alterations. The testing is part of approval procedures and testing strategies of the chemical and pharmaceutical industry, as well as risk assessment of food ingredients. Due to the wide potential spectrum of DNA damages, it is imperative to consider multiple endpoints to systematically assess genotoxicity. As defined in the OECD guidelines, genotoxicity testing includes assays that measure direct, irreversible damage to the DNA that is transmissible to the next generation (i. e. mutagenicity), as well as tests that evaluate directly the induced DNA damage that may or may not result in permanent alterations (and is therefore no direct evidence of mutagenicity) [76]. In both cases *in vitro* and *in vivo* models (mostly rodents) are used and guidelines recommend a test battery starting with testing for gene mutation in bacteria, followed by *in vitro* assays using mammalian cell lines, before recommending an *in vivo* test system [80-82]. Although these tests are routinely used, they present

crucial limitations (i. e. lack of xenobiotic metabolism and bacteria-specific reactions [291], use of tumor cells), which affect the usefulness of the assays to predict the genotoxic potential of a substance *in vivo*. With the emergence of a stronger awareness of animal welfare in scientific experiments, classic and well-established *in vivo* studies are increasingly attempted to be replaced by equally meaningful tests, which follow the 3R (refine, reduce, replace) principle. [292, 293] For this purpose, as well as to overcome present limitations, current efforts include the usage of 3D cell culture models or alternative *in vivo* model organisms. Within this study, the model organism *C. elegans* was applied for genotoxicity testing. The well-established *in vitro* method of DNA alkaline unwinding [9, 10] was optimized for detecting the proportion of dsDNA in *C. elegans* and was verified using validated genotoxins in order to provide a rapid genotoxicity evaluation in a metazoan organism.

4.2 Materials and Methods

4.2.1 Worm cultivation and exposure to positive controls

For assay development, the wild type (WT) N2 Bristol *C. elegans* strain was used, which was provided by the *Caenorhabditis Genetic Center* (CGC; University of Minnesota).

Worms were cultivated on agar plates at 20 °C as described by Brenner, 1974 [256]. After synchronization and hatching, L1 (larval stage 1) worms were seeded on OP50 *E. coli* covered NGM plates until the population reached L4 without further interference. For treatment *t*BOOH and BLM were used as positive controls in ranges of 0 – 5 mM *t*BOOH and 0 – 80 µM BLM for 1 h. BLM sulfate was purchased from Selleckem (NSC125066) and *t*BOOH from Merck (CAS 75-91-2). Both chemicals were used as received and diluted in 85 mM NaCl to the desired concentration. 3000 L4 larvae were incubated in liquid (85 mM NaCl) in the absence of *E. coli* while rotating slowly to ensure equal substance uptake. Afterward, samples were washed at least three times with 85 mM NaCl + 0.01% Tween® before continuing with the survival or alkaline unwinding assay.

4.2.2 Survival

The toxicity of the substances was determined using the survival assay as described previously [143]. After treatment, a specific number of worms were transferred to OP50-

seeded NGM plates. Alive and dead worms were manually counted 24 h post-treatment. The vitality of the animals was checked via the mechanical stimulus of touch using a platinum/zirconium wire, which stimulates the worms to move. Any worms that did not respond to the stimulus were considered dead.

4.2.3 Adapted alkaline unwinding for use in *C. elegans*

After treatment, worms were placed in 1 mL alkaline unwinding buffer (AU buffer; 0.5 M NaH_2PO_4, 0.5 M Na_2HPO_4, 0.1 M EDTA, pH 7.5). To reduce possible additional strand breaks during sample preparation, samples were kept on ice at all times and all experimental steps were performed in the dark. Worms were made assailable for the alkaline solution by using slight sonification and a large liquid volume (UP100H ultrasonic processor (Hielscher), 1 mL AU buffer, 2 x 20 sec on lowest setting, 100% amplitude). After centrifugation (1400 rpm, 2 min, 4 °C) and removal of the supernatant, 1.5 mL alkaline solution (0.9 M NaCl, 10 mM Na_2HPO_4, 0.03 N NaOH in dH_2O) was added to all samples. The DNA was allowed to unwind at RT in the dark for exactly 15 min, before neutralizing the solution with 0.1 N HCl (exact volume was adapted to reach pH 6.8 ± 0.02), sonification on ice (15 sec, highest setting), and adding SDS to a final concentration of 0.05%. The single- and double-stranded DNA were separated by successional elution of 0.15 M and 0.35 M potassium phosphate buffer over 1 mL hydroxyapatite columns at 60 °C. The amount of DNA for the single-stranded DNA (ssDNA) and dsDNA fraction were determined using Hoechst stain (Hoechst 33258 nucleic acid stain) at a final concentration of 7.5 x 10^{-7} M and the fluorescence was measured using a microtiter fluorescence reader (Infinite Pro, Tecan, Switzerland; 360 nm excitation wavelength and 455 nm emission wavelength). As described by Hartwig *et al.* 1993, staining availability of Hoechst was tested, which allowed calculations for dsDNA fraction (Eq. 1) [294]. For this, the fluorescent signals of ssDNA and dsDNA were compared, which yield 0.4 x lower values for dsDNA compared to ssDNA, resulting in the following calculation (Eq 1). Statistical evaluation was performed using Graph Pad Prism 9.

$$dsDNA = \frac{fluorescence\ dsDNA}{fluorescence\ dsDNA + (fluorescence\ ssDNA\ x\ 0.4)} \quad (1)$$

4.3 Results and Discussion

4.3.1 Method development

Alkaline unwinding was initially developed for cell culture systems [294, 295] and is a frequently utilised genotoxicity test, even though it does not belong to the primal OECD genotoxicity tests. Nevertheless, alkaline unwinding is a well-established and rapid assay, which can be categorized as an indicator genotoxicity test [75]. Similar to the alkaline COMET assay (which is (*in vitro*) also not part of the primal OECD genotoxicity tests), using alkaline unwinding one can quantify DNA strand breaks caused by genotoxins via direct interactions with the DNA; alkali labile sites; or as a consequence of transient strand discontinuities resulting from nucleotide- and base excision repair. [76, 296] In principle, the percentage of dsDNA is detected, which serves as a marker for genomic stability. A highly alkaline solution is used to enable the unwinding of the DNA and form ssDNA at sites of single-strand breaks. The quantification of dsDNA and ssDNA allows to draw conclusions regarding the amount of initial DNA single-strand breaks. Compared to the COMET assay, the procedure for alkaline unwinding does not call for isolation of intact cells, which can be complex in *C. elegans*. Despite being published [245], the COMET assay is experimentally demanding, as various cell types are present in worm extracts, background noise/ matrix is high, little comparable data is present and results are challenging to reproduce. For alkaline unwinding, the DNA within the worms needs to be accessible to the alkaline solution, but it is not necessary to isolate intact cells. Lysing the worms is the critical step during this method since it is of crucial importance that DNA damages are not caused by the lysing process itself. We found that gentle sonification (Ultrasonic Processor, UP 100H, 2 x 20 sec, in 1 mL liquid) works better for that purpose than using chemical dissipation of the cuticle (e. g. protein kinase K, pronase E, papain, Triton X-100), breaking of the cuticle with high pressure (French pressure cell press, as used for yeast cell lysis [297]) or slicing worms using syringes as described for germ cell isolation [298]. Except for the gentle sonification, the other methods resulted in additional DNA damage as we detected only very low amounts of dsDNA (data not shown). Making use of transgenic worm stains did not facilitate the workflow in this particular case. The tested *bus-5* deletion mutant (DC19, *bus-5*(br19) X), which presents higher porosity, and therefore higher cuticle permeability for various substances compared to the wild type (N2) strain [299], showed high levels of damage even in non-exposed controls. Mutant strains were therefore discarded as an alternative method for

the lysing process and did not facilitate the accessibility of the alkaline solution. Experiments regarding the optimal incubation time with the alkaline solution can be seen in Figure 10. The unwinding time was reduced from 30 min (used in cell samples) to 15 min as data indicate increased sensitivity of the worm DNA compared to DNA retrieved from cell culture (HepG2, BeWo b30) to the alkaline solution. This finding corresponds to earlier observations in a worm study pointing out that the *C. elegans* genomic DNA was detected to be degraded under alkaline electrophoresis condition used in a classical comet assay [300]. All following steps are identical to the *in vitro* setup (see Figure 11), which was adapted from Hartwig *et al.* 1993 [294]. To keep DNA damage caused by the experimental setup to a minimum, worm samples were prepared in the dark and on ice after the compound treatment process was finished. For calculation of the percentage of dsDNA, the affinity of the Hoechst 33258 dye to dsDNA and ssDNA was tested. In contrast to cell samples, where a factor of 2.1 is present, in dsDNA of worms the binding affinity is reduced by a factor of 0.4 of dsDNA compared to ssDNA. This, and the higher sensitivity of *C. elegans* DNA to the alkaline solution may indicate a slightly different coiling and stability of the DNA, which can also be a reason for the difficulties in the COMET assay, that has also been described by Park *et al.*, as they found increased DNA damage in worms incubated with alkaline solutions at pH 12.3 for 30 min compared to controls [300]. Additionally, both effects collectively may explain the high fluorescence following 30 min unwinding time (Figure 10 (A)). Nevertheless, when adapting the alkaline unwinding to worm DNA, this genotoxicity test proves to be meaningful, reliable, and practicable for high throughput.

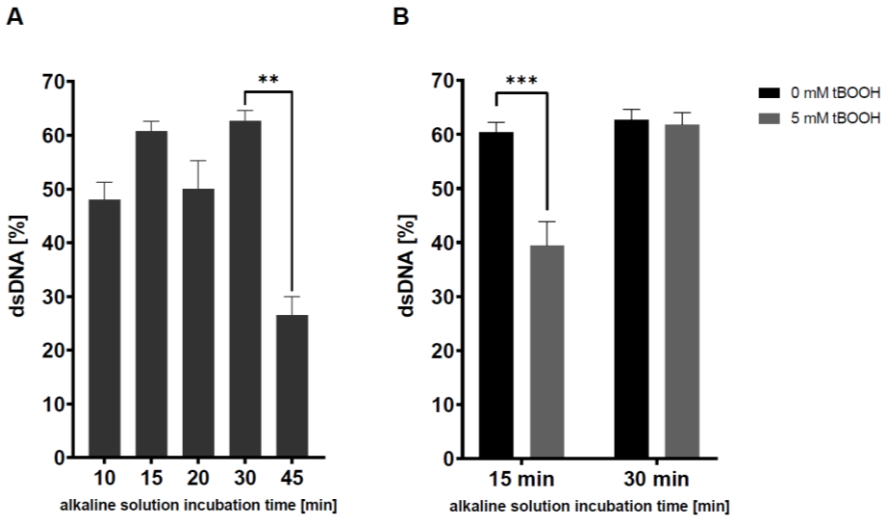

Figure 10 dsDNA [%] to total DNA concentration of *C. elegans* with different incubation times for the alkaline solution. [A] Comparison of percentage of dsDNA to total DNA concentration of *C. elegans* with different incubation times of alkaline solution in control worms. Highest basal levels of dsDNA can be reached when incubating the alkaline solution for 15 min or 30 min. [B] Percentage of dsDNA to total DNA concentration when exposing worms to 5 mM *t*BOOH for 1 h. Significant differences between negative (0 mM *t*BOOH) and positive (5 mM *t*BOOH) controls can only be detected when using the alkaline solution for 15 min. Data are expressed as means ± SEM of at least 6 independent experiments. For statistical analysis, the unpaired t-test was performed. ** $p < 0.01$ *** $p < 0.001$.

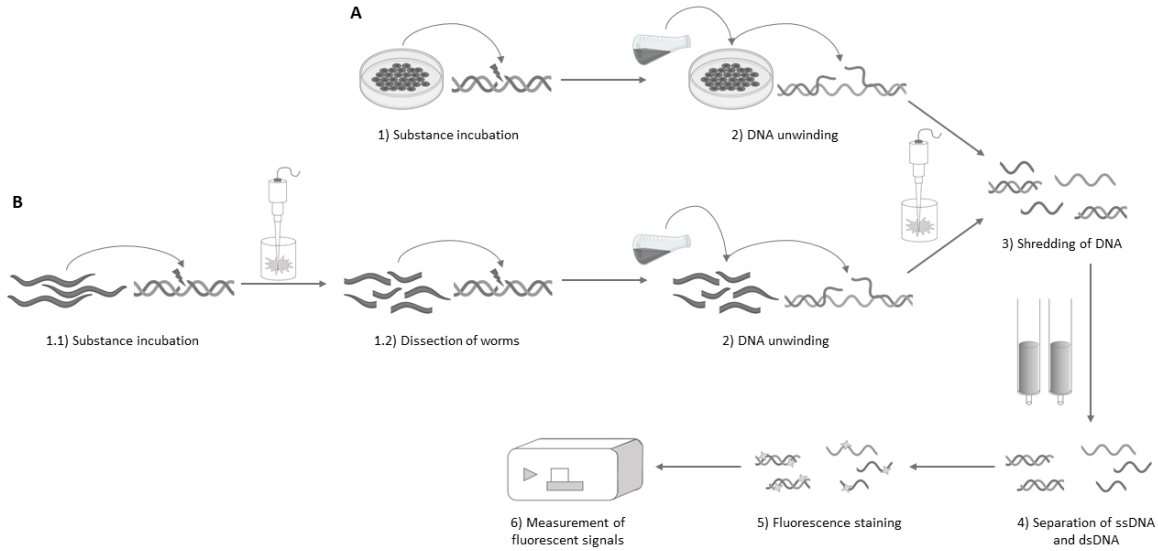

Figure 11 Schematic overview of the experimental setup for alkaline unwinding. Schematic overview of the experimental setup for alkaline unwinding in A) cell culture systems (Hartwig *et. al* [294] and B) *C. elegans* probes. While the alkaline solution can be directly added to exposed cell samples, worms need to be made accessible using an ultrasonic disruptor before adding the alkaline solution. After DNA unwinding, both probes are then sonicated to shred the DNA. Using hydroxyapatite, dsDNA and ssDNA can be separated and finally quantified using fluorescence staining.

4.3.2 Positive controls

For assay evaluation and verification, the positive controls *t*BOOH and BLM were used, as those chemicals are known to induce DNA strand breaks by different modes of action. *t*BOOH is a recognized inducer of oxidative stress and DNA damage in various *in vitro* and *in vivo* models, which is also effective and often applied in *C. elegans* [143, 276, 277]. It is proposed that the oxidant causes the iron-dependent formation of *tert*-butoxyl ($tBO^{\cdot}$) and *tert*-butyl peroxyl ($tBOO^{\cdot}$) radicals, resulting in cellular redox imbalance associated with lipid peroxidation, Ca^{2+}-dependent DNA cleavage, and apoptosis [301-303]. BLM is applied as an anti-cancer antibiotic. In comparison to *t*BOOH, BLM directly affects the DNA by causing athymic sites leading to single strand splitting [304]. Worms were incubated with both substances at sub-toxic concentrations for 1 h, which were determined in earlier studies [41] or survival assays (Figure 12). As expected, a highly significant and dose-dependent reduction of dsDNA is caused by exposing worms to *t*BOOH. Incubation of the substance of concentrations higher than the LD_{25} (2.5 mM *t*BOOH for 1h [41]), does not show any stronger effects, as the results show a maximum decrease of ~ 50% at this point (Figure 13 (A)). Exposure of *C. elegans* to BLM does also lead to a dose-dependent significant induction of strand breaks and resulting decrease of dsDNA at 20 µM and 40 µM BLM (≤ LD_{25}) compared to non-incubated control samples (Figure 13 (B)).

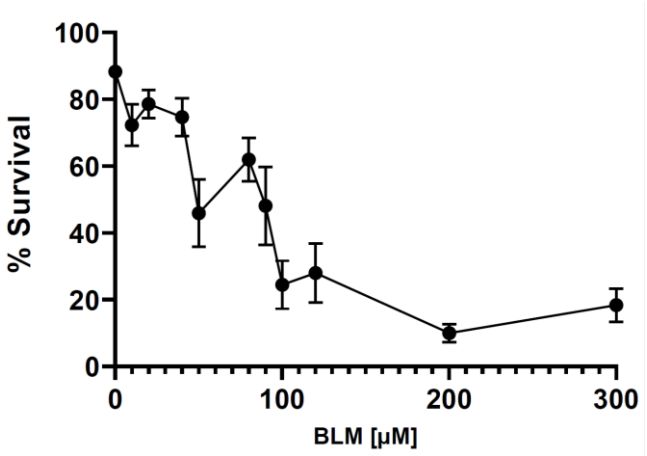

Figure 12 Survival of *C. elegans* (WT) treated with BLM for 1 h. Percentage of survival after treatment with BLM for 1 h in a concentration range of 0 – 300 µM BLM. Survival of worms was quantified 24 h after exposure. Data are expressed as means ± SEM of at least 3 independent experiments.

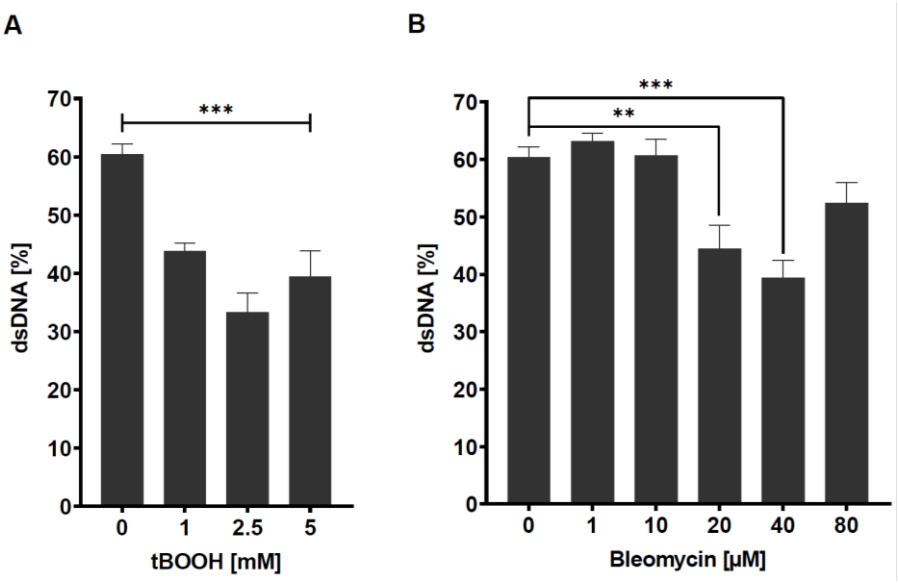

Figure 13 dsDNA [%] to total DNA concentration of *C. elegans* treated with *t*BOOH or BLM. Percentage of dsDNA to total DNA concentration of *C. elegans* treated with *t*BOOH [A] or BLM [B] for 1 h. Data are expressed as means ± SEM of at least 3 independent experiments. For statistical analysis, the unpaired t-test was performed. ** $p < 0.01$ *** $p < 0.001$.

4.3.3 Advantages of the model organism and alkaline unwinding compared to other genotoxicity tests

Factors that contribute to the genotoxicity potential of a compound on an organism are complex and often intertwined. Polymorphisms, age, gender, metabolic-enzyme expression, and lifestyle are a few examples that contribute to the vulnerability of an organism [305]. While most of these attributes can be modelled in rodent experiments, they are not preferentially used for first screenings and indicator tests due to high time and cost intensity. Bacteria assays and cell culture systems are often used for initial investigations as they are less expensive and ethically acceptable for broad-spectrum screening. Prokaryotes and eukaryotes have developed complex biochemical responses to DNA damage that activate numerous processes like activation of repair mechanisms, transient cell cycle arrests, transcriptional upregulation of response proteins, and in metazoans apoptosis as the last resort. Considering that the DNA damage response and DNA damage checkpoints in higher eukaryotes are more complicated than those found in prokaryotes or unicellular eukaryotes, an easily accessible metazoan model organism is required to study the more complex aspects of genotoxicity [207]. The use of *C. elegans* is a valuable addition to genotoxicity assessment, as the nematode can be used as model

organism for follow-up studies of *in vitro* testing and thus can improve the predictability for a possible genotoxic potential of a substance or treatment. With better predictability of genotoxicity, it would be possible to avoid unnecessary *in vivo* follow-up testing (and therefore replacement and reduction of animal testing). Genotoxicity testing in *C. elegans* is slowly getting more recognized, but validated methods are scarce. Besides the comet assay and rad-51 immunohistochemistry staining, very little is published for direct measurements of DNA damage in this model, and therefore a great need for additional, valid methods persists [245, 300, 306]. Detecting the compound-induced genomic instability by the alkaline unwinding method in worms can be useful for a) preliminary screening (high throughput), b) as follow up test of an *in vitro* positive result, c) for mechanistic studies (the xenobiotic metabolism is highly conserved in *C. elegans*) and d) exposure marker demonstrating that a substance is affecting the genomic stability. We are fully aware that the worm is a model organism with limitations, but it might provide a valuable addition to already existing strategies. The nematode is a multicellular and metabolising organism, which is not given in cell lines or bacteria cultures (as used for the Ames test), where a metabolic activation system in form of liver-derived enzymes has to be additionally added via S9 fraction [307]. Additionally, the worm has a rapid life cycle and short generation time which will allow high throughput testing [308, 309]. Most of the pathways involved in genomic integrity that are known through studies of bacteria, yeast, mammals, and human cell lines are also highly conserved in *C. elegans*, which makes the worm an experimental model greatly suited for research on processes involved in genomic stability [310, 311].

4.4 Limitations, Opportunities, and Future Directions

For method development, L4 larvae were chosen since they bear a fully developed DNA repair system but are not yet reproducing. Additionally, incubation of the positive controls was conducted in the absence of *E.coli* to avoid bacterial interferences. The two positive controls *t*BOOH and BLM were used as proof of principle for the AU assay in *C. elegans*. Both substances are validated DNA damage inducers (directly and indirectly) and no bioactivation is required for either of the substances. However, many other xenobiotics show only a genotoxic potential after being metabolised. Common examples are benzo[a]pyrene (BaP) and nitrosamines [312-314]. The great advantage of the nematode compared to *in vitro* models is that the toxicodynamic pathways (phase I + II

metabolism) needed for bioactivation are relatively similar to higher eukaryotes [315]. Phase I metabolising enzymes are necessary for the oxidation, reduction, and hydrolysis of xenobiotics and are broadly expressed in somatic cells of *C. elegans*. Over 85 cytochrome P450 isoforms have been identified in the nematode (compared to ~ 60 in humans) and many have been associated with xenobiotic metabolism [316]. Investigating substances that might only show their genotoxic potential after bioactivation is therefore very well possible in the nematode, but one must be aware of the differences that do exist between worms and mammals. For example, cytochrome P450 requires a heme cofactor and the coenzyme cytochrome P450 reductase. While *emb-8* is the worm´s homolog to the human P450 reductase, worms are not able to synthesize heme and need to scavenge this component from their diet [317]. Another metabolic difference can be found in the bioactivation of BaP, which causes the production of ROS and DNA adducts. In rodents and humans, BaP is predominantly metabolised by CYP1A1 leading ultimately to BaP-7,8-dihydrodiol-9,10-epoxide. While CYP1 enzymes do not exist in nematodes, studies still show the existence of DNA strand breaks in worms after BaP exposure, indicating a genotoxic potential of BaP caused by an alternative pathway of bioactivation [245, 318]. An additional challenge of utilising *C. elegans* for investigations regarding genomic stability is the current lack of data regarding enzyme activity, not only from metabolising enzymes but also enzymes that are involved in DNA repair – making research in this area even more important.

The optimized and with acute genotoxins validated method provides a rapid genotoxicity evaluation in the model *C. elegans.* In future studies, the scope of the application will be extended to the investigations of known substances which are genotoxic upon metabolic activation, as well as being applied more chronic exposure scenarios.

4.5 Acknowledgement

We thank Vanessa Brinkmann and Gerhard Fritz (Heinrich Heine University Düsseldorf, Medical Faculty, Institute of Toxicology) for valuable contributions to the here presented work. The N2 (WT) and DC19 *C. elegans* strains were provided by the CGC, which is funded by NIH Office Research Infrastructure Programs (P40 oD010440). We further thank the German Research Foundation (DFG) (Research Unit TraceAge (FOR 2558)).

4.6 Author Contribution

Experiments were designed and performed by MMN. Data analysis and interpretation were also done by MMN. JB and MMN wrote the manuscript. BW, AH and TS contributed to data interpretation, helped with ideas for experimental setup and revised the manuscript critically for important intellectual content. All authors were involved in compiling the manuscript and approved the final version. JB rendered this work possible.

Abstract

Although manganese (Mn) is an essential trace element, overexposure is associated with Mn-induced toxicity and neurological dysfunction. Even though Mn-induced oxidative stress is discussed extensively, neither the underlying mechanisms of the potential consequences of Mn-induced oxidative stress on DNA damage and DNA repair, nor the possibly resulting toxicity are characterized yet. In this study, we use the model organism *Caenorhabditis elegans* to investigate the mode of action of Mn toxicity, focusing on genomic integrity by means of DNA damage and DNA damage response. Experiments were conducted to analyze Mn bioavailability, lethality, and induction of DNA damage. Different deletion mutant strains were then used to investigate the role of base excision repair (BER) and dePARylation (DNA damage response) proteins in Mn-induced toxicity. The results indicate a dose- and time-dependent uptake of Mn, resulting in increased lethality. Excessive exposure to Mn decreases genomic integrity and activates BER. Altogether, this study characterizes the consequences of Mn exposure on genomic integrity and therefore broadens the molecular understanding of pathways underlying Mn-induced toxicity. Additionally, studying the basal poly(ADP-ribosylation) (PARylation) of worms lacking poly(ADP-ribose) glycohydrolase (PARG) *parg-1* or *parg-2* (two orthologue of PARG), indicates that *parg-1* accounts for most of the glycohydrolase activity in worms.

Chapter 5

Effects of Manganese on Genomic Integrity in the Multicellular Model Organism *Caenorhabditis elegans*

Based on:

Merle M. Nicolai, Ann-Kathrin Weishaupt, Jessica Baesler, Vanessa Brinkmann, Anna Wellenberg, Nicola Winkelbeiner, Anna Gremme, Michael Aschner, Gerhard Fritz, Tanja Schwerdtle and Julia Bornhorst, International Journal of Molecular Sciences, 2021. Oct. 22(20), 10905

DOI: 10.3390/ijms222010905

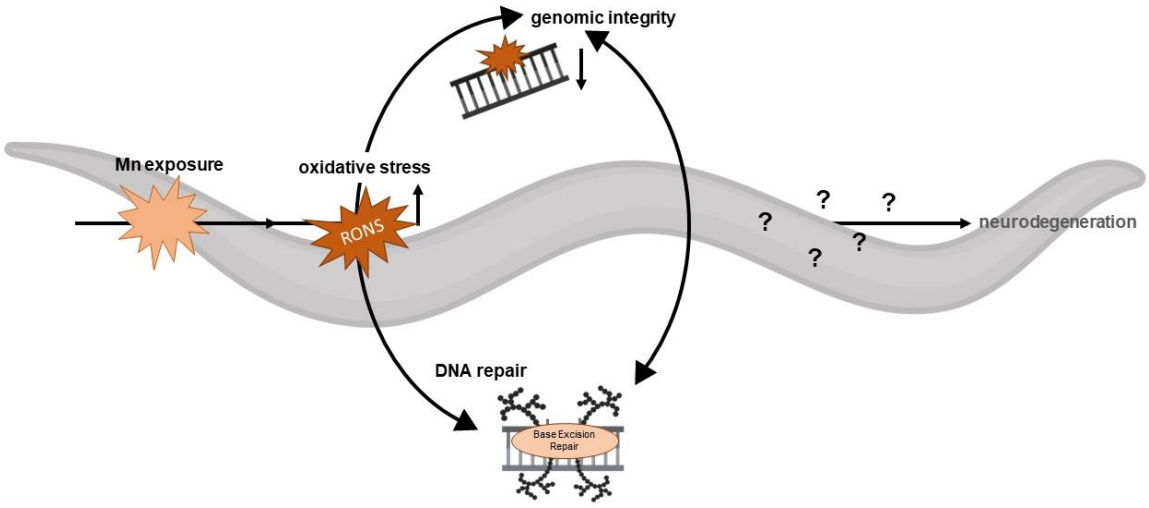

Figure 14 Graphical Abstract: Effects of manganese on genomic integrity in the multicellular model organism *Caenorhabditis elegans*.

Keywords

Manganese, oxidative stress, DNA repair, DNA damage response, *Caenorhabditis elegans*

5.1 Introduction

Exposure to the transition metal and essential trace element manganese (Mn) occurs both naturally and anthropogenically. Natural sources of Mn are diverse and ubiquitous with Mn being the 12th most abundant element in the earth´s crust. Mn does not usually exist in its elemental form, but is found as silicates, carbonates, and oxides [132]. The element can exist in several oxidative states, with Mn(II) and Mn(III) being the most common forms in biological systems [319]. Due to the rich natural occurrence of Mn in vegetables, cereal products, and drinking water, the adequate intake of 3 mg/day for adults is generally met [1]. Therefore, Mn deficiency has not been observed in humans [165]. Continuous scientific progress and rising industrial processes have led to increased release of Mn into the environment, which causes short- and long-term environmental and health risks [141]. Although the essential trace element is needed as a component for several enzyme systems [131, 320], overexposure is associated with various toxicity endpoints in humans [321]. For the general population, chronic overexposure due to

contaminated drinking water or food is of the greatest concern. Bioaccumulation of the metal can further increase the Mn concentration in specific regions or food items. An example is the significant bio-concentration of Mn in water by aquatic biota, which are taken up by marine and freshwater plants, phytoplankton, aquatic invertebrates, and finally fish [141]. In addition to natural sources, emission from mining, Mn alloy, production, welding, coke oven, dry battery manufacturing, Mn salt production, gasoline additive (MMT), and Mn-containing agrochemicals increase regional soil and water Mn concentrations to new extreme levels [132, 166]. Currently, South Africa, Russia, Gabon, Australia, and Brazil have the richest deposits for Mn [141]. High concentrations of inhaled Mn, mostly in an occupational setting, cause acute toxicity in the respiratory system. Even higher nutritional Mn exposure arises from long-term parenteral nutrition therapy [322, 323] or in formula-fed infants [150, 324].

Mn overexposure is associated with neurodegeneration and can have a negative impact on movement, cognition, emotion, and behavioural responses [140, 167]. Recently, several epidemiological studies have indicated an association between environmental exposure to Mn and neurological effects in children and adults. It has been observed that Mn accumulates in the dopamine-rich region of the basal ganglia, causing dopaminergic neurodegeneration [13, 161, 162]. In fact, *in vivo* extrapolations suggest a 1 – 5-fold increase in the Mn concentration in this region of the human brain under occupational exposure, causing dopaminergic neurodegeneration [325, 326]. Animal models have been used extensively to study the pathobiology of neurotoxicity by applying translationally human-relevant Mn concentrations [221]. Additionally, *in vitro* models have been used to understand Mn uptake, homeostasis, and toxicity to single cell lines. However, effective concentrations are not comparable between different cell lines and are not capable of reflecting the situation in a whole (human) organism. Despite the published investigations, little is known about the underlying mechanisms of neurodegeneration. A proposed mechanism for the pathological changes and symptoms of Mn overexposure is the induction of oxidative stress [183]. Excessive production of reactive oxygen and nitrogen species (RONS), either directly via a Fenton-like reaction or indirectly by inhibiting the respiratory chain in mitochondria, leads to increased interactions with macromolecules such as DNA [179]. Recent evidence from *in vitro* studies suggests that Mn may damage the DNA or disturb cellular DNA damage response pathways under conditions of either overload due to high exposure or disturbed homeostasis [10]. The

resulting DNA damage in combination with an insufficient DNA repair system might contribute to the neurological dysfunction [41, 186]. However, the results regarding the genotoxic potential of Mn are inconsistent and further studies are needed to clarify whether Mn species are genotoxic. The soil-dwelling nematode *Caenorhabditis elegans* (*C. elegans*) is a well-established model organism used for investigating developmental biology, aging, neurobiology, and genetic toxicology, as well as toxicity testing. 60 – 80% of *C. elegans* genes have human homologs and most DNA repair pathways found in mammals are conserved in the worm [309, 315, 327, 328]. Easy genetic manipulation and the short life cycle allow us to use forward genetics to gain knowledge about specific genes involved in the DNA damage response. Accordingly, this study was conducted to address these open questions in an *in vivo* model organism to gain further insight into the underlying mechanisms of Mn-induced adverse effects, focusing on genomic integrity by means of DNA damage and DNA damage response.

5.2 Results and Discussion

5.2.1 Excessive Mn exposure causes concentration- and time-dependent increase of Mn content and lethality

To investigate Mn uptake after acute Mn exposure, L4 *C. elegans* wild types were incubated with $MnCl_2$ both for 1 h and 4 h at various concentrations between 0 mM – 250 mM $MnCl_2$ or 0 – 60 mM $MnCl_2$, respectively. The results presented in Figure 15 indicate dose- and time-dependent uptake of Mn that inversely correlates with the survival rate of the worms. Nematodes incubated with 250 mM $MnCl_2$ for 1 h show a total Mn content of ~4.7 ng Mn/µg protein (Figure 15 (A)). N2 (WT) exposed to $MnCl_2$ for 4 h reach similar total body concentrations at 60 mM $MnCl_2$ (approximately $1/4^{th}$ of the corresponding concentration for 1 h) (Figure 15 (B)). Lethality increases at 100 mM $MnCl_2$ (1 h) and above, reaching an approximated LD_{50} at 200 mM $MnCl_2$ for 1 h. Lethality testing after 4 h exposure indicates an LD_{50} value of ~50 mM $MnCl_2$. Similar lethality results were already seen by Neumann *et al.* [41] where the dosing regime was comparable, whereby small varieties might be caused by different laboratory settings [221]. All further experiments were conducted with nematodes exposed to $MnCl_2$ at sub-toxic to toxic concentrations (in detail: up to 250 mM $MnCl_2$ for 1 h (survival 37 ± 6%); up to 60 mM $MnCl_2$ for 4 h (survival 40 ± 4%)), as genotoxic chemicals are expected to induce decreased

genomic integrity at doses that do not trigger extensive cell death and might follow a non-linear dose-response relationship in genotoxicity testing [329, 330].

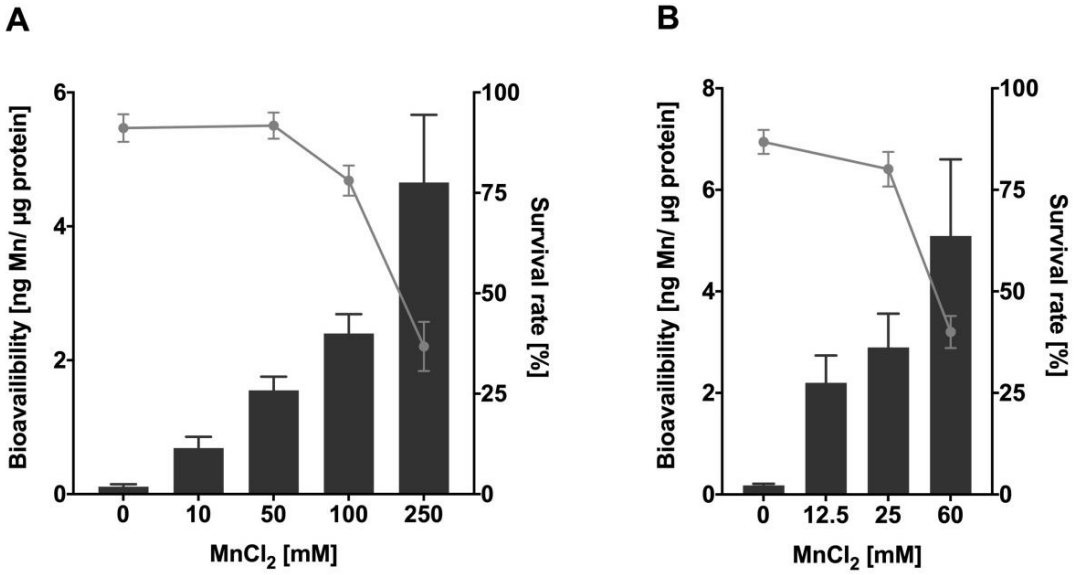

Figure 15 Mn bioavailability and lethality of N2 (WT) after 1 h and 4 h Mn overexposure. Results show dose- and time-depending survival curves [%] and concentration-dependent Mn uptake [ng Mn/ µg protein] of L4 stage N2 (WT) following [A] 1 h and [B] 4 h $MnCl_2$ exposure. Survival of worms was quantified 24 h after exposure and bioavailability was measured analytically via ICP-OES. Data are expressed as means ± SEM of at least four independent experiments.

5.2.2 Mn causes a decrease in genomic integrity and the formation of oxidative DNA damage at sub-toxic and toxic concentrations

Mn-induced toxicity is implicated to be mediated by induction of oxidative stress [331, 332], which can cause increased interactions of RONS with macromolecules such as DNA [7, 333]. Oxidative DNA damage is one of the main mutagenic events in germline cells and genomic integrity is especially important as *C. elegans* germline is the site of cell mitosis, meiosis, and oocyte maturation [334-336]. Nevertheless, genomic integrity is equally important in post-mitotic cells, which are found outside of the mature nematode´s germline and are irreversibly withdrawn from the cell cycle [337, 338]. We decided to investigate the DNA damage in total worms, therefore looking into global effects of Mn on the organism´s genome without differentiating between cell types or tissues, especially, since post-mitotic cells incur DNA damage over a protracted time [338]. As our studies show that the bioavailability at LD_{50} values for 1 h and 4 h was proportional to time and concentration (Figure 15), we decided to focus on the investigation of DNA

damage after 1 h $MnCl_2$ exposure. Previous studies also showed that 1 h Mn exposure already causes adverse outcomes for various oxidative stress endpoints in *C. elegans*, suggesting that this exposure scenario could also lead to DNA damage [41]. Initially, we focused on quantifying DNA strand breaks, which are caused directly by exogenous or endogenous sources or resulting as DNA repair intermediate and can cause loss of information and mutations, DNA-protein crosslinks, and can also have strong effects on the secondary DNA structure [127-129]. For quantification, the alkaline unwinding method was utilised, which uses the percentage of dsDNA out of total DNA as a marker for genomic integrity. DNA strand breaks provoke DNA strands to unwind at those sites in an alkaline environment, leading to a decrease of dsDNA. Results of the alkaline unwinding assay show a significant dose-dependent decrease of the percentage of dsDNA after 1 h Mn exposure, starting at sub-toxic concentrations (50 mM $MnCl_2$) (Figure 16 (A)). At 250 mM $MnCl_2$ dsDNA is reduced from 60% to 40%, indicating an increase of DNA strand breaks and a decrease of genomic integrity. DNA strand breaks have multiple upstream causes, one source may be oxidative DNA modifications or apurinic/ apyrimidinic (AP) sites formed during DNA repair [7, 118].

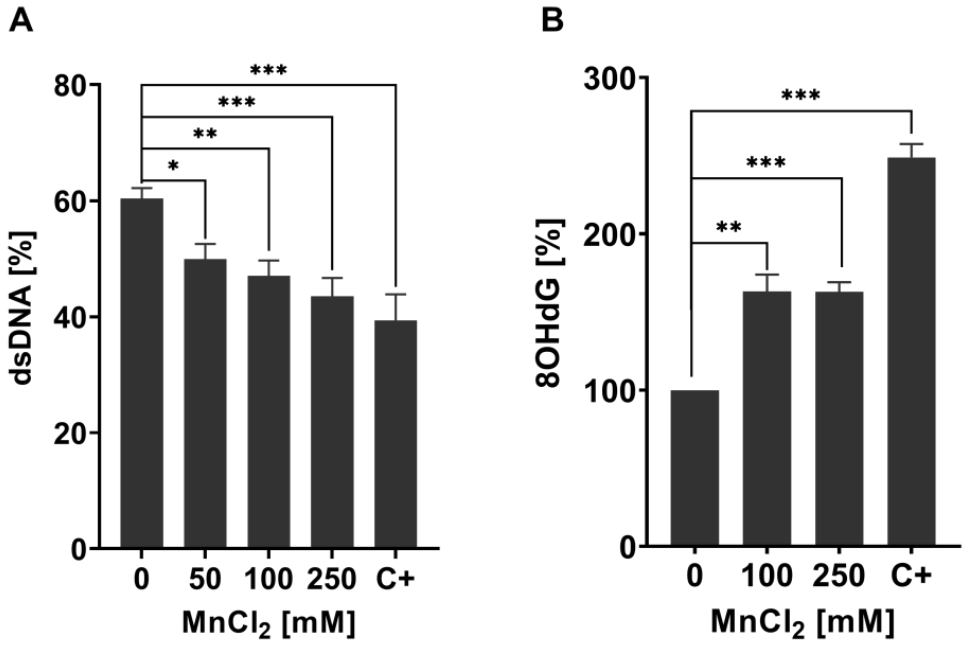

Figure 16 Changes in genomic stability-related markers in Mn exposed N2 (WT) *C. elegans*. Changes in genomic stability-related markers in Mn exposed N2 (WT) *C. elegans*. [A] Percentage of dsDNA to total DNA concentration of N2 (WT) *C. elegans* treated with $MnCl_2$ for 1 h. 40 µM Bleomycin for 1 h was used as the positive control (C+). [B] Relative 8OHdG levels of N2 (WT) exposed to 100 mM and 250 mM $MnCl_2$ for 1 h. 6.5 mM *t*BOOH was used as positive control (C+). Data are expressed as means ± SEM of at least three independent experiments. For statistical analysis, the unpaired t-test was performed.

Oxidative DNA modifications (and also other base modifications) are repaired via BER (see Figure 17). The damaged base is, in both mammals and worms, excised by glycosylases, leaving AP sites, which are then processed further to DNA single-strand breaks by endonucleases before being repaired by further BER repair enzymes [311, 339, 340]. To investigate the origin of DNA strand breaks and potential RONS-induced oxidative DNA damage after Mn exposure, 8OHdG was measured utilising the OxiSelect™ Oxidative DNA Damage ELISA kit. Guanine is likely the most intensely investigated DNA base for oxidative DNA damage, as its low oxidation potential makes it particularly susceptible to incur RONS-induced damage [92, 341]. The interaction of singlet oxygen with guanine leads to the formation of 8-oxo-7,8-dihydroguanine (8oxodG) and 8OHdG, which are in equilibrium with each other and are equally used as biomarkers in both *in vitro* and *in vivo* studies [342]. The base modification disrupts cellular functions by altering protein-DNA binding and the DNA secondary structure, which can cause changes in genome stability, gene regulation, and telomere protection [88, 90, 343, 344]. 8OHdG was shown to be a reliable oxidative DNA damage marker in nematodes, proven by Ahn *et al.* [345]. Here, silver nanoparticles caused an increase of the base modification, demonstrating that 8OHdG formation also occurs in *C. elegans* under oxidative stress conditions. The method, as applied by Ahn *et al.* [345], was improved by quantifying the content of dC and a respective isotopically labelled IS (dC-IS) after hydrolysis using HPLC-MS/MS. This allowed normalization to the respective hydrolysis rate as well as the actual DNA content. A significant increase in damage was induced by a 1 h Mn exposure to 100 mM and 250 mM $MnCl_2$ (Figure 16 (B)). Differences between those two doses were not detectable. These findings of decreased genomic integrity (increase of DNA strand breaks and oxidatively modified DNA bases) caused by Mn are in line with studies performed in neuroblastoma cells (SH-SY5Y) [9] and further corroborate the results of Yang *et al.* [346], which show that Mn induces increased levels of 8OHdG in the striatum of mice. Other investigations in mammals and (neuronal) cell lines come to the same conclusion [10, 338], but studies performed by Sava *et al.* and Oikawa *et al.*, suggested that Mn causes an increase of 8oxodG levels of neuronal cells (PK-12), but only if co-incubated with dopamine or melanin [11, 347]. Another *in vitro* study was performed on Mn-toxicity resistant cells (SCOV-3 clones) and showed that these cells have an increased ability of DNA repair, by means of enhanced PARP and AP endonuclease activity compared to the non-resistant original cell line. This indicates that

formation of Mn-induced DNA damage is compensated by the higher DNA repair levels of those cells [348].

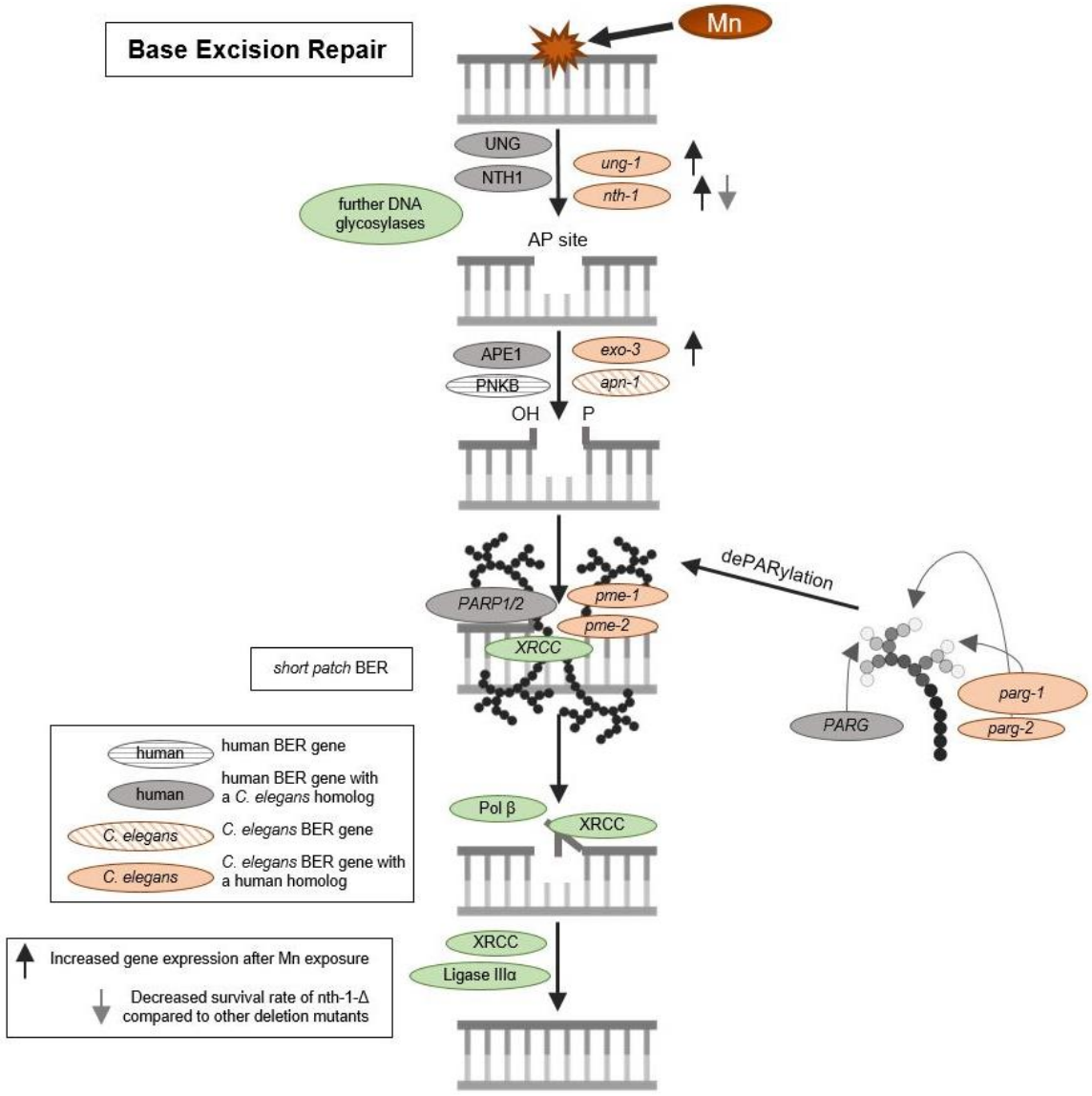

Figure 17 Schematic overview of base excision repair and DNA damage response. Schematic overview of base excision repair and DNA damage response. BER is initiated by DNA N-glycosylases, which cleave the glycosylic bond linking the altered (oxidised pyrimidic) base and the deoxyribose, resulting in AP site formation. AP-endonucleases will then remove the base-free deoxyribosylphosphate. The resulting single nucleotide gap can be filled either by short patch BER or long patch BER. In the case of short patch BER, the single-nucleotide gap is simply filled and ligated by DNA polymerase β and DNA ligase. If long patch BER occurs, polymerase δ or ε will replace part of the damaged DNA strand beyond the gap by extending the 3´strand. A flap endonuclease will then remove the displaced DNA strand and the remaining nick will be ligated by a DNA ligase III. PARylation facilitates the recruitment of XRCC and other BER enzymes and PAR chains are removed again by PARGs.

5.2.3 Increased Mn-caused DNA damage does not lead to the formation of apoptotic bodies

We then proceeded to examine if those doses of Mn causing increased lethality and genotoxic events, also lead to the formation of apoptotic bodies in the N2 (WT). Surprisingly, acridine orange staining showed no induction in the formation of apoptotic bodies with incubations of 50 mM, 100 mM, or 250 mM $MnCl_2$ for 1 h (Figure 18). This suggests that other cell death pathways lead to the increased lethality after Mn overexposure. 200 J/m^2 UV-C was used as the positive control and induced apoptosis as anticipated.

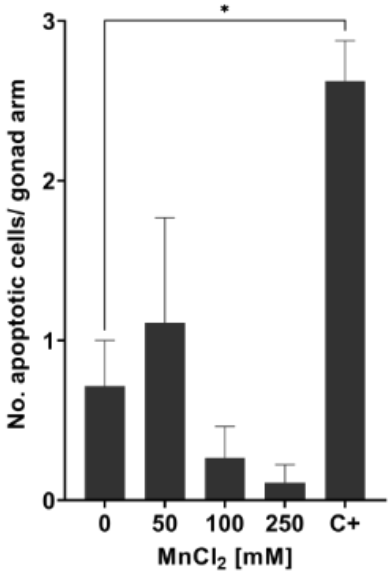

Figure 18 Measurement of apoptotic bodies in N2 (WT) *C. elegans* using acridine orange staining. The number of apoptotic cells per gonad arm was determined 24 hours after treating wild type *C. elegans* with $MnCl_2$ at sub-toxic and toxic concentrations. 200 J/m^2 UV-C radiation was used as positive control (C+). Data are expressed as means ± SEM of two independent experiments, with ≥ 10 worms per sample. For statistical analysis, the unpaired t-test was performed.

5.2.3 Gene expression studies indicate activation of BER after Mn exposure in addition to slight modification of AP site incision activity

DNA damage caused by Mn-induced oxidative stress may further trigger an induction or dysregulation of DNA repair pathways. BER is the main pathway of DNA repair of oxidative DNA damage in mammals [349], and most likely also in *C. elegans* [311]. The repair pathway is highly conserved in the nematode and functional homologs exist for

most repair enzymes (see Figure 17). After 1 h exposure, gene expression studies showed a significant increase in the uracil-glycosylase *ung-1* (homolog to human UNG) and AP-endonuclease *exo-3* (homolog to human APE1) at 100 mM and 250 mM $MnCl_2$ compared to non-exposed worms (Figure 19). The 4 h incubation with 25 mM and 60 mM $MnCl_2$ caused a significant increase in gene expression of *ung-1*, the N-glycosylase *nth-1* (homolog to human NTH1), and *exo-3*, which all act in the initiation of the BER. While in mammals, NTH1 is responsible for the detection and removal of oxidised pyrimidines, it is assumed that the *C. elegans* homolog *nth-1* can also detect and remove oxidised purines, such as 8OHdG. A homolog for the glycosylase OGG1, that removes 8OHdG in mammals, is lacking in *C. elegans* [350, 351].

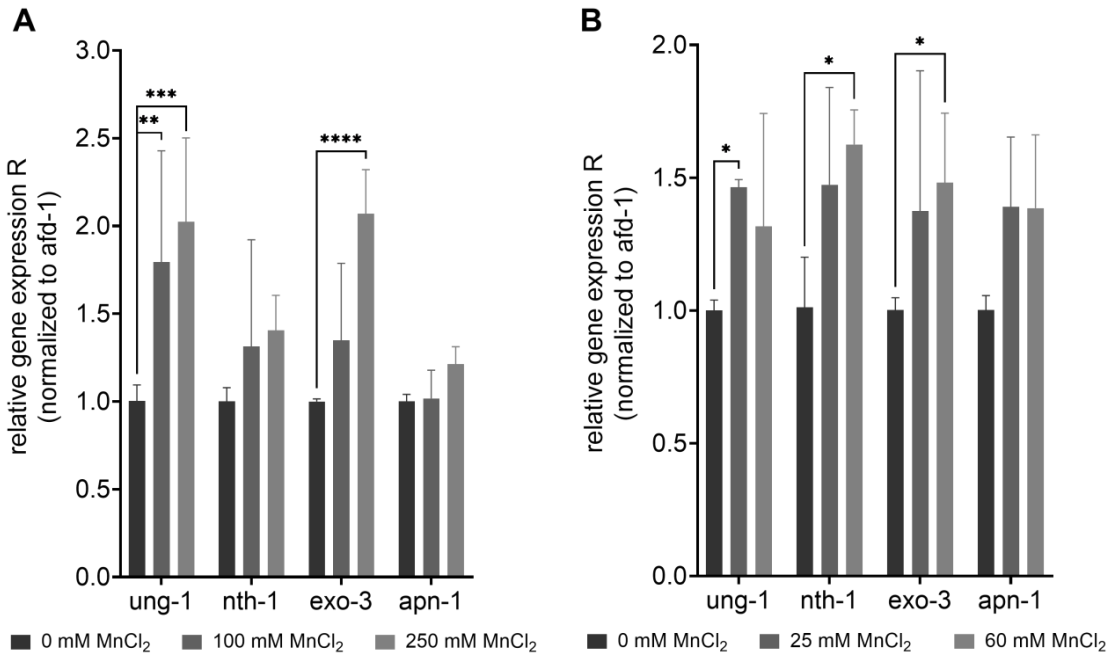

Figure 19 Increase of gene expression of BER-involved genes after excessive $MnCl_2$ exposure. N2 (WT) were exposed to $MnCl_2$ for [A] 1 h (0 mM, 100 mM, and 250 mM) and [B] 4 h (0 mM, 25 mM, and 60 mM) and the relative gene expression of *ung-1*, *nth-1*, *exo-3* and *apn-1* compared to non-treated worms was analysed. Data are expressed as means ± SEM of four independent experiments. For statistical analysis, the 2way ANOVA with Tukey´s multiple comparisons test was performed.

The incision activity assay was applied to study the effect of Mn on the capacity to incise AP sites after excessive exposure to the trace element. No significant changes were observed after 1 h Mn exposure with doses of 50 mM, 100 mM, or 250 mM $MnCl_2$ (Figure 20 (A)). After the 4 h incubation with Mn, at the highest concentration (60 mM

$MnCl_2$) incision activity towards the AP site containing oligonucleotide was significantly reduced (63% ± 7.5%) compared to non-exposed N2 (WT) (Figure 20 (B)). Olaparib was used as positive control. In general, not much data regarding DNA repair after Mn exposure is published, especially when looking into incision activity of nematodes. While BER incision activity was measured in mice with varying trace element status [352], the effect of Mn alone on DNA repair efficiency has yet to be studied. Other studies focus on the sensitivity of different BER deficient species/ cells towards Mn, but not the adverse consequences of Mn on DNA repair (e.g. [353]). Further research is therefore called for, especially considering the importance of BER in post-mitotic cells like neurons [338]. A failure of DNA damage in those cells might be associated with neurodegeneration after genotoxic events.

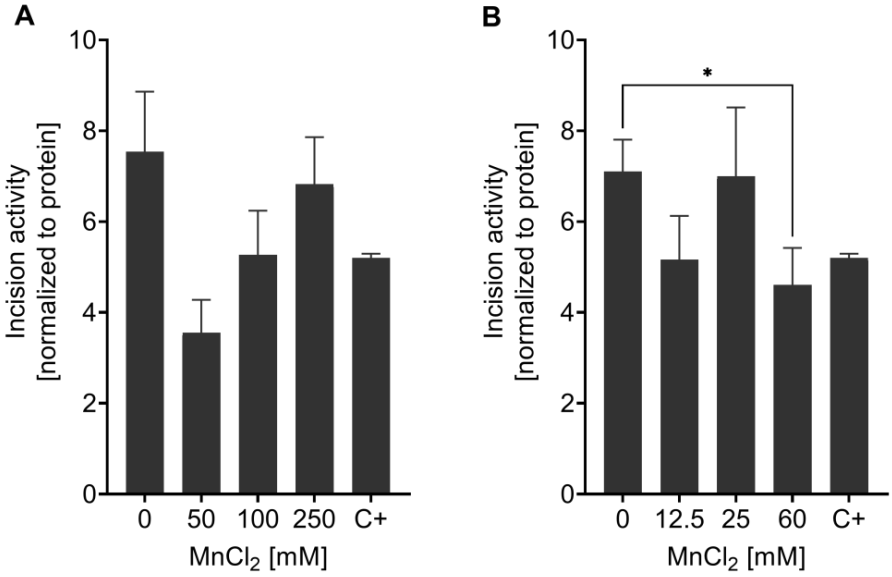

Figure 20 Measurement of AP site incision activity after Mn exposure. BER incision activity was determined towards an AP site analogue containing oligonucleotide by non-radioactive incision activity assay in N2 (WT). Worms were exposed to MnCl2 for [A] 1 h (0 mM, 50 mM, 100 mM, and 250 mM) and [B] 4 h (0 mM, 12.5 mM, 25 mM, and 60 mM). Olaparib was used as a positive control (C+) at 200 µM for 1 h. Data are expressed as means ± SEM of four independent experiments. For statistical analysis, the unpaired t-test was performed.

5.2.4 Reverse genetic studies indicate a slight phenotype of the nth-1(Δ) mutant and significant differences in parg-1 and parg-2 activity

To investigate the individual roles of BER-involved enzymes in response to Mn, the knock-down strains *ung-1(Δ)*, *nth-1(Δ)*, *exo-3(Δ)*, and *apn-1(Δ)* were examined for distinct Mn-dependent phenotypes. The induction of oxidative stress by Mn exposure observed in wild-type *C. elegans* by Neumann *et al.* 2019 [41] was also observed in the investigated deletion mutants defective in a single BER protein (Supporting Information, Figure 34), but Mn concentration-dependent differences between the strain were not detectable. However, changes in lethality after excessive Mn exposure were observed for the *nth-1*(Δ) strain. A functional knock-down of the N-glycosylase *nth-1* caused higher sensitivity towards Mn following 1 h exposure (Figure 21 (A)). This supports the hypothesis that nth-1 in *C. elegans* may also be capable of detecting and excising 8OHdG as discussed above. However, no differences in the survival rate were observed after 4 h incubation with $MnCl_2$. Further studies found that the *exo-3(Δ)* strain is hypersensitive to other oxidising agents, reflected in decreased life span and brood size, developmental delay, and abnormal vulval organogenesis [339, 354], but lethality data shown here do not capture the sensitivity of that strain under the given conditions.

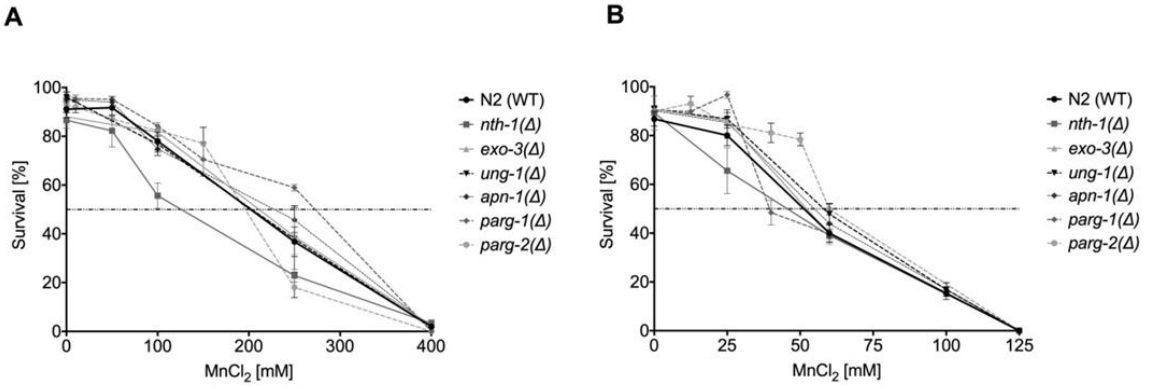

Figure 21 Dose-response curves of $MnCl_2$ on BER- and DNA damage response-deletion mutants compared to wild type *C. elegans*. Worms were incubated with various concentrations of $MnCl_2$ for [A] 1 h or [B] 4 h. Data are expressed as means ± SEM of at least three independent experiments.

For investigations regarding the DNA damage response, we build on the studies performed by Neumann *et. al* 2019 [41], who investigated PARylation in N2 (WT) and *pme1(Δ)* (orthologue of human PARP1) and *pme-2(Δ)* (orthologue of human PARP2) strains. These results show that after 1 h and 4 h incubation Mn does not exert any effects of PAR induction in wild-type *C. elegans*. While deletion of the genes, responsible for the induction of PARylation, caused an overall basal reduction of R-Ado levels, exposing *pme-1(Δ)* worms to 250 mM $MnCl_2$ for 1 h caused a significant increase of PARylation [41]. While the poly(ADP-ribose) polymerases PARP-1 and 2 both have obvious roles in DNA repair by binding to the DNA damage site and post-translationally modifying proteins to form "recruitment platforms" for other proteins needed for DNA repair, such as XRCC1 [107, 355], it is also discussed that the poly(ADP-ribose) glycohydrolase PARG co-operates to facilitate downstream cellular DNA repair processes [101]. PARG is responsible for the degradation of PAR, releasing monomeric ADP-ribose moieties [113], which might be needed for DNA damage response at different damage sites. It is also posited, that once PARylation caused the recruitment of XRCC1, removal of the PAR chain facilitates the translocation of XRCC1 from PAR directly to the DNA strand break and increases the repair kinetics of downstream processes [114]. In contrast to humans, worms have two functional orthologues of the glycohydrolase [356, 357]. Evaluation of basal PAR levels of these two PARG deletion mutant strains *parg-1(Δ)* and *parg-2(Δ),* showed significant differences between the glycohydrolase activities (Figure 22 (A)). A knock-down of *parg-1(Δ)* caused basal PAR levels to increase 70-fold (699 pmol PAR/ mg DNA) compared to wild-type and *parg-2(Δ)* (10 pmol PAR/ mg DNA). This data suggest that the main degradation activity is exerted by *parg-1* and that *parg-2* is not able to compensate for a deficiency. These results are corroborative of those by Janisiw *et al.*, which showed by immunostaining that *parg-1* has the main PAR glycohydrolase activity in the *C. elegans* germline [358]. Present knowledge on the functional role of *parg* is scarce, especially in the context of global effects in whole organisms. When exposing those three strains (*parg-1(Δ), parg-2(Δ),* and N2 (WT)) to Mn, a significant induction of PAR was not observed (Figure 22 (B)). PAR levels of the wild-type strain N2 (WT) and mutant strain *parg-2(Δ)* were comparable, while PARylation in *parg-1(Δ)* was both, less inducible by the positive control *t*BOOH, as well as less suppressed by the PAR inhibitor Olaparib. This is most likely due to the already high basal PAR levels in this strain.

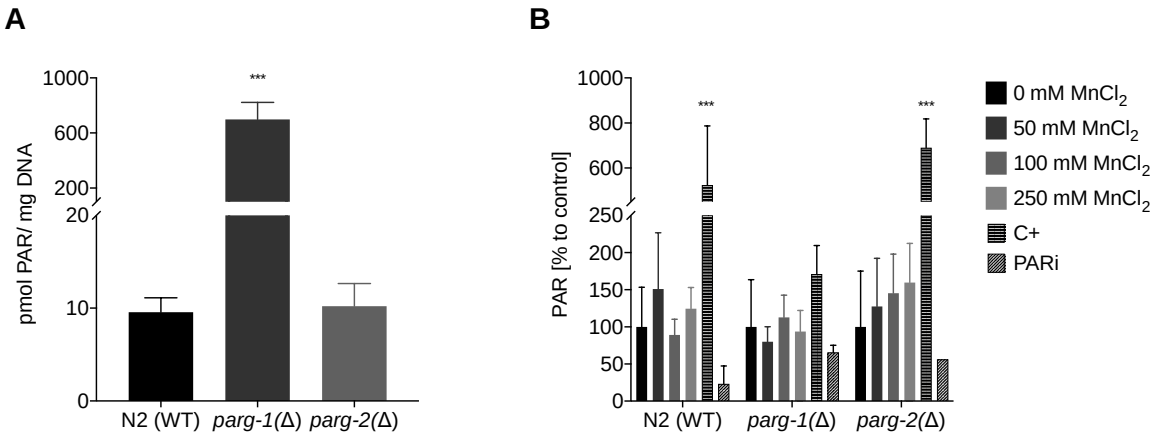

Figure 22 Determination of PARylation levels via HPLC-MS/MS. [A] Comparison of the basal PARylation levels in non-treated N2 (WT), *parg-1(*Δ), and *parg-2(*Δ) worms. [B] Relative PARylation levels of N2 (WT), *parg-1(*Δ), and *parg-2(*Δ) worms treated with 1 h $MnCl_2$ at sub-toxic and toxic concentrations. PAR levels are normalized to the DNA amount and compared relatively to the respective untreated control. 6.5 mM *t*BOOH (1 h) was used as positive control (C+) and 100 µM Olaparib (1 h) as PAR inhibitor (PARi). Data are expressed as means ± SEM of at least three independent experiments. For statistical analysis, the unpaired t-test was performed.

5.3 Materials and Methods

5.3.1 *C. elegans* maintenance and exposure to Mn

The *C. elegans* wild type N2 (WT) and the deletion mutant strains *nth-1(Δ)* (ok724), *ung-1(Δ)* (tm2862), *parg-1(Δ)* (gk120), and *parg-2(Δ)* (ok980) (all from *Caenorhabditis* Genetics Center (CGC), Minneapolis, USA) and *exo-3(Δ)* (tm4374), *apn-1(Δ) (tm6691)* (Mitani laboratory, National BioResource Project, Japan) were cultivated on *E. coli*-covered 8P plates at 20 °C as described in previous studies and by Brenner 1974 [143, 256]. After synchronization, eggs were allowed to hatch overnight and L1 larvae were seeded on NGM plates with OP50 *E. coli* as the food source. Worms were allowed to reach L4 larvae stage without further interference. For Mn exposure, 3000 synchronized L4 worms per sample were incubated in liquid (85 mM NaCl) with $MnCl_2$ (99.9% Manganese(II) chloride tetra-hydrate, Sigma-Aldrich 203734) for 1 h and 4 h in the absence of *E. coli* at different concentrations between 0 mM – 250 mM $MnCl_2$. Afterwards, worms were washed at least three times with 85 mM NaCl + 0.01% Tween®, before shock-freezing the pellets in liquid nitrogen for storage at -80 °C or directly proceeding with the following experiments.

5.3.2 ICP-OES measurement of Mn bioavailability

For analysis of Mn uptake, inductively coupled plasma-optical emission spectrometry (ICP-OES (Spectro)) was used. Frozen samples were homogenized by three freeze-thaw cycles and sonication (UP100H ultrasonic processor (Hielscher), 3 x 20 sec, 100% amplitude, highest setting), dried, and finally, acid-assisted digested (HNO_3:H_2O_2; 1:1) at 95 °C. The following device parameters were chosen for the analytical measurements: plasma power: 1400 W, refrigerant gas flow: 12 L/min, auxiliary gas flow: 1 L/min, nebulizer gas type, and flow: MicroMist, 1 L/min, and wavelength: 257.611 nm. The purity of the plasma torch argon was greater than 99.99%. For quantification, an external calibration was conducted using a multi-element mix (Spetec-645) and measurement accuracies were assessed using single-cell protein standards certified for trace elements (Commission of the European Communities, Community Bureau of References, BCR). For analysis, the Spectro Smart Analyzer software was used and all samples were normalized to protein content measured by BCA analysis (bicinchoninic acid assay-kit (Thermo Scientific)).

5.3.3 Lethality studies after Mn exposure

The acute toxicity of Mn was determined by lethality testing. After 1 h and 4 h treatment, a known number of worms was transferred to OP50-seeded NGM plates. Alive and dead worms were manually counted 24 h after the treatment. Animals that did not respond to the mechanical stimulus of touch (using a platinum/ zirconium wire) were considered as dead.

5.3.4 Measurement of DNA damage after Mn exposure utilising alkaline unwinding

The adapted alkaline unwinding assay was employed as described previously [359]. Shortly, worms were placed in 1 mL alkaline unwinding buffer (AU buffer; 0.5 M NaH_2PO_4, 0.5 M Na_2HPO_4, 0.1 M EDTA, pH 7.5) after Mn treatment and were made assailable to the alkaline solution by using slight sonication (1 mL AU buffer, 2 x 20 sec on lowest setting, 100% amplitude). After centrifugation and removal of the supernatant, 1.5 mL alkaline solution (0.9 M NaCl, 10 mM Na_2HPO_4, 0.03 N NaOH in dH_2O) was added

to all samples. Unwinding was conducted at room temperature (RT) in the dark for exactly 15 min, before neutralizing the solution with 0.1 N HCl, sonication on ice (15 sec, highest setting), and adding SDS to a final concentration of 0.05%. The single- and double-stranded DNA were separated by successional elution of 0.15 M and 0.35 M potassium phosphate buffer over 1 mL hydroxyapatite columns at 60 °C. The amount of the single-stranded DNA (ssDNA) and double-stranded DNA (dsDNA) fractions was determined using Hoechst stain (Hoechst 33258 nucleic acid stain) at a final concentration of 7.5 x 10^{-7} M and the fluorescence was measured using a microtiter fluorescence reader (Infinite Pro, Tecan; 360 nm excitation wavelength and 455 nm emission wavelength). The percentage of dsDNA indicates the genomic integrity of the worms as in alkaline environments, ssDNA occurs at sites of DNA strand breaks, and higher levels of dsDNA correlate with higher levels of genome integrity. The anti-cancer drug bleomycin was used as positive control at a concentration of 40 µM for 1 h.

5.3.5 ELISA measurement of 8OHdG

The OxiSelect™ Oxidative DNA Damage ELISA kit (Cell Biolabs, Inc.) was used for the rapid detection and quantification of 8-hydroxyguanine (8OHdG) in DNA samples obtained from N2 (WT) pellets, as described by Ahn *et al.* 2014 [345] but with some modifications as described in the following. The DNA was isolated from 3000 animals each, using the Qiagen Tissue and Blood DNA extraction kit, following manufacturer's instructions. DNA content was measured using a NanoDrop, samples were aliquoted to ~40 µg DNA/ sample. After vacuum drying the samples, enzymatic hydrolysis was used to get mononucleotides. For this, dried DNA samples were dissolved in 10 µL dH_2O and butylated hydroxytoluene (BHT) at a final concentration of 6.5 mM was added to each sample. Then, dsDNA was separated into single DNA strands by incubating all samples for 3 min at 100 °C while shaking. Immediate cooling on ice for another 2 min allows the DNA to re-form double helixes, but more loosely than before. At this point, 2.5 µL of 50 µM desoxy-cytosine (dC) internal standard (IS) was added to each analyte for later normalization. 5 µL Na-Succinate/ $CaCl_2$ (100 mmol/L 50mmol/L, pH 6) buffer were added before pipetting 1.6 µL 0.556 U/µL micrococcus nuclease to each sample. The mixture was vortexed thoroughly before adding 2.5 µL 0.001 U/µL phosphodiesterase. All samples were vortexed once again and shortly centrifuged. Enzyme incubation was conducted at 37 °C overnight. The next day, 2 µL 1 U/µL alkaline phosphatase was added and incubated

for another 2 h at 37 °C. Lastly, samples were filtered using a 10 kDa cut-off filter (Nanosep 10K, Pall), and samples were centrifuged for 20 min at 13,000 rpm at RT. 2 µL of each sample were used for cytosine quantification via HPLC-MS/MS for normalization (as described by Finke, Winkelbeiner *et al.* 2020 [360]), the rest was used for the semi-quantitative measurement of 8OHdG via the competitive inverse ELISA kit. Manufacturer's instructions were followed and all requisite reagents were included in the kit. As positive control, 6.5 mM *tert*-butyl hydroperoxide (*t*BOOH) was used.

5.3.6 Measurement of apoptotic bodies

For determination of apoptosis, early L4 larvae were incubated with $MnCl_2$ for 1 h in liquid followed by a 24 h regeneration period on a lawn of *E. coli*-covered NGM plates. For measurement of the apoptotic bodies, worms were incubated with acridine orange as described in Gartner *et al.* [361], and individual nematodes were anesthetized with 15 mM sodium azide as described before. Worms were examined under the fluorescence microscope (Olympus CJX41) at 40x magnification and apoptotic bodies were counted in the posterior germline loop. 200 J/m^2 UV-C irradiation was used as the positive control.

5.3.7 Quantitative real-time PCR analysis for gene expression studies

Gene expression studies were performed using TaqMan™ Gene expression assays. RNA was isolated using the TRIzol® method from incubated worm pellets as described previously [331]. 1 µg of isolated RNA was used for cDNA synthesis utilising the High Capacity cDNA Reverse Transcription Kit (Applied Biosystems). The quantitative real-time PCR (BioRad) using TaqMan™ Gene expression Assay probes (Life Technologies) for each gene was used and *afd-1* (actin homolog) was used as the housekeeping gene for normalization. Fold difference was determined via the comparative $2^{-\Delta\Delta Ct}$ method. The following probes were used: *afd-1* (Assay ID: Ce02414573_m1), *nth-1* (Assay ID: Ce02445360_g1, *ung-1* (Assay ID: Ce02453385_m1), *exo-3* (Assay ID: Ce02423726_g1), and *apn-1* (Assay ID: Ce02435571_g1).

5.3.8 Measurement of incision activity for AP sites

For AP site incision activity analysis, the method of non-radioactive base excision repair (BER) incision activity described by Winkelbeiner *et al.* 2020 [352] was used. After extract preparation of samples with 3000 worms each and protein quantification via BCA, 5 µg of protein were used for each sample for optimal determination of enzyme activity. Extracts were incubated with the fluorescently labelled DNA lesion containing hairpin-oligonucleotides (AP site analogue containing). Using polyacrylamide gel electrophoresis (PAGE), intact and incised oligonucleotides were separated and quantified via fluorescence measurement. The ratio of intact and incised oligonucleotides correlates with the incision activity of glycosylases involved in BER. The PAR polymerase (PARP) inhibitor Olaparib was used as positive control at 200 µM for 1 h.

5.3.9 Analysis of PAR levels via HPLC-MS/MS

Preparation of samples for poly(ADP-ribose) (PAR) extraction was conducted with 3000 worms per sample. All steps were conducted as described before [41, 362]. In brief, the worm´s cuticles were broken by four freeze-thaw cycles before homogenizing the samples with a tissue disruptor (Qiagen) in 1 mL 20% ice-cold trichloroacetic acid. Samples were washed twice with 70% EtOH and dried at 37 °C. Afterwards, pellets were resuspended in 400 µL 0.5 M KOH and incubated at 37 °C for 50 min. After removal of cell debris, supernatant was neutralized with 4.8 M MOPS (pH 5.9) and DNA concentration was measured via the Hoechst method for later normalization. 2.5 pmol ^{13}C,^{15}N labelled-PAR was added as an internal standard before digesting the nucleic acids with DNase and RNase, followed by digestion by protein kinase K overnight. Samples were enriched by the High Pure miRNA isolation kit (Roche) and digested to the monomeric units with alkaline phosphatase and phosphodiesterase I. All enzymes were removed with a 10 kDa cut-off filter (Nanosep 10K, Pall). The analytes were vacuum-dried and resuspended in water for HPLC-MS/MS analysis. PAR analysis was conducted on an Agilent HPLC system (Agilent 1260 Infinity II) coupled to a Sciex triple quadrupole-mass spectrometer (Sciex QTrap 6500+) equipped with an electrospray ion source operating in positive mode (ESI+). Separation was conducted using a Hypersil Gold aQ 150 x 2.1 mm particle size 3 micron and corresponding pre-column and an isocratic flow with 1% ACN + 0.01% formic acid and 99% water + 0.01% formic acid was used. The flow rate was 0.3 mL/min.

The following optimized source parameters were used: curtain gas = 35, collision gas = medium, ion spray voltage = 5500, temperature = 600, ion source gas 1 = 40, ion source gas 2 = 40, declustering potential = 66, entrance potential 10, and collision cell exit potential = 8. Quantification was conducted in MRM mode and the transitions of m/z = 400 > 136 (collision energy = 27) and m/z = 415 > 146 (collision energy = 27) for ribosyladenosine (R-Ado) and $^{13}C,^{15}N$ R-Ado, respectively. 6.5 mM *t*BOOH was used as positive control (described previously [41]) and 100 mM Olaparib was used as a PARP inhibitor.

5.3.10 Statistical analysis

Statistical analyses were performed using GraphPad Prism 9 (GraphPad Software, La Jolla, USA). Significance is depicted as *: $p<0.05$, **: $p<0.01$, and ***: $p<0.005$ compared to respective untreated mutant strains or N2 (WT).

5.4 Conclusions

Mn is constantly being introduced into the environment and rising industrial use of this transition metal causes increased pollution and exposure. It is therefore imperative to understand the short- and long-term environmental and health risks of the exposure to this metal, as well as the underlying pathways of its toxicity. Utilising the multicellular model organism *C. elegans* allowed us to investigate the adverse effects of Mn. The results of the current study are shedding more light on the underlying mechanisms of Mn-induced toxicity attributing to oxidative stress. Moreover, Mn-induced DNA damage (decreased genomic integrity), interfered with DNA repair and DNA damage responses. The increase in BER gene expression upon Mn exposure implies that the decreased genomic integrity results in activation of BER. PARylation and apoptosis were not triggered by excessive Mn exposure in this study design. To validate the results further, more studies on proteins linked to PARylation are required. Regarding BER specifically, the results show a significant role for *nth-1*, although further investigations are needed to understand the underlying mechanistic pathways. To confirm or refute the hypothesis that observed oxidative DNA damage caused by Mn is associated with the Mn-induced neurodegeneration examined in other studies, neurodegeneration assays are needed.

5.5 Acknowledgement

This work was supported by the DFG Research Unit TraceAge (FOR 2558, BO4103/4-2). Additional funding was obtained from the DFG project BO4103/2-1.

5.6 Author Contributions

Experiments were designed and mostly performed by MMN, AKW conducted the experiments regarding PARylation. VB and AW performed and analysed the acridine orange staining. JB (Jessica Baesler) performed the gene expression studies. NW helped with experimental set-up and AG assisted with experimental execution. Data analysis and interpretation were performed by MMN, JB (Julia Bornhorst) and MMN conceptualized the study and wrote the manuscript. MA, GF and TS contributed to data interpretation, helped with ideas for experimental setup, and revised the manuscript critically for important intellectual content. All authors were involved in compiling the manuscript and approved the final version. JB (Julia Bornhorst) rendered this work possible. All authors have read and agreed to the published version of the manuscript.

Abstract

Manganese (Mn) is an essential trace element, but overexposure is associated with toxicity and neurological dysfunction. Accumulation of Mn can be observed in dopamine-rich regions of the brain *in vivo* and Mn-induced oxidative stress has been discussed extensively. Nevertheless, Mn-induced DNA damage, adverse effects of DNA repair, and possible resulting consequences for the neurite network are not yet characterized. For this, LUHMES cells were used, as they differentiate into dopaminergic-like neurons and form extensive neurite networks. Experiments were conducted to analyze Mn bioavailability and cytotoxicity of $MnCl_2$, indicating a dose-dependent uptake and substantial cytotoxic effects. DNA damage, analysed by means of 8-oxo-7,8-dihydro-2´-guanine (8oxodG) and single DNA strand break formation, showed significant dose- and time-dependent increases of DNA damage upon 48 h Mn exposure. Furthermore, the DNA damage response was increased which was assessed by analytical quantification of poly(ADP-ribosyl)ation (PARylation). Gene expression of the respective DNA repair genes was not significantly affected. Degradation of the neuronal network is significantly altered by 48 h Mn exposure. Altogether, this study contributes to the characterization of Mn-induced neurotoxicity, by analysing the adverse effects of Mn on genome integrity in dopaminergic-like neurons and respective outcomes.

Chapter 6

Mechanistic Studies on the Adverse Effects of Manganese Overexposure in Differentiated LUHMES Cells

Based on:

Merle M. Nicolai, Barbara Witt, Sharleen Friese, Vivien Michaelis, Lisa Hölz-Armstrong, Maximilian Martin, Franziska Ebert, Tanja Schwerdtle and Julia Bornhorst

Submitted to: Food and Chemical Toxicology

Highlights

- Manganese decreases the DNA integrity of differentiated LUHMES cells
- Degradation of the neurite network is induced by manganese overexposure
- Analytical measurement of 8oxodG allows semi-quantitative analysis *in vitro*

Keywords

Manganese, LUHMES, DNA integrity, DNA repair, neurodegeneration, oxidative stress

6.1 Introduction

Manganese (Mn) is an essential trace element required as a cofactor for many cellular systems involved in growth, metabolism, neuronal functions, and cellular homeostasis [131, 320]. The ubiquitous divalent metal is naturally occurring in food (nuts, grains, vegetables) and drinking water in varying concentrations and a deficiency in humans has therefore not been observed [150, 363]. Due to the increasing industrial use of Mn and its mining, environmental exposure has been rising immensely in some regions, causing risks of adverse health effects to exposed humans [141]. Chronic Mn overexposure is associated with neurodegeneration, and recently published epidemiological studies also link the overexposure of the trace element to various neurological effects in children and adults all over the world [132, 166]. Recent results from Michalke *et al.* 2021 indicate, that the neural barriers in general strictly control the passage of transition metals into the cerebrospinal fluid, but less so for Mn [158]. This finding elevates the problematic nature of rising environmental Mn levels. Physiological concentrations of Mn in the human brain are estimated to be between 5.32 – 14.03 ng Mn/mg protein (corresponding to 20.0 – 52.8 µM Mn) [160], but bioavailability studies showed that Mn can accumulate strongly upon overexposure. Concentrations vary greatly between different brain regions, whereby the accumulation is especially high in mitochondria of the dopamine-rich region of the basal ganglia, particularly the *substantia nigra* [13, 161, 162]. The primary target cells in Mn-induced neurotoxicity are discussed to be astrocytes and neuronal cells [187-189]. While the association between Mn and neurodegeneration is avowed, little is known about the mechanistic pathways behind the adverse effects of Mn on movement,

cognition, emotion, and behavioural responses, with severe neurological dysfunctions similar to Parkinson's disease [140, 183, 364]. A better understanding of the neurotoxic mechanism is therefore of highest importance. Mn, as a transition metal, can induce increased formation of reactive oxygen and nitrogen species (RONS), either directly by Fenton-like reactions or indirectly by inhibiting the respiratory chain in mitochondria [365, 366]. Especially neurons are enriched in mitochondria and possess a rather high metabolic turn-over [367]. Increased RONS in turn might increasingly interact with macromolecules, such as proteins, lipids, and DNA; potentially causing DNA damage and/ or impairment of the DNA damage response [87, 179, 180]. It has been shown before, that Mn overexposure causes oxidative stress *in vitro* and *in vivo* and an increase of DNA damage and disturbed DNA damage response under high Mn conditions [10, 41, 183, 184]. Nevertheless, results regarding the genotoxic potential are inchoate and the fate of neurotoxic endpoints is still unclear. Especially to safeguard the cellular genome from (oxidative) damage in post-mitotic neurons which incur DNA damage, the DNA damage response is of central importance [338]. Therefore, we decided to focus the investigations on Mn-induced DNA damage and cellular DNA damage response in neuronal cells and the consequences on the neuronal network. For that reason, the Lund human mesencephalic (LUHMES) cell line was chosen for experimental investigations. Once differentiated, which is achieved by treatment of the neurons with tetracycline, cyclic AMP (cAMP), and glial-derived neurotrophic factor (GDNF), the cells exit the cell cycle and develop into dopaminergic-like neurons within one week. At this point, they express dopaminergic neuron-specific biochemical markers and develop an extensive neurite network [231, 232]. LUHMES are TET-off immortalized cells and are derived from embryonic human mesencephalons. This cellular system offers a high physiological relevance, acceptable culture procedures, and a large culture scale, needed for efficient and meaningful investigations of the mechanisms underlying Mn-induced neurotoxicity.

6.2 Materials and Methods

6.2.1 Cell culture of human neurons

LUHMES were cultivated and differentiated as described previously [368, 369]. In short, undifferentiated LUHMES cells were seeded on pre-coated dishes (50 µg/mL poly-L-ornithine hydrobromide (Sigma Aldrich), 1 µg/ mL fibronectin from bovine plasma

(Sigma Aldrich)). For proliferation medium, advanced DMEM/F12 (Life Technologies GmbH) was supplemented with N2 supplement (Life Technologies GmbH), 2 mM L-glutamine (Biochrom), and 40 ng/mL recombinant human basic fibroblast growth factor (FGF, R&D Systems). The differentiation process was initiated after 24 h of cultivation by changing the proliferation medium to differentiation medium (Advanced DMEM/F12, supplemented with N2, 2 mM L-glutamine, tetracycline (Sigma Aldrich), dibutyryl cyclic adenosine monophosphate sodium salt (cAMP, Sigma Aldrich), recombinant human cell-derived neurotrophic factor (GDNF, R&D Systems)). Two days later, cells were seeded on pre-coated culture dishes with a defined cell density of 150,000 cells/cm^2. The medium was replaced 48 h after seeding. Cells are completely differentiated and qualified for treatment after six days.

6.2.2 Incubation with $MnCl_2$, preparation of the stock solution, dosage information/ regimen

Cells were exposed to $MnCl_2$ for 24 h or 48 h with 10 – 1000 µM $MnCl_2$ for cytotoxicity assays and bioavailability studies were performed at 25 – 300 µM $MnCl_2$, as this concentration span proved to be most relevant for cytotoxicity. The genotoxic potential of Mn was assessed after 48 h at various sub-toxic concentrations (around the most sensitive effective concentration of 30% (EC_{30}) in cytotoxicity assessment) or in a time-dependent manner.

Stock solutions of $MnCl_2$ (> 99.9% purity, Sigma Aldrich) were prepared in sterile dH_2O, filtered and diluted shortly before the experiment.

6.2.3 Bioavailability of Mn, and other trace elements

For assessment of the bioavailability of Mn, copper (Cu), magnesium (Mg), calcium (Ca), iron (Fe), zinc (Zn), and selenium (Se) cells were differentiated and seeded in pre-coated 24-well cell culture plates. After Mn exposure, cells were pelletized on ice using RIPA (NaCl, Tris (pH 7.6), EDTA (pH 7.6), sodium-deoxycholate (Sigma Aldrich), Triton™ X-100, and 10% sodium dodecyl sulphate (Roth)). To ensure complete cell rupture, cells were sonicated (UP100H ultrasonic processor (Hielscher), 6 sec, 100 % amplitude, cycle 0.5) and centrifuged at 15,500 x g for 20 min at 4 °C. The protein level of the supernatant

was measured via the Bradford assay (Bio-Rad Laboratories) for normalization. For acid-assisted digestion, the cell suspensions were firstly dried overnight at 60 °C. Afterwards, 500 µL digestion solution (35% H_2O_2, 65% HNO_3; 1:1) were added to the cell pellets, mixed well, and finally digested overnight at 95 °C. For analysis, digested pellets were resuspended in 1 mL 10% HNO_3 and 10 µg/L Rhodium as internal standard and mixed well before diluting the analytes 1:1 in 10% HNO_3.

The analytical quantification was conducted by inductively-coupled plasma coupled to tandem mass spectrometry (ICP-MS/MS, both Agilent) using the following parameters: plasma RF power 1550 W, plasma gas flow 15 L/min, auxiliary gas flow: 0.9 L/min, nebulizer gas (argon) flow 4.3 mL/min, and nebulizer gas (helium) type MicroMist®. The certified reference material NIST Trace Elements in Natural Water 1640A (LGC Standards GmbH) were used for internal quality control. The following mass to charge (*m/z*) ratios were used for trace element and internal standard (IS) identification and quantification: Mn *m/z* 55 → 55, Fe *m/z* 56 → 56, Cu *m/z* 63 → 63, Zn *m/z* 66 → 66, and rhodium *m/z* 103 → 103.

6.2.4 Cytotoxicity testing

Cytotoxicity was assessed by investigating the dehydrogenase activity, mitochondrial membrane potential, and cell number. For this, cells were differentiated and seeded in pre-coated 96-well cell culture plates.

Dehydrogenase activity

Dehydrogenase activity was measured by the resazurin reduction assay as described before [368]. The method is based on the reduction of the blue non-fluorescent redox dye resazurin to the pink fluorescent resorufin by intracellular dehydrogenases. NADH is used as the cofactor. After incubation with $MnCl_2$, the medium was replaced with a 5 µg/ mL resazurin solution (7-hydroxy-3H-phenoxazin-3-one-10-oxide sodium salt (Sigma Aldrich), differentiation medium). Incubation lasted for 3 h at 37 °C before measuring the fluorescence (Tecan Infinite Pro M200, Tecan) with excitation: 530 nm and emission: 590 nm).

Mitochondrial membrane potential normalized to cell number

Mitochondrial membrane potential and cell number were determined simultaneously using MitoTracker™Orange CMTMRos (Invitrogen) [370, 371] and Hoechst 33258 (Merck) staining [372]. After incubation with $MnCl_2$, the medium was replaced with 300 nM MitoTracker™Orange CMTMRos in assay buffer (80 mM NaCl, 75 mM KCl, 25 mM D-glucose, 25 mM HEPES pH 7.4) for 30 min at 37 °C. After incubation, cells were fixed with 3.7 % formaldehyde in assay buffer for 10 min at 37 °C. After replacing the formaldehyde with assay buffer, fluorescence was measured at excitation: 544 nm and emission: 590 nm. Thereupon, cell membranes were permeabilized using 2.2% Triton™ X-100 (Sigma Aldrich) for 10 min at 37 °C to allow Hoechst 33258 staining. For this, 6 µM Hoechst 33258 in PBS was incubated at 37 °C for 30 min, before replacing the solution once again with assay buffer. Fluorescence was measured with the fluorescence plate reader (ex: 355 nm, em: 460 nm). The mitochondrial membrane potential was calculated and normalized to the cell number.

6.2.5 Detection of 8oxodG using HPLC-MS/MS

The oxidative DNA damage 8-oxo-7,8-dihydro-2´-guanine (8oxodG) was quantified analytically by high-performance liquid chromatography coupled to tandem-mass spectrometry (HPLC-MS/MS). For this, cells were differentiated and seeded into 25 cm^2 flasks and incubated with $MnCl_2$. Cells were pelletized and the DNA was isolated using the Qiagen Tissue and Blood DNA extraction kit, following the manufacturer's instructions. After vacuum drying the DNA samples, enzymatic hydrolysis was used to obtain mononucleotides, which is based on methods by Greer *et al.* (2015) and Finke *et al.* (2020) [360, 373]. Dried DNA samples were dissolved in 10 µL dH_2O and 6.5 mM butylated hydroxytoluene (BHT) was added to each sample. Then, dsDNA was separated into single DNA strands by incubating all samples for 3 min at 100 °C while shaking. Immediate cooling on ice for another 2 min allows the DNA to re-form double helixes, but more loosely than before. At this point, isotope-labelled internal standards (IS) for 8oxodG and deoxycytidine (dC) were added to each analyte for later normalization. 5 µL sodium-succinate/ $CaCl_2$ (100 mmol/ 50mmol/l, pH 6) buffer were added before pipetting 1.6 µL 0.556 U/µL micrococcus nuclease to each sample. The mixture was vortexed thoroughly before adding 2.5 µL 0.001 U/µL phosphodiesterase. All samples were vortexed

thoroughly for enzyme incubation overnight at 37 °C. Afterward, 2 µL 1U/µL alkaline phosphatase were added for an incubation of 2 h at 37 °C. All enzymes were obtained from Sigma-Aldrich. Lastly, samples were filtered using a 10 kDa cut-off filter (Nanosep 10K, Pall), and samples were centrifuged for 20 min at 13,000 rpm at RT. HPLC-MS/MS was conducted using an Agilent HPLC system (Agilent 1260 Infinity II) coupled to a Sciex triple quadrupole-mass spectrometer (Sciex QTrap 6500+). Separation was conducted using a YMC Triart-PFP column (reversed-phase; hybrid silica material modified with pentafluorophenyl propyl; 3 x 150 mm; 3 µm; 120 Å) and a corresponding pre-column of the same material. Samples were separated at a flow rate of 0.3 mL/min, using a 15 min mobile phase gradient with 5 mM ammonium formate in dH_2O (pH 4.2) and 5 mM ammonium formate in MeOH as eluents. Electrospray ionization in positive ion mode (ESI+) was used for ionization. Quantifier mass transition of 8oxodG (*m/z* 284→168) was used in relation to the mass transition of 8-oxo-dG-^{13}C,-$^{15}N_2$ (*m/z* 287→171). For normalization, dC was measured in samples diluted 1:200 in dH_2O. All analysed mass *m/z* transitions (Table 5), MS parameter (Table 6), and the LC mobile phase gradient (Table 7) can be found in the Supporting Information.

6.2.6 Determination of DNA single-strand breaks by alkaline unwinding

Quantification of DNA strand breaks was realized by alkaline unwinding, a method described before [184, 374], and adapted for LUHMES cells. Briefly, cells were incubated with $MnCl_2$ in 12-well cell culture plates and washed with ice-cold PBS. An alkaline solution (0.03 M NaOH, 0.02 M Na_2HPO_4, and 0.9 M NaCl) was added to each sample and incubated in the dark for 30 min. After neutralizing, transfer of the cell pellets into glass tubes, sonification of the cell mixtures, and addition of sodium dodecyl sulphate (SDS), single- and double-stranded DNA (ssDNA/ dsDNA) were separated using 60 °C tempered hydroxyapatite columns. The ssDNA and dsDNA were eluted using 0.15 M and 0.35 M potassium phosphate buffers, respectively. By adding Hoechst dye to the obtained DNA solutions and measuring the fluorescence using a microplate fluorescence reader (Tecan, SPECTRA Fluor), relative DNA fractions can be determined. The calculation of DNA strand breaks is based on calibrations with X-ray irradiations as described by Hartwig *et al.* [375].

6.2.7 Quantification of poly(ADP-ribosyl)ation (PAR) levels

For analysis of PAR levels, an isotope-diluted LC-MS/MS method was adapted from a previously published method [41, 362, 376]. Cells were differentiated and seeded in 12-well cell culture plates. After Mn exposure cells were washed with 1.5 mL ice-cold PBS before adding 1.5 mL of ice-cold 20% (w/v) TCA for cell lysis and precipitation of macromolecules. Afterward, cells were placed on ice and acid-insoluble materials were scraped from the cell culture dish using a cell scraper before transferring the cell suspension into a 2 mL reaction tube. Cell culture dishes were washed with another 0.5 mL ice-cold 20% (w/v) TCA to ensure complete transferal. The samples were centrifuged (3000 x g at 4 °C for 5 min) and pellets were washed twice with 500 µL ice-cold 70% EtOH. After the last washing step, samples were air-dried at 37 °C. The alkaline treatment was initiated by adding 255 µL 0.5 M KOH to detach protein-bound PAR. Pellets were resolved at 37 °C while shaking (600 U/min) constantly until no pellet was visible. This may take up to 70 min (depending on cell number used) and vortexing was done for 30 s every 20 min. When the solution was clear, 50 µL 4.8 M MOPS were added and mixed in for neutralization. 30 µL of the solution were stored at -80 °C for determination of DNA concentration by the Hoechst method [41].

2.5 pmol of ^{13}C,^{15}N labelled-PAR were added to each sample, before adding 6.25 µL 2 M $MgCl_2$, 2.5 µL 100 mM $CaCl_2$, 15.5 µL 2 mg/mL DNAse (Qiagen) and 2.5 µL 10 mg/mL RNAse (ThermoFisher Scientific) for nucleic acid digestion. The mixture was incubated at 37 °C on a shaker (400 U/min). After a 3 h incubation, 1.25 mL 40 mg/mL protein kinase K were added, mixed well, and samples were further incubated overnight. To enrich samples for PAR, a High Pure miRNA kit (Roche) was used. 624 µL binding buffer were added to each sample before adding 400 µL binding enhancer. The solutions were re-suspended until completely clear and 700 µL were transferred onto a high pure column and centrifuged at 15,700 x g for 30 s. The flow-through was discarded and the last centrifugation step was repeated until the entire mixture was filtered. The filter was washed with 200 µL washing buffer (15,700 x g for 30 s) and dried by centrifuging at 15,700 x g for 1 min. The columns were placed into new reaction tubes and 100 µL dH_2O were added for another centrifugation step (15,700 x g for 1 min). Columns were discarded and the digestion of the purified PAR was initiated by adding 342 µL of digestion master mix (60 µL 10 mM MgAc, 60 µL 250 mM NH_4Ac, 220 µL dH_2O, 1 µL 10 U/µL alkaline phosphatase, 1 µL 0.5 U/µL PDE). Samples were vortexed and incubated for 3 h at 37 °C

while shaking (400 U/min). After incubation, samples were transferred to Nanosep Omega 10K filter and filtered at 13,000 x g for 10 min to remove the enzymes. Samples were then vacuum-dried and pellets resuspended in 25 µL Millipore dH_2O for HPLC-MS/MS measurements. Quantification of PAR was conducted using an Agilent 1260 Infinity LC system coupled with an Agilent 6490 triple quadrupole-mass spectrometer (LC-MS/MS) (both Agilent) interfaced with an electron-ion source operating in the positive ion mode (ESI+) which is described in detail by Neumann *et al.* (2020) [41].

6.2.8 Gene expression screening of DNA repair associated genes

Relative mRNA expressions of genes involved in the relevant repair pathways were analysed using the qPCR-based method. Cells were differentiated and seeded in 25 cm^2 cell culture flasks. After Mn exposure (20 µM, 48 h (EC_{30})) cells were trypsinised, centrifuged, washed with ice-cold PBS, and pellets were stored at −20 °C. Using the "NucleoSpin RNA II kit" (Machery-Nagel), RNA was isolated and the concentration was measured using a Nanodrop (ThermoFisher Scientific). 1 µg RNA was used for reverse-transcribed to cDNA by using the "qScript Kit" (Quanta Biosciences). Primer sequences and efficiencies, thermal cycling programs and calculations of relative gene expressions for the 96-well based RT-qPCR method were described in Ebert *et al.* 2016 [377]. Actin serves as the housekeeping gene.

6.2.9 Assessment of neurite toxicity via tubulin staining

For the assessment of Mn toxicity on the neurite network, immunofluorescence staining of the neuronal cytoskeleton protein βIII-tubulin was conducted, followed by a semi-automatic quantification of the neurite mass as described by Witt *et al.* 2017 [378]. Briefly, differentiated LUHMES cells were seeded on pre-coated 18 mm glass coverslips and cells were incubated with $MnCl_2$ for 48 h. Afterward, cells were fixed with PBS containing 1% formaldehyde (Roth), washed with PBS containing 0.05% Tween® 20 solution, permeabilized with PBS containing 0.2% Triton™ X-100, washed again, and incubated with 1% bovine albumin in PBS for 30 min at RT. The primary antibody (anti-tubulin β3 [TUBB3], Clone: Tuj1, BioLegend GmbH) was incubated overnight at 4 °C before incubating the secondary antibody (Alexa Fluor® 488 goat anti-mouse IgG, Invitrogen) for 1 h at RT, both in blocking buffer (PBS, 1% bovine albumin). For low background

signalling, several washing steps with washing buffer were carried out after each antibody incubation. Lastly, cells were mounted in Vectashield mounting medium containing DAPI (Vector Laboratories), and the neuronal network was assessed on a Leica DM6 B wide-field fluorescence microscope, equipped with a microscope lens HC Plan APO 10X and 20X/0.70, a CTR6 LED lamp and a cooled Leica DFC 365 FX CCD camera. For quantification of the neurite mass, the LAS X Core 2D Analyse imaging software (Leica) was used. The relative fluorescence of the intensity of neuronal network surrounding the nuclei (identification via DAPI staining), was measured. A minimum of 20 images per sample was evaluated for neurite mass.

6.2.10 Statistical analysis

Statistical analyses were performed using GraphPad Prism 9 (GraphPad Software, La Jolla, USA). Statistical tests performed are listed in the respective figure captions and significance is depicted as *: $p<0.05$, **: $p<0.01$, and ***: $p<0.005$ compared to respective untreated control.

6.3 Results and Discussion

6.3.1 Cellular bioavailability, cytotoxicity, and adverse effects of Mn on the mitochondrial membrane potential

For investigations of Mn uptake by neurons, differentiated LUHMES cells were incubated with $MnCl_2$ for 24 h and 48 h with various concentrations of up to 300 µM $MnCl_2$, and 50 µM $MnCl_2$ respectively. The cellular Mn concentrations increased in a dose- and time-dependent manner in both incubation periods (Figure 23) for up to the highest tested concentrations each. Cells incubated with 300 µM $MnCl_2$ for 24 h showed a total Mn content of ~0.56 µg Mn/mg protein. A 48 h incubation with 50 µM $MnCl_2$ resulted in a total Mn concentration of ~0.12 µg Mn/mg protein. The same concentration of $MnCl_2$ after only 24 h incubation caused an increase of the cellular concentration to 0.078 µg Mn/mg protein, indicating that the Mn uptake is almost directly proportional to the incubation time. This linear uptake of Mn after 24 h and 48 h incubations was not observed in earlier studies using different human cell lines (CCF-STTG1 (CCL-185™), A549 or HeLa cells) [184, 366, 379]. Astrocytes for example do not show significant differences in Mn uptake

after either 24 h or 48 h exposure to the same $MnCl_2$ concentration. In addition, comparing the cellular Mn concentrations of astrocytes and neurons, Mn bioavailability is 15 – 20 times higher in LUHMES cells [379]. The effect of excessive Mn uptake on the status of other trace elements was also investigated in LUHMES, as other studies suggest an interrelation of other trace elements in uptake and homeostases [380]. Analysis of Cu, Mg, Ca, Fe, Zn, and Se indicated that the overexposure of differentiated LUHMES cells with up to 40 µM Mn for 48 h does not significantly affect the homeostasis of these trace elements (Supporting Information,

Figure 35). The cytotoxicity assessment was likewise conducted for cells exposed to $MnCl_2$ for 24 h and 48 h. The metabolic activity was determined using the resazurin assay, which measures the dehydrogenase activity. Concentrations of ≥ 50 µM $MnCl_2$ caused a highly significant decrease of the metabolic activity for both incubation times (Figure 24 (A and B)), which is dose- and time-dependent. The EC_{30} is estimated to be ~150 µM $MnCl_2$ and 40 µM $MnCl_2$ after a 24 h incubation and 48 h, respectively (Figure 24 (C)). The decrease of the cell number yielded more sensitive cytotoxic concentrations of $MnCl_2$ in the differentiated neurons compared to the resazurin assay. Highly significant decreases of cell numbers after 24 h and 48 h incubation were reached at concentrations of ≥ 25 µM $MnCl_2$. The approximated EC_{30} values are at 58 µM $MnCl_2$ for 24 h Mn exposure and > 25 µM $MnCl_2$ after 48 h Mn exposure. These results indicate that neurons are a highly important target for Mn-induced toxicity as they are much more sensitive than other brain-associated cell lines. Astrocytes incipient cytotoxic effects at incubation concentrations of 1000 µM for 24 h [379].

Measuring the mitochondrial membrane potential using MitoTracker® Orange allowed us to draw conclusions regarding the effect of Mn on mitochondrial function. Excessive levels of free radicals can disturb the mitochondrial integrity, which in turn can cause further formation of RONS. Additionally, Mn ions showed to induce H_2O_2 generation at the binding site of the complex II of the respiratory chain in mitochondria [381]. Mitochondrial membrane potential is therefore a likely target of Mn-induced oxidative stress. Exposing differentiated LUHMES cells for 24 h affected the potential already at low concentrations (≤ 50 µM $MnCl_2$) and a 50% reduction can be seen at 75 µM $MnCl_2$ (Figure 25 (A)). Even higher concentrations (≥ 200 µM $MnCl_2$) lead to a constant low level of ~ 15% compared to non-exposed cells. Incubation with Mn for 48 h showed an EC_{30} of 25 µM $MnCl_2$ (Figure 25 (B)), which is, likewise to the 24 h incubation, marginally under

the EC_{30} cytotoxicity values. The disturbance of the membrane potential by Mn shown in this study can correlate with oxidative stress, as the endpoint is both, an indicator for a cause and consequence of increases in RONS. This is in line with previous studies (*in vitro* and *in vivo*) that have shown before that Mn causes an increase in oxidative stress [10, 41, 184]. Consequences of oxidative stress, especially in neurons, are of great concern, due to the inability of self-replenishment of post-mitotic cells. On account of the almost linear cellular bioavailability and estimated EC_{30} values, we decided to conduct all following mechanistic studies after a 48 h Mn exposure with 0 µM, 20 µM, and 40 µM $MnCl_2$. This allowed the investigation of genotoxic endpoints at concentrations of sub-toxic (10 µM and 20 µM $MnCl_2$) and toxic concentrations (40 µM $MnCl_2$).

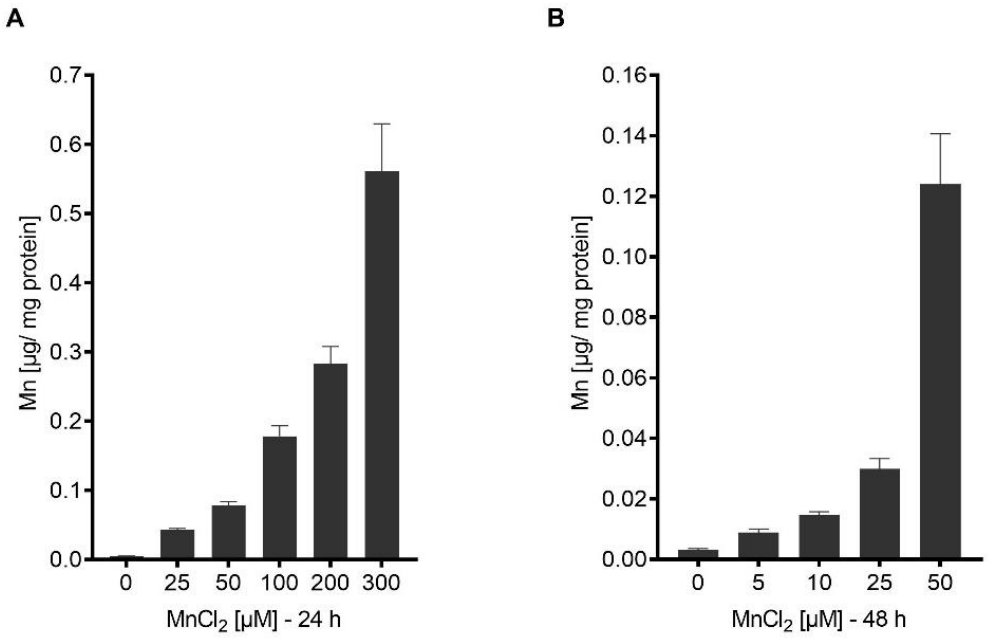

Figure 23 Mn bioavailability in LUHMES cells after Mn overexposure. Results show dose- and time-depended Mn uptake [µg Mn/ mg protein] in differentiated LUHMES cells following a [A] 24 h and [B] 48 h incubation. Bioavailability was measured analytically via ICP-MS/MS. Data are expressed as means ± SD of at least six independent experiments.

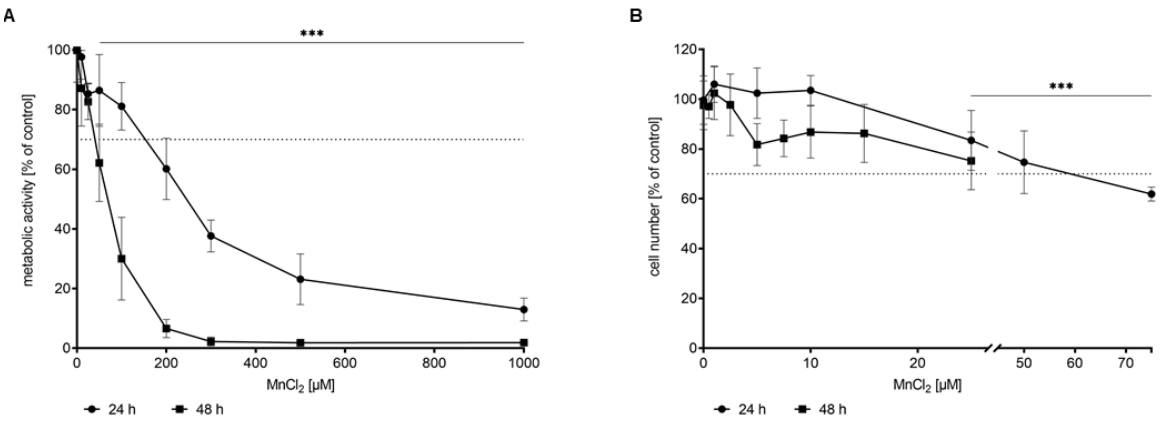

C

EC_{30} [µM]		
	Resazurin (metabolic activity)	Hoechst (cell number)
24 h	150	58
48 h	40	> 25

Figure 24 Cytotoxicity assessment of LUHMES cells after 24 h and 48 h Mn overexposure. [A] The metabolic activity measured via the resazurin reduction assay decreases dose- and time-dependently after $MnCl_2$ incubation. [B] Measurement of the cell number via the Hoechst assay indicates a decrease of cell number that is concentration-, but not time-dependent. [C] Comparison of the EC_{30} levels of the different endpoints. Data are expressed as means ± SD of at least six independent experiments. For statistical analysis, the 2way ANOVA with Dunnett´s multiple comparisons test was performed.

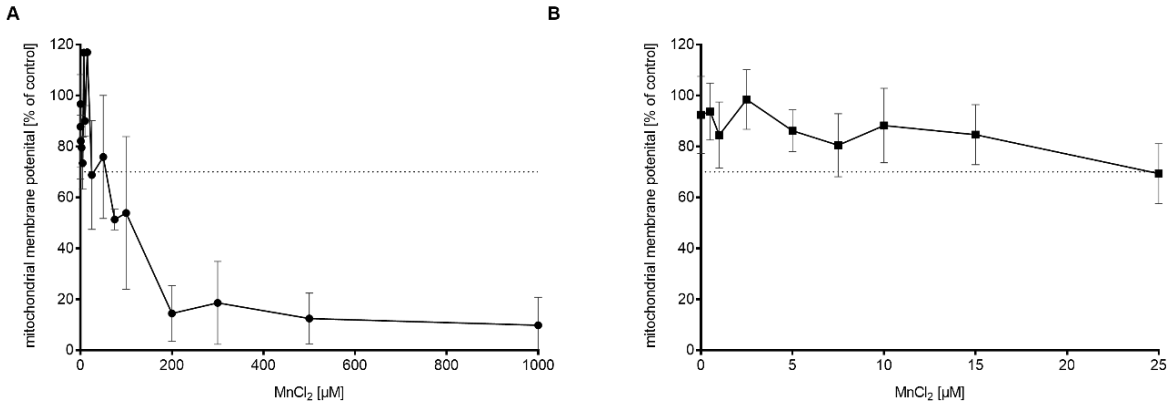

Figure 25 Measurement of mitochondrial membrane potential using MitoTracker™ Orange. Results show a dose-dependent decrease of the mitochondrial membrane potential after [A] 24 h and [B] 48 h $MnCl_2$ incubation of differentiated LUHMES cells. Data are expressed as means ± SD of at least six independent experiments.

6.3.2 Mn overexposure reduces the DNA integrity of post-mitotic neurons

Oxidative DNA damage is a major adverse outcome of oxidative stress, causing genomic integrity to be in jeopardy. An imbalance of antioxidant systems and oxidative stress can induce increased interactions of RONS with macromolecules such as DNA, causing DNA damage [7, 333]. While genomic stability is immensely important in cells that still undergo mitosis and meiosis (e. g. germline cells), it is equally important in post-mitotic cells, which are irreversibly withdrawn from the cell cycle [337, 338]. DNA damage can occur in the nuclei and even more in mitochondrial DNA. The latter is especially important for neuronal cells, due to their high mitochondrial mass and great energy dependence [382, 383]. A slow build-up of DNA damage in the genome causes loss of information that transfers from DNA to proteins. This could increase the transcription of defective proteins, their accumulation, cell death, and eventually neurodegeneration and disease [382, 384]. For this study, we decided to investigate DNA damage in the entirety of the neurons, not only mitochondrial DNA modifications, to elucidate the effect of Mn on the DNA integrity of the whole post-mitotic cell. For this, differentiated LUHMES cells were again exposed to Mn for 48 h at sub-toxic and toxic concentrations. First, 8oxodG was analytically quantified by HPLC-MS/MS, after isolating and hydrolysing the DNA of $MnCl_2$ incubated cells. The simultaneous quantification of the cytosine content allowed normalization to the respective hydrolysis rate as well as the actual DNA content. 8oxodG is the most investigated and likely the most frequently occurring oxidative DNA base modification, due to the low oxidation potential of guanine [385]. The interaction of singlet oxygen with guanine leads to the formation of 8oxodG and 8-hydroxyguanosine (8OHdG), which are in equilibrium with each other and are equally used as biomarkers in both *in vitro* and *in vivo* studies [92, 341, 342]. The results of the analytical quantification show that exposure of differentiated LUHMES cells to Mn caused a linear increase of the DNA damage, which is significantly different at 40 µM $MnCl_2$ compared to non-incubated cells (Figure 26). At this concentration, the level of oxidative DNA damage is three times higher as compared to control cells. If repaired, 8oxodG, and other oxidative DNA modifications, are repaired mainly via base excision repair (BER), which causes single-strand breaks as repair intermediates [386]. The damaged bases are excised by glycosylases, leaving apurinic/ apyrimidinic (AP) sites, which are then processed further by endonucleases to DNA single-strand breaks before being repaired by further BER repair enzymes [311, 339, 340]. Apart from DNA repair, strand breaks can be caused

directly by exogenous or endogenous sources and can lead to loss of information and mutations, DNA-protein crosslinks, and alterations of the secondary DNA structure [127-129]. Quantifying the percentage of double-stranded DNA (dsDNA) and thereby strand breaks per cell using the alkaline unwinding assay allows us to draw conclusions regarding the overall genomic integrity. In Mn-incubated cells, again for 48 h, a high increase of DNA strand breaks is detectable compared to control cells, already starting at 10 µM MnCl2 (Figure 27 (A)). Exposure to 20 µM $MnCl_2$ caused a further increase to $4*10^3$ strand breaks per cell. Doubling the incubation concentration does not further increase the damage and a plateau is reached with 50% dsDNA. When looking at the time-dependent effect of Mn exposure, a coherence is visible between the amount of strand breaks and exposure time. The neurons were incubated with 20 µM $MnCl_2$ for 0 h, 2 h, 4 h, 8 h, 24 h, or 48 h and the data suggest a consistent increase of DNA strand breaks and decrease of dsDNA (Figure 27 (B)). The results of both genotoxicity endpoints indicate significant induction of DNA strand breaks and oxidative DNA damage 8oxodG. These results are in line with other *in vitro* [9, 10, 338] and *in vivo* [346] studies that investigated DNA damage (DNA strand breaks and DNA base modifications) after Mn exposure, employing the alkaline COMET assay or analytical and immunohistochemical analysis of oxidative base modification.

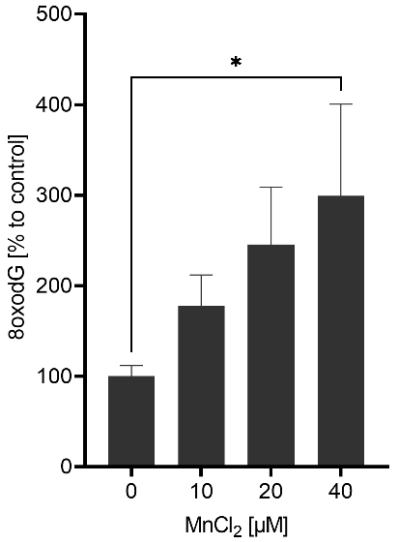

Figure 26 Induction of 8oxodG formation in LUHMES cells after 48 h Mn exposure. The increased formation of 8oxodG was measured analytically via HPLC-MS/MS. Sub-toxic (10 µM – 20 µM $MnCl_2$) and toxic (40 µM $MnCl_2$) concentrations of Mn cause a dose-depend increase of oxidative DNA damage that is significantly higher at 40 µM $MnCl_2$ compared to control cells. Data are expressed as means ± SD of at least six independent experiments. For statistical analysis, the ordinary one-way ANOVA with Dunnett´s multiple comparisons test was performed.

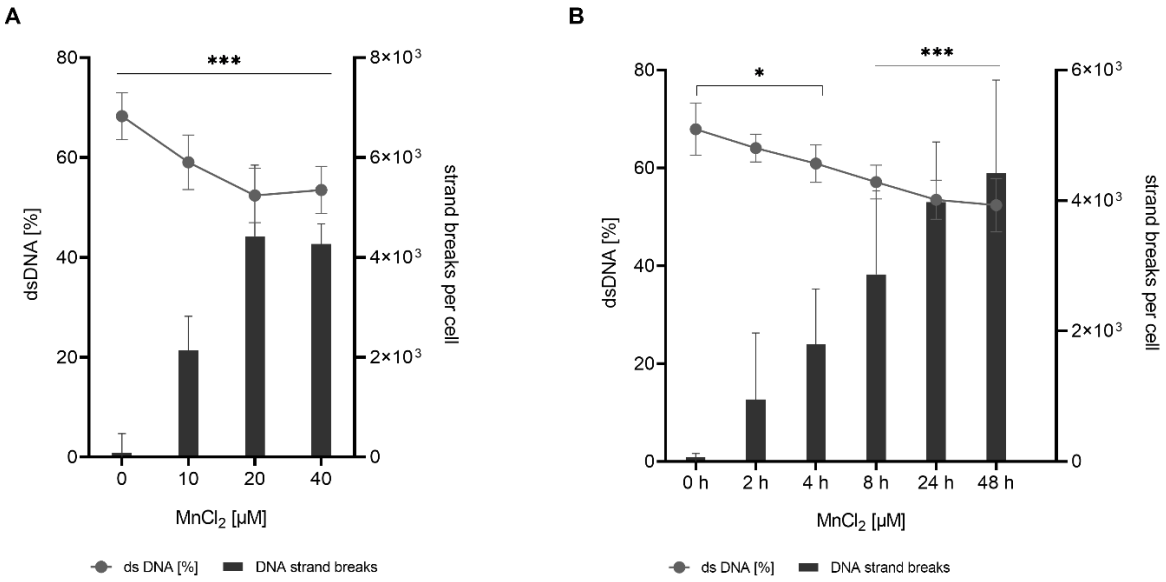

Figure 27 Measurement of dsDNA [%] and strand breaks per cell using the alkaline unwinding assay as marker for genomic integrity. [A] Differentiated LUHMES cells were exposed to 0 µM, 10 µM, 20 µM and 40 µM $MnCl_2$ for 48 h. [B] Differentiated LUHMES cells were incubated with 20 µM $MnCl_2$ for different exposure times (0 h, 2 h, 4 h, 8 h, 24 h, and 48 h). Data are expressed as means ± SD of at least nine independent experiments. For statistical analysis, the 2way ANOVA with Dunnett´s multiple comparisons test was performed.

6.3.3 Induction of the DNA damage response and increased DNA repair gene expression are results of Mn overexposure

Unrepaired DNA damage may trigger cell death, making an effective DNA repair crucial for neuronal survival. The DNA damage response involves different pathways and genes responsible for sensing and responding to DNA damage and therefore initializing DNA repair, apoptosis, and in case of proliferating cells cell cycle regulation [387]. Poly(ADP-ribose) (PAR) signalling is one of the first activated pathways upon DNA damage and is needed to ensure access of repair protein to the DNA lesion in the otherwise tightly packed DNA double-helix [388, 389]. The PAR polymerase (mainly PARP1) recognizes and binds to DNA lesions, and then catalyses the formation of PAR chains on close-by histones and itself [390-392]. These PAR chains can act as binding platforms for downstream pathway proteins, e.g. XRCC1, which initializes the DNA repair [393]. Relative PAR levels can be analytically quantified as a measure of the onset of the early DNA damage response. Results of this study showed that PARylation in 10 µM and 40 µM $MnCl_2$-treated differentiated LUHMES cells were significantly higher compared to non-

incubated cells, indicating a response to DNA damage (Figure 28 (A)). PARylation has also been identified as a sensitive endpoint in other brain cells. Previous studies in astrocytes identified an efficient disturbance of PARylation upon Mn exposure [366]. Gene expression studies allow the conclusion that the increased levels of PARylation in Mn-exposed LUHMES might be regulated by enzyme activity or protein translation; not on RNA level. The gene expression analysis of PARP1 and genes involved in base and nucleotide excision repair showed no significant changes in Mn-exposed cells compared to controls (Figure 28 (B)). A slight increase in gene expression can be detected for OGG1, which encodes for the bifunctional 8-oxoguanine DNA glycosylase. This glycosylase removes 8oxodG and initializes the base excision repair by nicking the DNA backbone [394]. There is evidence that OGG1 is involved in the repair of oxidative damage in neurons and high gene expression levels were found in the *substantia nigra* of patients suffering from neurodegenerative diseases [395]. The results of this study indicate that Mn does not have a strong effect on OGG1 but further studies are needed to confirm the results on a protein and enzyme activity level.

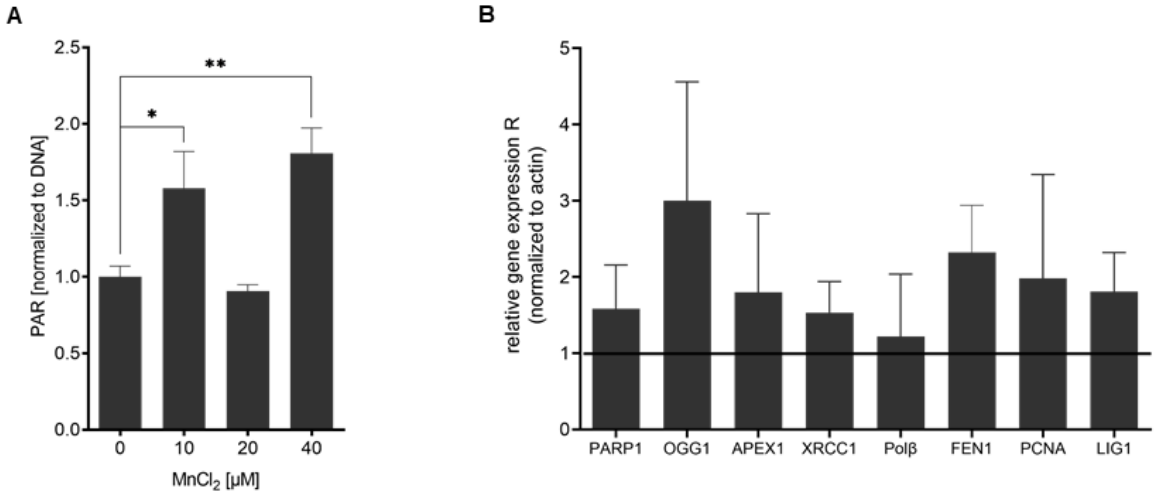

Figure 28 Analysis of DNA damage response and DNA repair in differentiated LUHMES cells upon Mn exposure. [A] Analytical measurement of relative PAR induction after 48 h MnCl2 (10 µM – 40 µM) exposure via HPLC-MS/MS. [B] Measurement of relative gene expression of DNA damage response and BER-involved genes after 48 h incubation with 20 µM MnCl2. Data are expressed as means ± SD of at least four (A) or three (B) independent experiments. For statistical analysis, the unpaired t-test was performed.

6.3.4 Decreased tubulin expression indicate Mn caused neurodegeneration

Immunofluorescence staining of the neuronal cytoskeleton protein βIII-tubulin was used to investigate the adverse effects of Mn on the neurite network. Maintenance of the long intercellular synaptic connections is required for the propagation of electrochemical signals across vast cellular distances [396]. Changes in the synaptic morphology are linked to neurodegeneration and adverse changes can be observed in patients with Parkinson´s disease [397, 398]. Differentiated LUHMES cells are well suitable for neurite toxicity testing, as they form extensive dendrite outgrowth and neuronal networks [231, 232]. The immunofluorescence staining of cells incubated with 20 µM or 40 µM $MnCl_2$ for 48 h showed a significant decrease compared to non-incubated cells (Figure 29 (A)). Both concentrations caused a relative decrease of around 20%. The degradation of the neurite network is also visible in the exemplary microscopic pictures shown in Figure 29 (B). The results indicate an adverse effect of Mn on the tubulin expression and therefore neuronal network. These results are in line with observations by Stanwood *et al.* 2009 that showed that acute Mn exposure induces early and profound changes in neurite length and integrity of primary mesencephalic culture cells at sub-toxic Mn concentrations (100 µM $MnCl_2$) [399].

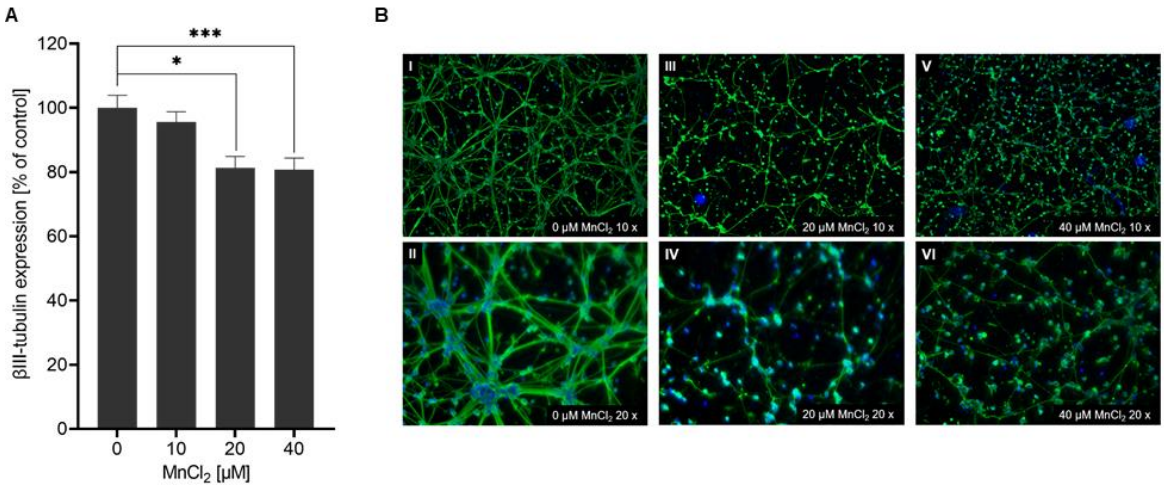

Figure 29 Immunofluorescence staining of βIII-tubulin for assessment of neurite mass. [A] Semi-automatic measurement of the relative βIII-tubulin expression in immunofluorescence-stained differentiated cells. LUHMES were incubated for 48 h with 0 µM, 10 µM, 20 µM or 40 µM MnCl2. Data are expressed as means ± SD of at least 2 independent experiments. For statistical analysis, the ordinary one-way ANOVA with Dunnett´s multiple comparisons test was performed. [B] Representative microscopic images of the neuronal network of LUHMES cells after 48 h Mn exposure with 0 µM (I + II), 20 µM (III + IV), and 40 µM (V + VI) $MnCl_2$. βIII-tubulin was stained with TUBB3 and Alexa Fluor® 488 (portrayed in green) and nuclei using DAPI (portrayed in blue). 10 x and 20 x objectives were used.

6.4 Conclusion

Mn is a ubiquitous trace element and due to increased industrial use, rising exposure to the transition metal is unavoidable. While Mn overexposure has been linked to neurodegeneration before, understanding the underlying neurotoxic mechanisms is imperative. Utilising the LUHMES cell line allowed us to investigate the adverse effects of Mn on dopaminergic-like neurons. Determination of bioavailability and cytotoxicity of $MnCl_2$ allowed us to find the right dosing regimen for investigations of Mn-induced DNA damage and DNA damage response/ DNA repair. Additionally, the results indicate that mitochondria function is disturbed, which can be both a consequence and cause of RONS. An increase of 8oxodG and a decrease of the dsDNA in Mn-exposed cells indicate a loss of genomic integrity. While the DNA damage response was triggered by Mn exposure, gene expression studies revealed only minor alterations in BER-involved genes. The neurite network, assessed via immunofluorescence staining of tubulin, on the other hand, showed significant adverse changes induced by Mn. Altogether, the results of this study are shedding more light on the underlying mechanisms of Mn-induced neurotoxicity. The outcome of the investigations confirms the hypothesis that Mn at high exposure leads to increased genomic instability. Future studies of specific endpoints of oxidative stress could help to understand the nature of Mn-induced RONS. For a deeper insight, studies of repair enzyme expression and activity levels are required. Especially the link between genomic instability and the degradation of the neurite network is of high interest and will be the focus of follow-up repair studies to understand the persistence and consequences of DNA damage in more detail.

6.5 Acknowledgement

We thank Prof. Dr. Marcel Leist (University of Konstanz) and Prof. Dr. Stefan Schildknecht (Albstadt-Sigmaringen University) for providing the LUHMES cells and tips and tricks on their handling. This work was supported by the DFG Research Unit TraceAge (FOR 2558, BO4103/4-2). Additional funding was obtained from the DFG project BO4103/2-1.

6.6 Author Contributions

Experiments were designed by JB and BW, and mostly performed by BW, SF, and MMN. MM and LHA conducted the experiments regarding bioavailability and PARylation. FE performed the gene expression studies. Data analysis and interpretation were done by MMN. JB and MMN conceptualized the study and wrote the manuscript. VM and TS contributed to data interpretation, helped with ideas for experimental setup, and revised the manuscript critically for important intellectual content. All authors were involved in compiling the manuscript and approved the final version. JB and TS rendered this work possible.

Chapter 7

General Discussion and Future Perspectives

7. General Discussion and Future Perspectives

The association of the trace element Mn and neurodegeneration has been shown in various *in vitro*, *in vivo,* and epidemiological studies. High Mn exposure is associated with various adverse neurological effects. In physiological ranges, the trace element is needed for a large number of cellular processes, and exposure is omnipresent in food, drinking water, occupational settings, or the environment. A deficiency has therefore not been reported for the general population. Chronic overexposure, on the other hand, is of higher importance, not only in an occupational setting but also for vulnerable population groups discussed in Chapter 2.4 [132, 140, 166, 167, 321].

This work was conducted to elucidate the underlying mechanisms of oxidative stress, DNA damage, DNA repair, and their functional interaction in Mn-induced neurodegeneration. In that process, it was pursued to utilise the multicellular model organism *C. elegans* as an alternative to the classic *in vitro* and *in vivo* systems for genotoxicity testing and provide a full test system for oxidative stress-mediated genotoxicity. Additionally, the dopaminergic-like LUHMES cell line was used to increase the focus of this research on underlying mechanisms of changes in DNA integrity and the resulting neuronal cell fate.

Before starting to investigate any adverse effects of Mn-induced neurotoxicity, the focus was set on establishing new and reliable methods for the analysis of oxidative stress and genomic integrity in the model organism *C. elegans*. While the nematode has many advantages, not at least being a multicellular and metabolizing organism, using the worm has the great drawback that it is not yet routinely used for oxidative stress and genotoxicity assessment. Validated methods for oxidative stress and DNA integrity endpoints are therefore still scarce.

7.1 CLox as a Highly Sensitive Oxidative Stress Biomarker in *C. elegans*

Oxidative stress is defined as a state where levels of oxidants exceed the detoxifying capacity of cellular antioxidant systems [25]. Oxidants are endogenous and/ or exogenous highly reactive species containing one or more unpaired electrons, namely free radicals. Due to their high reactivity, they pull electrons from other molecules to attain increased stability. Thereby the attacked molecules lose their electrons and become free radicals themselves. Thus starting a chain-reaction that can cause damage to cellular

macromolecules, like lipids, proteins and DNA [400]. These oxidative-stress induced damages of various cellular components can then induce impairment of many macromolecular functions and pathways, associated with numerous diseases, cell death pathways and other toxicity endpoints [240-242]. Investigating the oxidative stress status, its induction and target pathways, as well as possible endpoints, is not only important for mechanistic studies but is also of clinical relevance. Various different reactive species can exist in cells, and their location can be very specific to certain cellular compounds [401-403]. This causes the assessment of oxidative stress to be challenging. The target endpoints of RONS are diverse, site-specific and show different sensitivity, all depending on the nature of the oxidant [53, 404]. Many different oxidative stress biomarkers are routinely used for the assessment of oxidative stress *in vitro* and *in vivo* (an overview of some examples are given in chapter 2.1.1), but not all are relevant for every test substance or test system. Assessment of multiple endpoints is therefore always recommended to ensure a comprehensive investigation of the oxidative stress status. An additional factor influencing the choice of biomarker is the preference of the detection methods. On the one hand, using dyes usually has the advantage of being relatively easy and quick. On the other hand, staining can be less specific, radicals are often short-lived, and analyses are semi-quantitative. Analytical measurements are highly specific and quantitative, but the molecules of interest might not be stable enough for a reliable assessment [53-55]. Carefully weighing up possible biomarkers and developing better options for the assessment of oxidative stress is therefore of high priority.

By developing an online two-dimensional liquid chromatography method for measurements of the peroxidation of CL (described in Chapter 3), a sensitive and quantitative method for oxidative stress detection specific to the oxidation of lipids in the mitochondria of *C. elegans* was developed. CL possess a high level of unsaturation, making this biomarker a very early and sensitive indicator of RONS. Additionally, the fact that CL are exclusively mitochondrial-bound phospholipids might be especially of interest for substances like Mn that disrupt the respiratory chain resulting in an increase of RONS at the site of mitochondria [246, 247, 252]. CL activity is directly linked to mitochondrial activity, and their oxidation can cause mitochondrial dysfunction leading to subsequent failure of downstream processes and production of even more RONS [250, 253, 254]. Furthermore, CL oxidation impacts the production of ATP, which is needed for many cellular processes, like the DNA damage response or neurite outgrowth [100, 405,

406]. The HILIC pre-separation and heart-cut set-up increased the sensitivity and selectivity of this method needed for CLox detection, as they are usually low in abundance. This set-up also allowed to skip time-consuming sample preparation. The method was initially developed for *C. elegans* probes and proved to be a highly sensitive oxidative stress marker in nematodes, but can also be used for other *in vitro* or multicellular model/ animal model organisms. In addition, using the online two-dimensional LC method, we were able to investigate the cardiolipin distribution in *C. elegans* on a molecular level, something that has not been done in the nematode before and gives further insights into the mitochondrial membrane structure.

The method was then additionally adapted and altered to suit the selective analysis of sphingolipids in *C. elegans* (published by Scholz *et al.* in 2021) [407], which allows feasible, reproducible, and robust analysis of this lipid class. Sphingolipids exert many different cellular functions, e.g. stabilising of cell membranes and bioactive roles in cell signalling, and changes in the sphingolipid concentration are associated with cardiovascular diseases and neurodegeneration alike, making this an additional, new and relevant investigatory endpoint for many pathways [408], including metal-induced neurodegeneration [409].

Other popular oxidative stress biomarkers can likewise be used for investigations of RONS and assessment of their targets in *C. elegans*. The ratio of GSH and GSSG exemplarily can be measured analytically or via the biochemical redox assay described before [41, 52]. *In vivo* staining of the transparent worm by MitoTracker™ is another common method used for oxidative stress assessment in *C. elegans* [410]. Nevertheless, investigating CL distribution and its oxidation productions proved to be a highly sensitive and feasible oxidative stress marker in *C. elegans* which now can be used to investigate the underlying mechanisms of neurodegeneration and other oxidative stress-related pathologies in a multicellular organism. Especially for research on substances possibly disturbing mitochondria function (like Mn), this endpoint is of high relevance due to the exclusive existence of CL in mitochondria.

7.2 Genotoxicity Testing in *C. elegans* via Alkaline Unwinding

C. elegans has increasingly been used for toxicity testing in a wide variety of endpoints, but particularly genotoxicity assessment in the nematode is still scarce, despite the many advantages of *C. elegans* [315, 411, 412]. Classical genotoxicity testing relies on various

in vitro and *in vivo* methods that measure mutations, chromosomal aberrations, and in the case of indicator tests, DNA damage itself [75]. The advantage of these methods is that the experimental setup, as well as data interpretation, are described extensively in TGs. The fact that they are also routinely used adds to results comparability and high reproducibility [76]. Adding *C. elegans* as a test model for genotoxicity assessment might allow to overcome some of the limitations found in *in vitro* and animal experiments. Bacterial or cell culture experiments can give first insights into the genotoxic potential of substances, but their single-cell nature and lack of metabolism are diminishing their transferability to higher evolved organisms [291, 413]. *C. elegans* as a model organism is an experimental bridge between *in vitro* and animal models. The nematode is a multicellular, metabolizing organism that contains various cell types and tissues. Thus, one can conduct meaningful and more complex investigations without having to immediately opt for cost- and time-intensive animal experiments. Furthermore, utilising *C. elegans* might allow the reduction of unnecessary animal experiments [292, 293]. Currently, the only genotoxicity test included in *in vitro*/ *in vivo* OECD TGs that was adapted to *C. elegans* is the alkaline COMET assay [245] which is time-intensive, experimentally demanding, and hard to reproduce due to high background noise in worm samples. Additionally, during the method development for alkaline unwinding (Section 4.3.1), it was observed that *C. elegans* DNA is much more sensitive to the alkaline solution compared to DNA isolated from human cell pellets (HepG2 liver carcinoma cell line), which is in line with previous investigations by Park *et al.* [300]. Thus, it is likely that high amounts of DNA damage are readily artificially caused during the alkaline COMET assay, which includes a denaturation step at high pH. Opting for the neutral COMET assay for *C. elegans* probes might be an alternative but limits the DNA damage detection from simultaneous measurement of single-strand breaks, double-strand breaks and alkali labile sites to only DNA double-strand breaks. Depending on the test substance and its resulting kind of DNA damage, this might still be a very sensitive method to detect DNA damage on a single-cell level [71, 414, 415].

Other DNA damage detection methods in *C. elegans* rely on antibody staining (8OHdG or indirectly via the repair enzyme gene rad-51/ *cep-1*) or very indirectly by concluding the relative change of DNA damage from survival rates of transgenic strains lacking specific DNA repair enzymes [345, 416, 417]. The transparent body of the nematode allows *in vivo* fluorescence staining and enables visualisation of the damage location [309]. A practical

downside of being dependent on antibody staining is that many, if not most, antibodies do not bind specifically in *C. elegans* probes, and the demand for better *C. elegans* antibodies production is not strong enough yet. Utilising transgenic strains can provide information regarding possible DNA damage endpoints and underlying mechanisms but prohibits any assertions regarding the damage amount, kind, or location.

By establishing the AU assay in *C. elegans*, described in Chapter 4, we developed a method that can be used for preliminary high throughput screening, valuable follow up tests of positive *in vitro* results, genomic stability assessment, and mechanistic investigations. Thus, creating a rapid tool to better decide if a substance should be further investigated in animal experiments. AU is not part of the OECD guidelines, neither *in vitro* nor *in vivo*, but could be categorized as an indicator test. This method allows the detection of DNA strand breaks caused directly, via AP sites, or as a consequence of DNA repair, and can therefore be used to analyse the genotoxic potential of a wide variety of chemicals.

In future studies, it could be of high interest to extend the AU by a method including the bacterial-derived formamidopyrimidine-DNA glycosylase (FPG) protein as described by Hartwig *et al.* [418]. FPG is an enzyme that specifically cleaves 8OHdG (and to small amounts 8-hydroxy-adenine) and thus, in addition to generally detecting DNA strand breaks, also specifically oxidative DNA damage can be analysed. Other lesion-specific enzymes could likewise be used, as it is frequently done for COMET assays. Exemplarily, the endonuclease III (recognition of oxidised pyrimidines) and the 3-methyl-adenine DNA glycosylase II (detection of alkylated bases) can give valuable information on different kinds of DNA lesions, which might occur as a natural background "noise" or might be specifically induced by a genotoxic agent [419]. This is not only interesting for Mn-toxicity research but for genotoxicity assessment in *C. elegans* in general.

The germline of *C. elegans* offers a possibility for cell-specific genotoxicity investigations. In *C. elegans*, the germline is a distinct "compartment" with two U-shaped gonad arms, which have defined mitotic and meiotic regions, and gametes move through those regions during gametogenesis [336]. Fluorescent staining of DNA damage and DNA repair markers can be conducted to draw indirect conclusions about DNA integrity in the heritable germline cells at different stages of the gamete development [420]. In addition, by isolating and collecting the germline, one could quantify the DNA damage directly in the heritable germline cells using AU to quantify the DNA lesions.

The COMET and AU assay are the first of the classic genotoxicity tests adapted to *C. elegans*, but other assays (e.g. micronuclei test, mutation screening) could in principle be established for nematode probes as well. This could significantly improve the informative value and ethical conditions of genotoxicity testing and is therefore a main focus for further research.

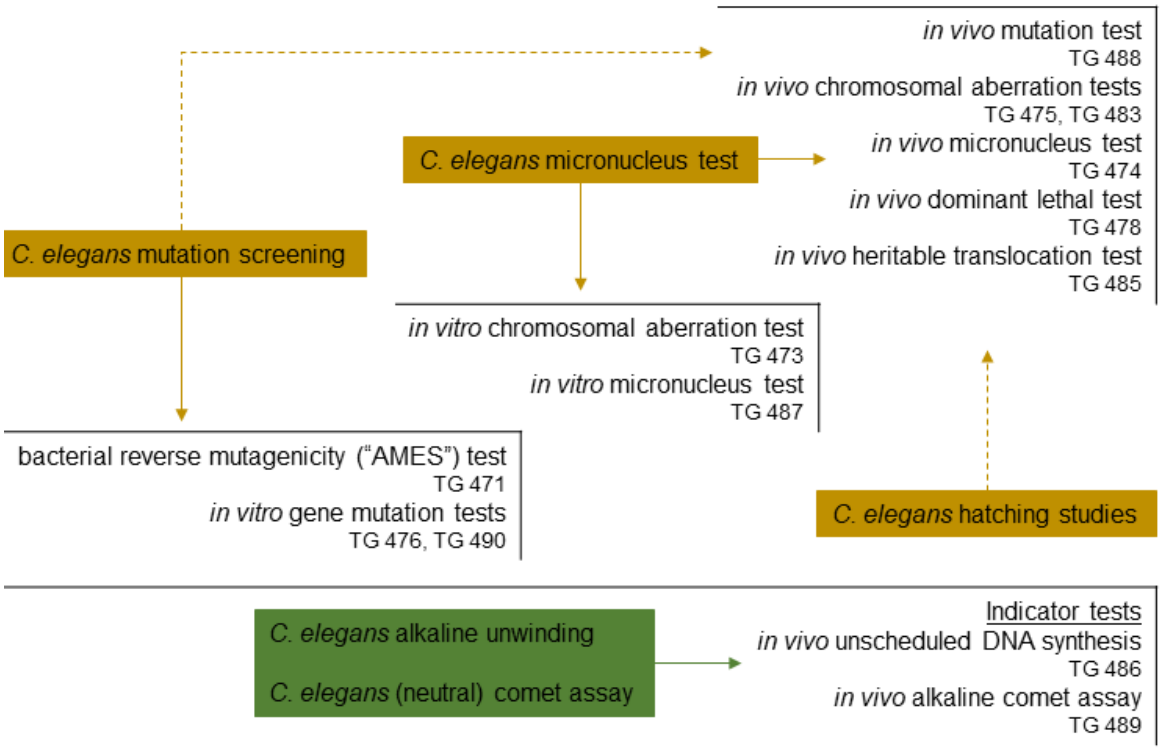

Figure 30 Overview of the OECD TGs for genotoxicity testing and possible *C. elegans* methods. Green: genotoxicity tests in *C. elegans* that are published and could be used as indicator tests. Yellow: methods that might be adaptable to *C. elegans* probes or are already used but not for genotoxicity assessment yet.

7.3 Investigations of Bioavailability, Oxidative Stress, DNA Integrity, and Survival after Mn Exposure in *C. elegans*

The second part of this research project focused on investigations of underlying mechanisms of Mn-induced neurotoxicity, focusing on oxidative stress and DNA integrity. By utilising *C. elegans*, we were able to conduct the research on a complete organism rather than individual single cell lines. Chapter 5 highlights the findings of DNA damage induction and DNA repair after Mn exposure. Before any mechanistic studies

were conducted, the bioavailability of Mn and survival rate after exposure were determined for optimal dose-finding for genotoxicity assessment. This is necessary for many reasons, including that genotoxins are expected to induce DNA damage at doses that do not trigger extensive cell death or the fact that genotoxicity might follow a non-linear dose-response relationship [329, 330]. Bioavailability strongly depends on the exposure scenario, larval stage, and compound species (reviewed in detail by Taylor *et al.* [221]) and should therefore always be determined before conducting further research. The results indicate not only a concentration-dependent but also a time-dependent uptake of Mn. This allowed us to reduce the exposure scenarios to only sub-toxic (50 mM $MnCl_2$) and toxic (100 mM, 250 mM $MnCl_2$) concentrations of Mn after 1 h of exposure.

Further bioavailability studies focusing on subcellular bioavailability and distribution could elucidate the cell compartment-specific Mn accumulation. This is especially interesting for mitochondria, as in the case of higher mitochondrial Mn accumulation, the levels of CLox should increase as well, causing a reduced mitochondrial function (as described in Section 7.1). Also of interest is the bioavailability and accumulation after long-term Mn incubation and the resulting adverse effects on genomic integrity, neurodegeneration, and possible adaptive effects. For this, incubation must be performed on agar plates covered with inactivated *E. coli* (as described by Baesler *et al.* [225]) rather than the incubation in liquid that was performed for the studies in Chapter 5, which might have the advantage of a more transferrable exposure scenario to other organisms [221].

The genotoxicity assessments (8OHdG and alkaline unwinding) indicate induction of DNA damage after Mn exposure, which is likely caused by Mn-induced oxidative stress shown in previous studies and different organisms [41, 183, 332]. While the results of the gene expression studies and analytical measurements of PAR indicate induction of DNA repair and increase of BER gene transcription after Mn exposure, specific functional deletion of single BER enzymes did not alter Mn-induced toxicity (as assessed by the survival rate). While these targeted investigations shed more light on oxidative-stress induced DNA damage and induction of PARylation, DNA repair and other stress mechanisms might need to be analysed in a more general way. Future studies should therefore focus on less-targeted investigations, for example, by transcriptomics, proteomics, or global post-translational modification analysis [421].

First transcriptome analyses have already been conducted in cooperation with Marcello Pirritano and Prof. Dr. Martin Simon (University of Wuppertal) and might indicate

improper protein folding as a consequence of Mn-induced oxidative stress and cause for decreased genomic integrity (data not shown) by inhibiting DNA repair, but the evaluation is still ongoing. In fact, the unfolded protein response under endoplasmic reticulum stress is associated with altered DNA damage and DNA repair [422]. Moreover, PARylation causes the formation of long, branched and negatively charged PAR chains [423] that might cause alterations of protein folding of close-by enzymes.

Another further research goal is direct investigations of the neurotoxicity of Mn and its link to other neurodegenerative diseases in a living organism. Previous studies showed that the neurotransmitter release is affected by Mn and that Manganism, Parkinson's disease and other neurodegenerative diseases are closely linked [13, 172, 173]. However, studies focused on DNA damage induction, and DNA repair in deletion mutants (e.g. *pdr-1, djr-1,* and *pink-1* gene deletions/ function knock-downs) could help to further understand similarities and differences of the underlying mechanisms [424]. In addition to investigating DNA integrity in Parkinson's-associated *C. elegans* mutant strains, investigating CLox in *pink-1* (human: *PINK-1*) and *pdr-1* (human: *PARKIN/ PARK-2*) could be of high relevance. These genes encode for enzymes that are located in mitochondrial membranes and are associated with mitochondrial quality control. Mutations in those genes are linked to mitochondrial damage [425]. Investigating changes in CLox status of single deletion strains or multiple deletion mutants (e.g. BER and Parkinson´s disease-relevant genes) compared to wild type worms might elucidate the nature of the mitochondrial dysfunction in (Mn-induced) neurodegeneration further.

7.4 Effects of Mn on Genome Integrity and Neurite Outgrowth in LUHMES Cells

Dopaminergic neurons were identified as a major target of Mn, and by utilising the LUHMES cell line, we were able to investigate the adverse effects of Mn specifically on dopaminergic-like neurons [13, 161, 162]. Similar to the studies performed in *C. elegans*, bioavailability and cytotoxicity of Mn in the LUHMES cells were determined to find the right dosing regimen for investigations of Mn-induced DNA damage, DNA damage response, and DNA repair. Additionally, the mitochondrial function was shown to be affected by Mn, which can be both a consequence and a cause of RONS formation [426]. Further investigations of the adverse effect of Mn on mitochondrial function can be achieved by quantifying the CLox levels, which can provide information about the

oxidative stress status in LUHMES cells after Mn exposure, as well as the functionality of the mitochondrial membrane (see Section 7.1).

DNA strand breaks were analysed utilising the AU assay, and by analytical measurements of 8oxodG, the oxidative DNA damage was quantified precisely. Both methods indicate an overall decrease in genomic integrity after Mn exposure and are therefore in line with the results in *C. elegans*. While the DNA damage response increased after Mn exposure, gene expression studies revealed only minor alterations in BER-involved genes, also shown in the nematode. This indicates that DNA repair is regulated on the level of protein activity instead of on the transcriptional level.

Significant adverse changes were observed in the tubulin expression upon Mn exposure, which indicates a strong reduction of the neurite network. Combining these results of the investigations in LUHMES cells confirms the hypothesis that high Mn exposure causes a decrease of genomic integrity by inducing DNA damage. The role of DNA repair could not yet be elucidated completely. Studies regarding the repair kinetics might deepen the understanding of the DNA damage response and DNA repair capacity. AU can be used to assess the progress of DNA damage control over time (e.g. every 30 min after exposure for a longer time period), as described by Fleck *et al.* [427].

Of particular interest is the possible link between decreased genomic integrity and the degradation of the neurite network. One possible mechanism could be the induction of PARylation accompanied by high cellular energy consumption, which causes a decrease of ATP and NAD^+ availability needed for neurite outgrowth and regeneration of neurites [406, 428]. Thus, investigating the cellular status of energy-related nucleotides (ADP, AMP, ATP, NAD^+, and NADH) and PARylation activity simultaneously could be of high importance.

The here presented results additionally raise the question of whether Mn-induced neurodegeneration can be counteracted. One possibility might be the use of N-acetyl cysteine (NAC), which is a potent RONS scavenger and antioxidant. NAC is a precursor of GSH and *in vitro* studies by Qian *et al.* showed that NAC induces neuronal differentiation and neurogenesis [429]. *In vivo*, NAC showed to increase the enzymatic and non-enzymatic antioxidant levels of rats and significantly reduce the oxidative stress in old animals [430], and a case-control study in Parkinson´s disease patients indicates that NAC has a positive effect on the dopaminergic system in conditions of

neurodegeneration in humans [431]. While these studies focus on the antioxidant capacity of NAC, it would be of high interest to investigate the status of DNA integrity in LUHMES exposed simultaneously and time-displaced to Mn and NAC, to study the specific role of oxidative stress in Mn-induced toxicity as well as the neuroprotective effect of NAC upon Mn exposure.

Appendix

Supporting Information

9.1 Supporting Information Chapter 3

Table 2 Detailed information of the 2D-LC method utilising a heart-cut setup.

Pump 1 (HILIC)			Pump 2 (RP)			Valve	
time/ min	*flow mL/min*	*% B*	*time/ min*	*Flow mL/min*	*% B*	*time/ min*	*Position*
0	0.3	97	0	0.3	70	0	A
0.2	0.3	97	8.2	0.3	90	5.75	B
0.5	0.3	93	20.2	0.3	100	6.3	A
2.75	0.3	93	23.7	0.3	100	7.8	B
7.5	0.3	60	24	0.3	70	24	A
11	0.3	60					
11.5	0.3	97					
14.0	0.3	97					
14.1	0.05	97					
21.9	0.05	97					
22.0	0.3	97					

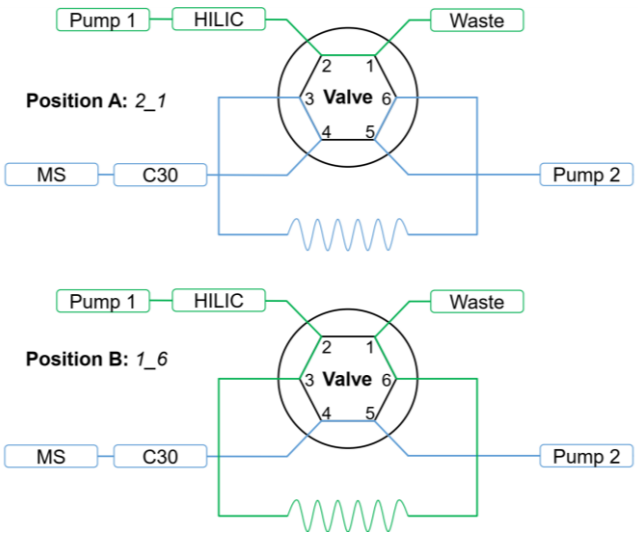

Figure 31 Overview of the used heart-cut setup by means of a dual gradient pump LC system and a six-port valve. In position A, 1D HILIC separation was carried out. By switching the valve to position B, the eluting analyte was transferred into a 400 µL sample loop. The analyte fraction was transferred to the RP column by switching the valve back to position A.

Table 3 Summary of identified cardiolipin species of *C. elegans* and oxidation products after *t*BOOH treatment Based on accurate mass (mass deviation less than ± 5 ppm) and MS/MS fragmentation experiments. The lipid nomenclature in this work is based on the recommendations of Liebisch *et al.* [263]. Fatty acyl (FA) composition of CL species are described as CL x:y, where x represents the total carbon number and y the total number of double bonds. CL 80:15 has a total number of 80 carbon atoms and 15 double bonds in total. Individual FA composition is specified using a slash for a specific position and an underscore were *sn*-1 and *sn*-2 position cannot be distinguished.

Identified CL species

Species	MS/MS	Ion	*m/z* exp	*m/z* calc	*δm/m* [ppm]	*rt* [min]
CL(74:7)	18:1/18:1/18:1_20:4	$[M-H]^-$	1478.0135	1478.0119	1.1	16.44
CL(74:8)	18:1_18:2/18:1_20:4	$[M-H]^-$	1475.9962	1475.9962	0.0	16.13
CL(74:9)	N/A	$[M-H]^-$	1473.9806	1473.9806	0.0	15.81
CL(74:10)	18:1_18:4/18:1_20:4	$[M-H]^-$	1471.9649	1471.9649	0.0	15.54
CL(74:11)	18:1_18:3_18:3_20:4	$[M-H]^-$	1469.9487	1469.9493	-0.4	15.20
CL(74:12)	N/A	$[M-H]^-$	1467.9344	1467.9336	0.5	14.97
CL(74:13)	N/A	$[M-H]^-$	1465.9190	1465.9180	0.7	14.70
CL(75:9)	17:1_20:3/18:1_20:4	$[M-H]^-$	1487.9966	1487.9962	0.2	16.11
CL(75:10)	17:1_20:4/18:1_20:4	$[M-H]^-$	1485.9803	1485.9806	-0.2	15.79
CL(75:11)	17:1_20:4/18:2_20:4	$[M-H]^-$	1483.9638	1483.9649	-0.8	15.46
CL(75:12)	15:1_20:3_20:4_20:4	$[M-H]^-$	1481.9475	1481.9493	-1.2	15.18
CL(75:13)	15:1_20:4/20:4/20:4	$[M-H]^-$	1479.9340	1479.9336	0.2	14.93
CL(76:9)	18:1/18:1/20:3_20:4	$[M-H]^-$	1502.0116	1502.0119	-0.2	16.29
	18:1_20:3/18:1_20:4					
CL(76:10)	18:1_20:4/18:1_20:4	$[M-H]^-$	1499.9963	1499.9962	0.1	15.99
CL(76:11)	18:1_20:4/18:2_20:4	$[M-H]^-$	1497.9800	1497.9806	-0.4	15.65
CL(76:12)	18:2_20:4/18:2_20:4*	$[M-H]^-$	1495.9641	1495.9649	-0.6	15.36
	18:1_18:2/20:3_20:4					
	18:2/18:2/20:4/20:4					
CL(76:13)	18:2_20:4/18:3_20:4*	$[M-H]^-$	1493.9482	1493.9493	-0.7	15.11
	18:4_20:4/18:1_20:4					
	18:2_18:3/20:4/20:4					
	18:1_18:4/20:4/20:4					
CL(76:14)	18:3_20:4/18:3_20:4	$[M-H]^-$	1491.9341	1491.9336	0.3	14.85
CL(76:15)	18:3_18:4_20:4_20:4	$[M-H]^-$	1489.9187	1489.9180	0.5	14.62
CL(77:9)	N/A	$[M-H]^-$	1516.0256	1516.0275	-1.3	16.69
CL(77:10)	18:1_20:4/19:1_20:4	$[M-H]^-$	1514.0119	1514.0119	0.0	16.35

Continuation Table 3

Species	MS/MS	Ion	*m/z* exp	*m/z* calc	*δm/m* [ppm]	*rt* [min]
CL(77:11)	18:3_19:1/20:3_20:4	$[M-H]^-$	1511.9952	1511.9962	-0.7	15.93
	17:1_20:3/20:3_20:4					
CL(77:12)	17:1_20:4/20:3_20:4	$[M-H]^-$	1509.9798	1509.9806	-0.5	15.66
	17:1_20:3/20:4/20:4					
	18:1_19:4/20:3_20:4					
	18:2_19:3/20:3_20:4					
	18:1_19:3/20:4/20:4					
CL(77:13)	17:1_20:4/20:4/20:4	$[M-H]^-$	1507.9638	1507.9649	-0.7	15.36
	18:2_19:3/20:4/20:4					
	18:2_20:4/19:3_20:4					
	19:3/19:3/19:3_20:4					
CL(77:13)+O	N/A	$[M-H]^-$	1523.9615	1523.9599	1.1	13.94
CL(77:14)	N/A	$[M-H]^-$	1505.9493	1505.9493	0.0	15.03
CL(77:15)	N/A	$[M-H]^-$	1503.9342	1503.9336	0.3	14.85
CL(78:10)	N/A	$[M-H]^-$	1528.0277	1528.0275	0.1	16.43
CL(78:11)	18:1_20:3/20:3_20:4	$[M-H]^-$	1526.0106	1526.0119	-0.8	16.07
CL(78:12)	18:1_20:3/20:4/20:4	$[M-H]^-$	1523.9956	1523.9962	-0.4	15.83
	18:1_20:4/20:3_20:4					
	18:2_20:3/20:3_20:4					
CL(78:13)	18:1_20:4/20:4/20:4	$[M-H]^-$	1521.9797	1521.9806	-0.6	15.53
	18:2_20:4/20:4_20:3					
	18:3_20:4/20:3/20:3					
CL(78:14)	18:3_20:4/20:3_20:4	$[M-H]^-$	1519.9639	1519.9649	-0.7	15.25
	18:2_20:4/20:4_20:4					
	18:1_20:4/20:4_20:5					
CL(78:14)+O	N/A	$[M-H]^-$	1535.9604	1535.9599	0.3	13.86
CL(78:15)	18:4_20:4/20:3_20:4	$[M-H]^-$	1517.9486	1517.9493	-0.5	15.00
	18:3_20:4/20:4/20:4					
	18:2_20:4/20:4_20:5					
CL(78:15)+O	N/A	$[M-H]^-$	1533.9448	1533.9442	0.4	13.63
CL(78:16)	18:4_20:4/20:4/20:4	$[M-H]^-$	1515.9341	1515.9336	0.3	14.77
CL(78:17)	N/A	$[M-H]^-$	1513.9166	1513.9180	-0.9	14.60
CL(79:11)	19:1_20:3/20:3_20:4	$[M-H]^-$	1540.0267	1540.0275	-0.5	16.56

Continuation Table 3

Species	MS/MS	Ion	*m/z* exp	*m/z* calc	*δm/m* [ppm]	*rt* [min]
CL(79:12)	19:1_20:4/20:3_20:4	$[M-H]^-$	1538.0119	1538.0119	0.0	16.18
	19:1_20:3/20:4/20:4					
CL(79:13)	19:1_20:4/20:4/20:4	$[M-H]^-$	1535.9950	1535.9962	-0.8	15.77
CL(79:14)	19:4_20:4/20:3/20:3	$[M-H]^-$	1533.9792	1533.9806	-0.9	15.48
	19:3_20:4/20:3_20:4					
	19:2_20:4/20:4/20:4					
CL(79:15)	19:4_20:4/20:3_20:4	$[M-H]^-$	1531.9639	1531.9649	-0.7	15.20
	19:3_20:4/20:4/20:4					
CL(79:15)+O	N/A	$[M-H]^-$	1547.9593	1547.9599	-0.3	13.82
CL(79:16)	19:4_20:4/20:4/20:4	$[M-H]^-$	1529.9492	1529.9493	-0.1	14.95
CL(80:12)	20:3/20:3/20:3/20:3	$[M-H]^-$	1552.0275	1552.0275	0.0	16.29
CL(80:13)	20:3_20:4/20:3_20:4	$[M-H]^-$	1550.0116	1550.0119	-0.2	16.00
CL(80:14)	20:3_20:4/20:3_20:4	$[M-H]^-$	1547.9951	1547.9962	-0.8	15.70
	20:3/20:3/20:4/20:4					
CL(80:14)+O	20:3_20:4:1/20:3_20:4	$[M-H]^-$	1563.9897	1563.9912	-0.9	14.16
CL(80:15)	20:3_20:4/20:4/20:4	$[M-H]^-$	1545.9791	1545.9806	-1.0	15.42
CL(80:15)+O	20:3_20:4/20:4:1_20:4	$[M-H]^-$	1561.9758	1561.9755	0.2	13.94
CL(80:16)	20:4/20:4/20:4/20:4	$[M-H]^-$	1543.9638	1543.9649	-0.7	15.14
	20:3_20:4:1/20:4/20:4					
CL(80:16)+O	20:4:1_20:4/20:4/20:4	$[M-H]^-$	1559.9608	1559.9599	0.6	13.79
CL(80:17)	20:4_20:5/20:4/20:4	$[M-H]^-$	1541.9473	1541.9493	-1.3	15.01

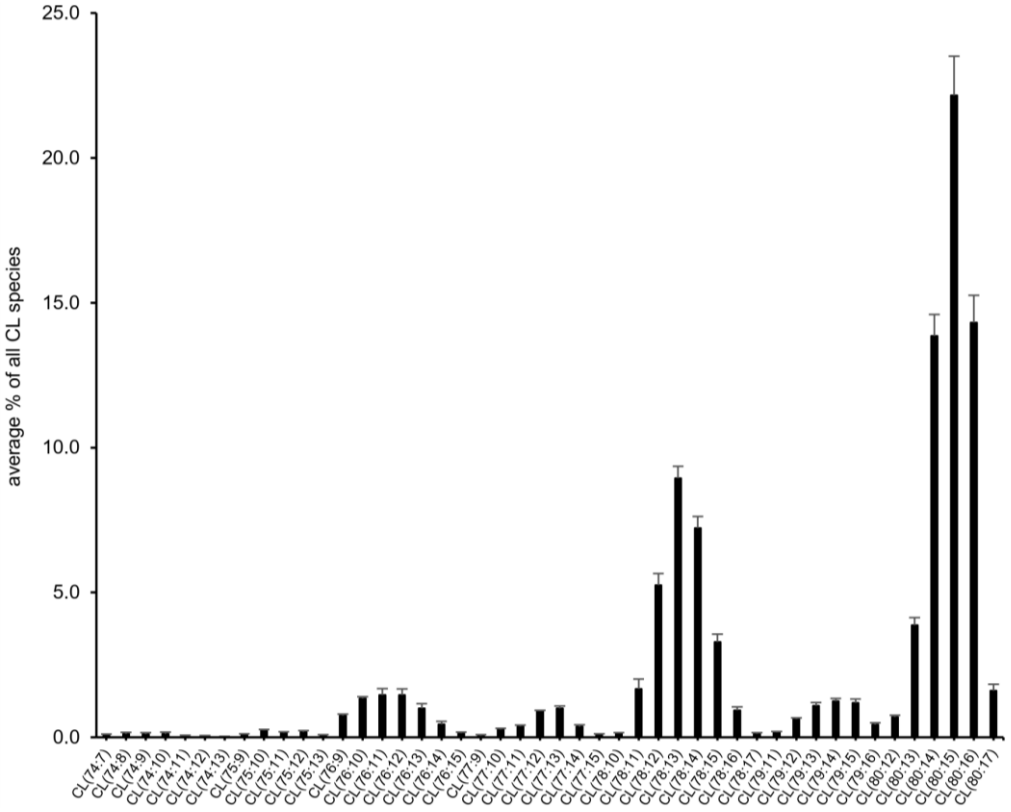

Figure 32 Overview of distribution of CL species in untreated *C. elegans* (WT).

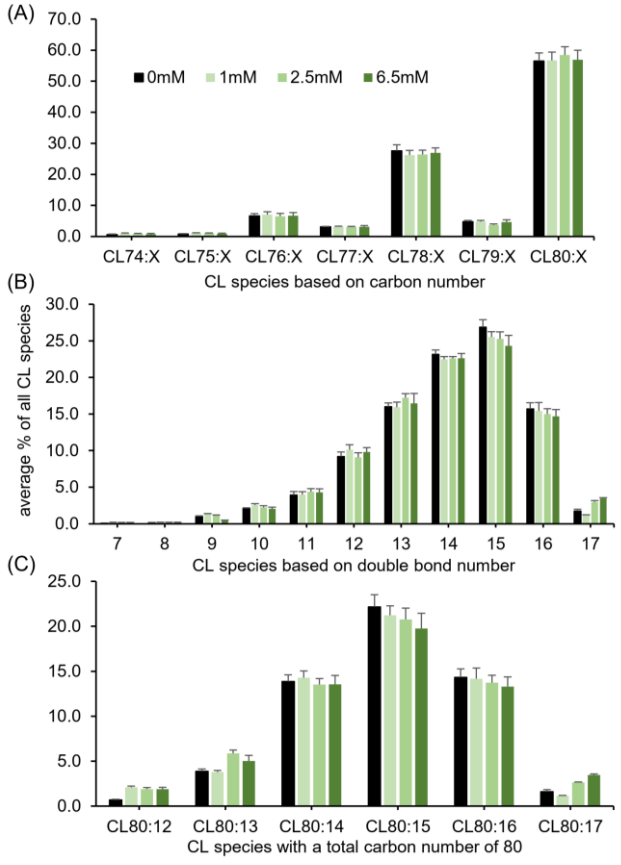

Figure 33 Comparison of CL species in untreated and with *t*BOOH treated *C. elegans*.

Table 4 Summary of CL distribution in treated and untreated *C. elegans* samples. Three biological replicates were analysed.

CL distribution mol % (n=3)

Species	Untreated	1 mM *t*BOOH	2.5 mM *t*BOOH	6.5 mM *t*BOOH
CL(74:7)	0.09 ± 0.02	0.20 ± 0.01	0.15 ± 0.03	0.16 ± 0.03
CL(74:8)	0.12 ± 0.05	0.20 ± 0.02	0.16 ± 0.04	0.19 ± 0.04
CL(74:9)	0.11 ± 0.05	0.19 ± 0.04	0.16 ± 0.05	0.16 ± 0.06
CL(74:10)	0.12 ± 0.06	0.16 ± 0.04	0.14 ± 0.05	0.12 ± 0.06
CL(74:11)	0.06 ± 0.01	0.10 ± 0.03	0.08 ± 0.04	0.06 ± 0.04
CL(74:12)	0.05 ± 0.01	0.08 ± 0.02	0.06 ± 0.03	0.04 ± 0.02
CL(74:13)	0.03 ± 0.01	0.04 ± 0.01	0.03 ± 0.02	0.02 ± 0.01
CL(75:9)	0.10 ± 0.02	0.21 ± 0.02	0.17 ± 0.01	0.13 ± 0.01
CL(75:10)	0.24 ± 0.03	0.35 ± 0.02	0.32 ± 0.03	0.27 ± 0.03
CL(75:11)	0.16 ± 0.04	0.21 ± 0.04	0.25 ± 0.03	0.19 ± 0.06
CL(75:12)	0.19 ± 0.04	0.24 ± 0.00	0.22 ± 0.02	0.21 ± 0.04
CL(75:13)	0.07 ± 0.03	0.08 ± 0.01	0.08 ± 0.02	0.08 ± 0.02
CL(76:9)	0.75 ± 0.05	0.79 ± 0.04	0.69 ± 0.03	0.81 ± 0.12
CL(76:10)	1.35 ± 0.06	1.72 ± 0.14	1.50 ± 0.14	1.61 ± 0.19
CL(76:11)	1.47 ± 0.22	1.53 ± 0.21	1.40 ± 0.20	1.43 ± 0.22
CL(76:12)	1.46 ± 0.20	1.48 ± 0.22	1.41 ± 0.24	1.41 ± 0.21
CL(76:13)	1.01 ± 0.16	0.98 ± 0.17	0.94 ± 0.17	0.92 ± 0.16
CL(76:14)	0.45 ± 0.10	0.41 ± 0.09	0.43 ± 0.09	0.40 ± 0.09
CL(76:15)	0.14 ± 0.04	0.14 ± 0.04	0.15 ± 0.05	0.12 ± 0.03
CL(77:9)	0.06 ± 0.03	0.13 ± 0.02	0.09 ± 0.03	0.07 ± 0.04
CL(77:10)	0.27 ± 0.05	0.33 ± 0.03	0.30 ± 0.03	0.25 ± 0.05
CL(77:11)	0.38 ± 0.04	0.46 ± 0.01	0.50 ± 0.02	0.48 ± 0.03
CL(77:12)	0.91 ± 0.02	0.91 ± 0.04	0.85 ± 0.05	0.90 ± 0.09
CL(77:13)	1.01 ± 0.07	0.95 ± 0.05	0.92 ± 0.06	0.97 ± 0.14
CL(77:13)+O	N/A	N/A	N/A	0.02 ± 0.02
CL(77:14)	0.37 ± 0.06	0.32 ± 0.07	0.33 ± 0.06	0.37 ± 0.13
CL(77:15)	0.09 ± 0.03	0.10 ± 0.02	0.09 ± 0.03	0.10 ± 0.05
CL(78:10)	0.15 ± 0.02	N/A	N/A	0.60 ± 0.07
CL(78:11)	1.68 ± 0.34	1.54 ± 0.13	2.14 ± 0.16	2.13 ± 0.21
CL(78:12)	5.25 ± 0.41	5.15 ± 0.35	4.66 ± 0.26	4.83 ± 0.36
CL(78:13)	8.95 ± 0.40	8.98 ± 0.53	8.34 ± 0.39	8.30 ± 0.57
CL(78:14)	7.23 ± 0.40	6.70 ± 0.32	7.02 ± 0.38	6.72 ± 0.28
CL(78:14)+O	N/A	0.07 ± 0.04	0.21 ± 0.09	0.33 ± 0.13
CL(78:15)	3.30 ± 0.27	2.96 ± 0.27	3.09 ± 0.20	3.00 ± 0.21
CL(78:15)+O	N/A	N/A	0.08 ± 0.03	0.11 ± 0.06

Continuation Table 4

Species	Untreated			1 mM *t*BOOH			2.5 mM *t*BOOH			6.5 mM *t*BOOH		
CL(78:16)	0.93	±	0.12	0.80	±	0.11	0.84	±	0.10	0.91	±	0.10
CL(78:17)	0.12	±	0.04	0.04	±	0.01	0.05	±	0.01		N/A	
CL(79:11)	0.18	±	0.03	0.15	±	0.01		N/A			N/A	
CL(79:12)	0.63	±	0.04	0.72	±	0.09		N/A		0.53	±	0.09
CL(79:13)	1.09	±	0.11	1.10	±	0.13	1.03	±	0.13	1.13	±	0.12
CL(79:14)	1.26	±	0.09	1.24	±	0.10	1.17	±	0.06	1.27	±	0.20
CL(79:15)	1.20	±	0.13	1.11	±	0.09	1.08	±	0.10	1.21	±	0.21
CL(79:15)+O		N/A			N/A			N/A		0.04	±	0.03
CL(79:16)	0.45	±	0.05	0.44	±	0.06	0.43	±	0.05	0.48	±	0.12
CL(80:12)	0.70	±	0.06	2.10	±	0.13	1.90	±	0.17	1.88	±	0.21
CL(80:13)	3.87	±	0.26	3.80	±	0.18	5.88	±	0.36	5.01	±	0.62
CL(80:14)	13.86	±	0.74	13.91	±	0.74	12.50	±	0.63	12.38	±	0.79
CL(80:14)+O		N/A		0.37	±	0.21	1.03	±	0.41	1.17	±	0.35
CL(80:15)	22.16	±	1.35	20.78	±	0.84	19.54	±	0.94	18.32	±	1.32
CL(80:15)+O		N/A		0.43	±	0.25	1.24	±	0.48	1.43	±	0.40
CL(80:16)	14.32	±	0.95	13.67	±	0.85	12.83	±	0.42	12.27	±	0.75
CL(80:16)+O		N/A		0.49	±	0.35	0.91	±	0.41	1.02	±	0.34
CL(80:17)	1.61	±	0.22	1.15	±	0.06	2.64	±	0.06	3.46	±	0.11

9.2 Supporting Information Chapter 5

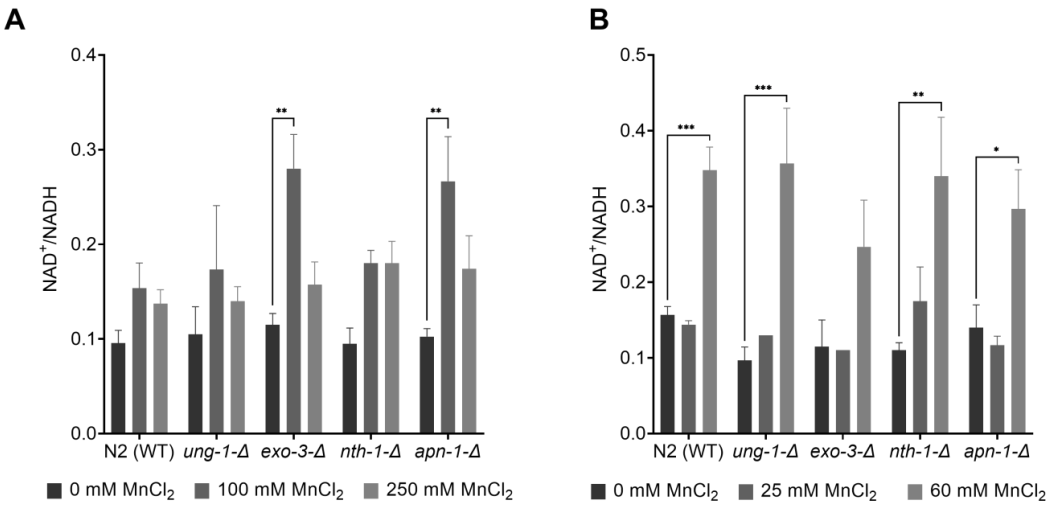

Figure 34 Changes of the NAD⁺/NADH ratio as measure of oxidative stress. Wild-type, N2 (WT), and BER-deletion mutants (*ung-1-Δ, exo-3-Δ, nth-1-Δ,* and *apn-1-Δ)* were incubated with $MnCl_2$ for [A] 1 h or [B] 4 h. Data are expressed as means ± SEM of at least three independent experiments. For statistical analysis, the unpaired t-test was performed.

9.3 Supporting Information Chapter 6

Table 5 Overview of the *m/z* transitions used for molecule identification and quantification in MRM modus of the HPLC-MS/MS method.

Analyte	*m/z*		RT [min]
	Q1	Q2	
8oxodG	284	168*	6.6
		139	
		112	
8-oxo-dG-^{13}C,-$^{15}N_2$	287	171*	6.6
		142	
		115	
dC	128	112*	5.5
		95	
dC-$^{15}N_3$	131	115*	5.5
		98	

* used as quantifier

Table 6 MS method parameters for the analytical quantification of 8oxodG/ dC via HPLC-MS/MS method.

Parameter		Parameter	
CUR	35	CAD	Medium
IS	5500	DP	70
TEM	450	EP	10
GAS1	50	CXP	10
GAS2	50		

Table 7 HPLC gradient flow used for the separation of 8oxodG/ dC.

time [min]	A [%]	B [%]	flow [L/ min]	Max pressure [bar]
0	95	5	0.3	400
5	40	60	0.3	400
6.9	30	70	0.3	400
7	20	80	0.3	400
8	20	80	0.3	400
11.2	95	5	0.3	400
14.3	95	5	0.3	400

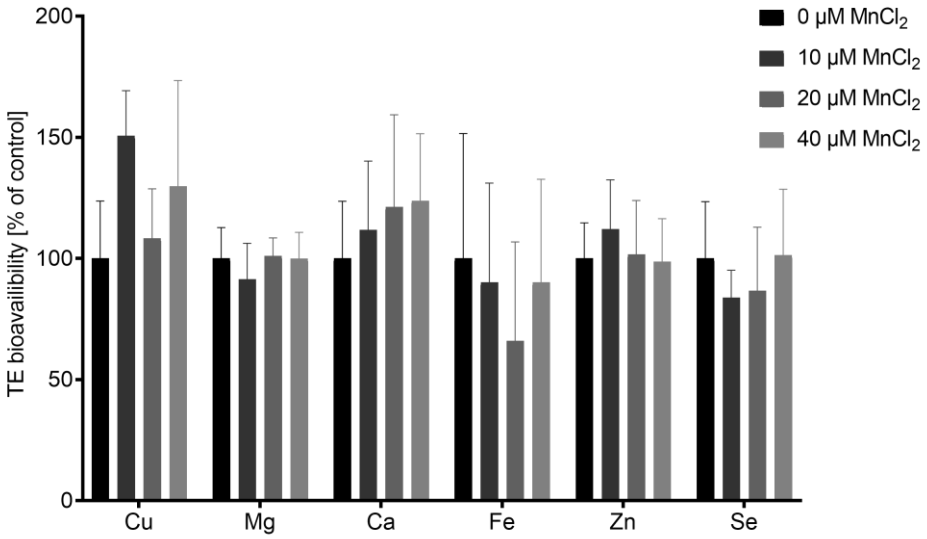

Figure 35 Comparison of the TE bioavailability after Mn exposure in differentiated LUHMES cells. Results indicate no changes in the bioavailability of copper, magnesium, calcium, iron, zinc, or selenium after 48 h exposure to 10 µM, 20 µM or 40 µM MnCl2. Data are expressed as means ± SD of at least two independent experiments.

References

1. EFSA Panel on Dietetic Products NaA. Scientific Opinion on Dietary Reference Values for manganese. EFSA Journal. 2013.
2. Caito S, Aschner M. Chapter 11 - Neurotoxicity of metals. In: Lotti M, Bleecker ML, editors. Handbook of Clinical Neurology. 131: Elsevier; 2015. p. 169-89.
3. Tinkov AA, Paoliello MMB, Mazilina AN, Skalny AV, Martins AC, Voskresenskaya ON, *et al.* Molecular Targets of Manganese-Induced Neurotoxicity: A Five-Year Update. Int J Mol Sci. 2021;22(9).
4. Erikson KM, Aschner M. Manganese: Its Role in Disease and Health. Met Ions Life Sci. 2019;19.
5. Li L, Yang X. The Essential Element Manganese, Oxidative Stress, and Metabolic Diseases: Links and Interactions. Oxid Med Cell Longev. 2018;2018:7580707-.
6. Smith MR, Fernandes J, Go YM, Jones DP. Redox dynamics of manganese as a mitochondrial life-death switch. Biochem Biophys Res Commun. 2017;482(3):388-98.
7. Poetsch AR. The genomics of oxidative DNA damage, repair, and resulting mutagenesis. Comput Struct Biotechnol J. 2020;18:207-19.
8. Ueda K, Okamoto Y, Aoki A, Jinno H. Catecholamine oxidation-mediated transcriptional inhibition in Mn neurotoxicity. J Toxicol Sci. 2020;45(10):619-24.
9. Stephenson AP, Schneider JA, Nelson BC, Atha DH, Jain A, Soliman KFA, *et al.* Manganese-induced oxidative DNA damage in neuronal SH-SY5Y cells: Attenuation of thymine base lesions by glutathione and N-acetylcysteine. Toxicology Letters. 2013;218(3):299-307.
10. Bornhorst J, Schwerdtle T. Chapter 24 DNA Damage Induced by Manganese. Manganese in Health and Disease: The Royal Society of Chemistry; 2015. p. 604-20.
11. Oikawa S, Hirosawa I, Tada-Oikawa S, Furukawa A, Nishiura K, Kawanishi S. Mechanism for manganese enhancement of dopamine-induced oxidative DNA damage and neuronal cell death. Free Radic Biol Med. 2006;41(5):748-56.
12. Flecknell P. Replacement, reduction and refinement. Altex. 2002;19(2):73-8.
13. Lin M, Colon-Perez LM, Sambo DO, Miller DR, Lebowitz JJ, Jimenez-Rondan F, *et al.* Mechanism of Manganese Dysregulation of Dopamine Neuronal Activity. The Journal of Neuroscience. 2020;40(30):5871-91.

14. Bowman AB, Kwakye GF, Herrero Hernández E, Aschner M. Role of manganese in neurodegenerative diseases. J Trace Elem Med Biol. 2011;25(4):191-203.
15. Fan XM, Luo Y, Cao YM, Xiong TW, Song S, Liu J, *et al.* Chronic Manganese Administration with Longer Intervals Between Injections Produced Neurotoxicity and Hepatotoxicity in Rats. Neurochem Res. 2020;45(8):1941-52.
16. Scholz D, Pöltl D, Genewsky A, Weng M, Waldmann T, Schildknecht S, *et al.* Rapid, complete and large-scale generation of post-mitotic neurons from the human LUHMES cell line. Journal of Neurochemistry. 2011;119(5):957-71.
17. Pizzino G, Irrera N, Cucinotta M, Pallio G, Mannino F, Arcoraci V, *et al.* Oxidative Stress: Harms and Benefits for Human Health. Oxid Med Cell Longev. 2017;2017:8416763-.
18. Rajendran P, Nandakumar N, Rengarajan T, Palaniswami R, Gnanadhas EN, Lakshminarasaiah U, *et al.* Antioxidants and human diseases. Clin Chim Acta. 2014;436:332-47.
19. Pacher P, Beckman JS, Liaudet L. Nitric oxide and peroxynitrite in health and disease. Physiol Rev. 2007;87(1):315-424.
20. Genestra M. Oxyl radicals, redox-sensitive signalling cascades and antioxidants. Cell Signal. 2007;19(9):1807-19.
21. Dröge W. Free radicals in the physiological control of cell function. Physiol Rev. 2002;82(1):47-95.
22. Deponte M. Glutathione catalysis and the reaction mechanisms of glutathione-dependent enzymes. Biochim Biophys Acta. 2013;1830(5):3217-66.
23. Birben E, Sahiner UM, Sackesen C, Erzurum S, Kalayci O. Oxidative stress and antioxidant defense. World Allergy Organ J. 2012;5(1):9-19.
24. Shahidi F, Zhong Y. Novel antioxidants in food quality preservation and health promotion. European Journal of Lipid Science and Technology. 2010;112(9):930-40.
25. Kohen R, Nyska A. Oxidation of biological systems: oxidative stress phenomena, antioxidants, redox reactions, and methods for their quantification. Toxicol Pathol. 2002;30(6):620-50.
26. Sato H, Shibata M, Shimizu T, Shibata S, Toriumi H, Ebine T, *et al.* Differential cellular localization of antioxidant enzymes in the trigeminal ganglion. Neuroscience. 2013;248:345-58.
27. Goldstein S, Meyerstein D, Czapski G. The Fenton reagents. Free Radic Biol Med. 1993;15(4):435-45.

28. van Genuchten CM, Peña J. Mn(II) Oxidation in Fenton and Fenton Type Systems: Identification of Reaction Efficiency and Reaction Products. Environ Sci Technol. 2017;51(5):2982-91.
29. Datta K, Suman S, Kallakury BV, Fornace AJ, Jr. Exposure to heavy ion radiation induces persistent oxidative stress in mouse intestine. PLoS One. 2012;7(8):e42224.
30. Valko M, Rhodes CJ, Moncol J, Izakovic M, Mazur M. Free radicals, metals and antioxidants in oxidative stress-induced cancer. Chem Biol Interact. 2006;160(1):1-40.
31. Ozguner F, Koyu A, Cesur G. Active smoking causes oxidative stress and decreases blood melatonin levels. Toxicol Ind Health. 2005;21(1-2):21-6.
32. Clavo B, Rodríguez-Esparragón F, Rodríguez-Abreu D, Martínez-Sánchez G, Llontop P, Aguiar-Bujanda D, *et al.* Modulation of Oxidative Stress by Ozone Therapy in the Prevention and Treatment of Chemotherapy-Induced Toxicity: Review and Prospects. Antioxidants (Basel). 2019;8(12).
33. Rumgay H, Murphy N, Ferrari P, Soerjomataram I. Alcohol and Cancer: Epidemiology and Biological Mechanisms. Nutrients. 2021;13(9).
34. Sarkar S, Yadav P, Bhatnagar D. Lipid peroxidative damage on cadmium exposure and alterations in antioxidant system in rat erythrocytes: a study with relation to time. Biometals. 1998;11(2):153-7.
35. Desai SN, Farris FF, Ray SD. Lipid Peroxidation. In: Wexler P, editor. Encyclopedia of Toxicology (Third Edition). Oxford: Academic Press; 2014. p. 89-93.
36. Zhang Y, Dai M, Yuan Z. Methods for the detection of reactive oxygen species. Analytical Methods. 2018;10(38):4625-38.
37. Kuznetsov AV, Kehrer I, Kozlov AV, Haller M, Redl H, Hermann M, *et al.* Mitochondrial ROS production under cellular stress: comparison of different detection methods. Anal Bioanal Chem. 2011;400(8):2383-90.
38. Ayuda-Durán B, González-Manzano S, González-Paramás AM, Santos-Buelga C. Caernohabditis elegans as a Model Organism to Evaluate the Antioxidant Effects of Phytochemicals. Molecules. 2020;25(14):3194.
39. Chakraborty S, Bornhorst J, Nguyen TT, Aschner M. Oxidative stress mechanisms underlying Parkinson's disease-associated neurodegeneration in *C. elegans*. Int J Mol Sci. 2013;14(11):23103-28.
40. Urban N, Tsitsipatis D, Hausig F, Kreuzer K, Erler K, Stein V, *et al.* Non-linear impact of glutathione depletion on *C. elegans* life span and stress resistance. Redox Biol. 2017;11:502-15.

41. Neumann C, Baesler J, Steffen G, Nicolai MM, Zubel T, Aschner M, *et al.* The role of poly(ADP-ribose) polymerases in manganese exposed *Caenorhabditis elegans*. J Trace Elem Med Biol. 2020;57:21-7.
42. Andrisic L, Dudzik D, Barbas C, Milkovic L, Grune T, Zarkovic N. Short overview on metabolomics approach to study pathophysiology of oxidative stress in cancer. Redox Biol. 2018;14:47-58.
43. Caito SW, Aschner M. Quantification of Glutathione in *Caenorhabditis elegans*. Curr Protoc Toxicol. 2015;64(618):6.18.1-6..6.
44. Livak KJ, Schmittgen TD. Analysis of relative gene expression data using real-time quantitative PCR and the 2(-Delta Delta C(T)) Method. Methods. 2001;25(4):402-8.
45. Mills MG, Gallagher EP. A targeted gene expression platform allows for rapid analysis of chemical-induced antioxidant mRNA expression in zebrafish larvae. PloS one. 2017;12(2):e0171025-e.
46. Corbisier P, Houbion A, Remacle J. A new technique for highly sensitive detection of superoxide dismutase activity by chemiluminescence. Anal Biochem. 1987;164(1):240-7.
47. Levine RL, Garland D, Oliver CN, Amici A, Climent I, Lenz AG, *et al.* Determination of carbonyl content in oxidatively modified proteins. Methods Enzymol. 1990;186:464-78.
48. Labuschagne CF, Stigter EC, Hendriks MM, Berger R, Rokach J, Korswagen HC, *et al.* Quantification of in vivo oxidative damage in *Caenorhabditis elegans* during aging by endogenous F3-isoprostane measurement. Aging Cell. 2013;12(2):214-23.
49. Rund KM, Ostermann AI, Kutzner L, Galano J-M, Oger C, Vigor C, *et al.* Development of an LC-ESI(-)-MS/MS method for the simultaneous quantification of 35 isoprostanes and isofurans derived from the major n3- and n6-PUFAs. Analytica Chimica Acta. 2018;1037:63-74.
50. Yue J, Wang P, Liu YH, Wu JY, Chen J, Peng RX. Fast evaluation of oxidative DNA damage by liquid chromatography-electrospray tandem mass spectrometry coupled with precision-cut rat liver slices. Biomed Environ Sci. 2007;20(5):386-91.
51. Hunter SE, Jung D, Di Giulio RT, Meyer JN. The QPCR assay for analysis of mitochondrial DNA damage, repair, and relative copy number. Methods (San Diego, Calif). 2010;51(4):444-51.

52. Wandt VK, Winkelbeiner N, Lossow K, Kopp JF, Schwarz M, Alker W, *et al.* Ageing-associated effects of a long-term dietary modulation of four trace elements in mice. Redox Biol. 2021;46:102083-.
53. Marrocco I, Altieri F, Peluso I. Measurement and Clinical Significance of Biomarkers of Oxidative Stress in Humans. Oxid Med Cell Longev. 2017;2017:6501046-.
54. Sidorova Y, Domanskyi A. Detecting Oxidative Stress Biomarkers in Neurodegenerative Disease Models and Patients. Methods Protoc. 2020;3(4).
55. Thérond P, Bonnefont-Rousselot D, Davit-Spraul A, Conti M, Legrand A. Biomarkers of oxidative stress: an analytical approach. Curr Opin Clin Nutr Metab Care. 2000;3(5):373-84.
56. Lu B, Yadav S, Shah PG, Liu T, Tian B, Pukszta S, *et al.* Roles for the Human ATP-dependent Lon Protease in Mitochondrial DNA Maintenance*. Journal of Biological Chemistry. 2007;282(24):17363-74.
57. Zmijewski JW, Moellering DR, Goffe CL, Landar A, Ramachandran A, Darley-Usmar VM. Oxidized LDL induces mitochondrially associated reactive oxygen/nitrogen species formation in endothelial cells. American Journal of Physiology-Heart and Circulatory Physiology. 2005;289(2):H852-H61.
58. Li Y, Zhu H, Kuppusamy P, Roubaud V, Zweier JL, Trush MA. Validation of lucigenin (bis-N-methylacridinium) as a chemilumigenic probe for detecting superoxide anion radical production by enzymatic and cellular systems. J Biol Chem. 1998;273(4):2015-23.
59. Song C, Mitter SK, Qi X, Beli E, Rao HV, Ding J, *et al.* Oxidative stress-mediated NFκB phosphorylation upregulates p62/SQSTM1 and promotes retinal pigmented epithelial cell survival through increased autophagy. PloS one. 2017;12(2):e0171940-
60. Kuzma M, Nyúl E, Mayer M, Fischer E, Perjési P. HPLC analysis of in vivo intestinal absorption and oxidative metabolism of salicylic acid in the rat. Biomedical Chromatography. 2016;30(12):2044-52.
61. Rahman I, Kode A, Biswas SK. Assay for quantitative determination of glutathione and glutathione disulfide levels using enzymatic recycling method. Nature Protocols. 2006;1(6):3159-65.
62. Weydert CJ, Cullen JJ. Measurement of superoxide dismutase, catalase and glutathione peroxidase in cultured cells and tissue. Nature protocols. 2010;5(1):51-66.
63. Alharby HF, Metwali EMR, Fuller MP, Aldhebiani AY. The alteration of mRNA expression of SOD and GPX genes, and proteins in tomato (Lycopersicon esculentum

Mill) under stress of NaCl and/or ZnO nanoparticles. Saudi Journal of Biological Sciences. 2016;23(6):773-81.

64. Barshishat-Kupper M, McCart EA, Freedy JG, Tipton AJ, Nagy V, Kim S-Y, *et al.* Protein Oxidation in the Lungs of C57BL/6J Mice Following X-Irradiation. Proteomes. 2015;3(3):249-65.
65. Chaudhuri AR, de Waal EM, Pierce A, Van Remmen H, Ward WF, Richardson A. Detection of protein carbonyls in aging liver tissue: A fluorescence-based proteomic approach. Mech Ageing Dev. 2006;127(11):849-61.
66. Vida C, de Toda IM, Cruces J, Garrido A, Gonzalez-Sanchez M, De la Fuente M. Role of macrophages in age-related oxidative stress and lipofuscin accumulation in mice. Redox Biol. 2017;12:423-37.
67. Rund KM, Heylmann D, Seiwert N, Wecklein S, Oger C, Galano JM, *et al.* Formation of trans-epoxy fatty acids correlates with formation of isoprostanes and could serve as biomarker of oxidative stress. Prostaglandins Other Lipid Mediat. 2019;144:106334.
68. Fang L, Teuchert M, Huber-Abel F, Schattauer D, Hendrich C, Dorst J, *et al.* MMP-2 and MMP-9 are elevated in spinal cord and skin in a mouse model of ALS. J Neurol Sci. 2010;294(1-2):51-6.
69. Muratori M, Tamburrino L, Marchiani S, Cambi M, Olivito B, Azzari C, *et al.* Investigation on the Origin of Sperm DNA Fragmentation: Role of Apoptosis, Immaturity and Oxidative Stress. Mol Med. 2015;21(1):109-22.
70. Weimann A, Belling D, Poulsen HE. Quantification of 8-oxo-guanine and guanine as the nucleobase, nucleoside and deoxynucleoside forms in human urine by high-performance liquid chromatography-electrospray tandem mass spectrometry. Nucleic Acids Res. 2002;30(2):E7-E.
71. Peycheva E, Georgieva M, Miloshev G. Comparison Between Alkaline and Neutral Variants of Yeast Comet Assay. Biotechnology & Biotechnological Equipment. 2009;23(1):1090-2.
72. Lindahl T, Barnes DE. Repair of endogenous DNA damage. Cold Spring Harb Symp Quant Biol. 2000;65:127-33.
73. Kawanishi S, Hiraku Y, Pinlaor S, Ma N. Oxidative and nitrative DNA damage in animals and patients with inflammatory diseases in relation to inflammation-related carcinogenesis. Biol Chem. 2006;387(4):365-72.
74. Erickson RP. Somatic gene mutation and human disease other than cancer: an update. Mutat Res. 2010;705(2):96-106.

75. Round GTGDSC. Guidance Document on Revisions to OECD Genetic Toxicology Test Guidelines. 2015.

76. OECD. Overview on genetic toxicology TGs2017.
77. Srinivas US, Tan BWQ, Vellayappan BA, Jeyasekharan AD. ROS and the DNA damage response in cancer. Redox Biol. 2019;25:101084.
78. Salehi F, Behboudi H, Kavoosi G, Ardestani SK. Oxidative DNA damage induced by ROS-modulating agents with the ability to target DNA: A comparison of the biological characteristics of citrus pectin and apple pectin. Scientific Reports. 2018;8(1):13902.
79. Shokolenko I, Venediktova N, Bochkareva A, Wilson GL, Alexeyev MF. Oxidative stress induces degradation of mitochondrial DNA. Nucleic Acids Res. 2009;37(8):2539-48.
80. EMA/CHMP/ICH. ICH guideline S2 (R1) on genotoxicity testing and data interpretation for pharmaceuticals intended for human use - Step 5. 2011.

81. Committee ES. Scientific opinion on genotoxicity testing strategies applicable to food and feed safety assessment. EFSA Journal. 2011;9(9):2379.
82. Phillips DH, Arlt VM. Genotoxicity: damage to DNA and its consequences. Exs. 2009;99:87-110.
83. Lindahl T, Nyberg B. Rate of depurination of native deoxyribonucleic acid. Biochemistry. 1972;11(19):3610-8.
84. Crow JF. The origins, patterns and implications of human spontaneous mutation. Nature Reviews Genetics. 2000;1(1):40-7.
85. Tubbs A, Nussenzweig A. Endogenous DNA Damage as a Source of Genomic Instability in Cancer. Cell. 2017;168(4):644-56.
86. Sedletska Y, Radicella JP, Sage E. Replication fork collapse is a major cause of the high mutation frequency at three-base lesion clusters. Nucleic Acids Res. 2013;41(20):9339-48.
87. Cooke MS, Evans MD, Dizdaroglu M, Lunec J. Oxidative DNA damage: mechanisms, mutation, and disease. The FASEB Journal. 2003;17(10):1195-214.
88. Fleming AM, Zhu J, Ding Y, Burrows CJ. 8-Oxo-7,8-dihydroguanine in the Context of a Gene Promoter G-Quadruplex Is an On–Off Switch for Transcription. ACS Chemical Biology. 2017;12(9):2417-26.

89. Wang R, Hao W, Pan L, Boldogh I, Ba X. The roles of base excision repair enzyme OGG1 in gene expression. Cellular and Molecular Life Sciences. 2018;75(20):3741-50.
90. Larsen E, Kwon K, Coin F, Egly J-M, Klungland A. Transcription activities at 8-oxoG lesions in DNA. DNA Repair. 2004;3(11):1457-68.
91. Fouquerel E, Barnes RP, Uttam S, Watkins SC, Bruchez MP, Opresko PL. Targeted and Persistent 8-Oxoguanine Base Damage at Telomeres Promotes Telomere Loss and Crisis. Molecular Cell. 2019;75(1):117-30.e6.
92. Margolin Y, Cloutier J-F, Shafirovich V, Geacintov NE, Dedon PC. Paradoxical hotspots for guanine oxidation by a chemical mediator of inflammation. Nature Chemical Biology. 2006;2(7):365-6.
93. Maki H, Sekiguchi M. MutT protein specifically hydrolyses a potent mutagenic substrate for DNA synthesis. Nature. 1992;355(6357):273-5.
94. Shibutani S, Takeshita M, Grollman AP. Insertion of specific bases during DNA synthesis past the oxidation-damaged base 8-oxodG. Nature. 1991;349(6308):431-4.
95. Markkanen E, Dorn J, Hübscher U. MUTYH DNA glycosylase: the rationale for removing undamaged bases from the DNA. Frontiers in Genetics. 2013;4(18).
96. Shibutani S, Takeshita M, Grollman AP. Translesional Synthesis on DNA Templates Containing a Single Abasic Site: a mechanistic study of the “A rule”*. Journal of Biological Chemistry. 1997;272(21):13916-22.
97. Sagher D, Strauss B. Insertion of nucleotides opposite apurinic apyrimidinic sites in deoxyribonucleic acid during in vitro synthesis: uniqueness of adenine nucleotides. Biochemistry. 1983;22(19):4518-26.
98. Suzuki T, Kamiya H. Mutations induced by 8-hydroxyguanine (8-oxo-7,8-dihydroguanine), a representative oxidized base, in mammalian cells. Genes Environ. 2017;39:2.
99. Jackson SP, Bartek J. The DNA-damage response in human biology and disease. Nature. 2009;461(7267):1071-8.
100. Bürkle A. Poly(ADP-ribose). The most elaborate metabolite of NAD+. Febs j. 2005;272(18):4576-89.
101. Harrision D, Gravells P, Thompson R, Bryant HE. Poly(ADP-Ribose) Glycohydrolase (PARG) vs. Poly(ADP-Ribose) Polymerase (PARP) - Function in Genome Maintenance and Relevance of Inhibitors for Anti-cancer Therapy. Front Mol Biosci. 2020;7:191.

102. Eustermann S, Wu WF, Langelier MF, Yang JC, Easton LE, Riccio AA, *et al.* Structural Basis of Detection and Signaling of DNA Single-Strand Breaks by Human PARP-1. Mol Cell. 2015;60(5):742-54.
103. Shieh WM, Amé JC, Wilson MV, Wang ZQ, Koh DW, Jacobson MK, *et al.* Poly(ADP-ribose) polymerase null mouse cells synthesize ADP-ribose polymers. J Biol Chem. 1998;273(46):30069-72.
104. Ruf A, Rolli V, de Murcia G, Schulz GE. The mechanism of the elongation and branching reaction of poly(ADP-ribose) polymerase as derived from crystal structures and mutagenesis. J Mol Biol. 1998;278(1):57-65.
105. Hayaishi O, Ueda K. Poly(ADP-ribose) and ADP-ribosylation of proteins. Annu Rev Biochem. 1977;46:95-116.
106. Hendriks IA, Larsen SC, Nielsen ML. An Advanced Strategy for Comprehensive Profiling of ADP-ribosylation Sites Using Mass Spectrometry-based Proteomics. Mol Cell Proteomics. 2019;18(5):1010-26.
107. Vyas S, Matic I, Uchima L, Rood J, Zaja R, Hay RT, *et al.* Family-wide analysis of poly(ADP-ribose) polymerase activity. Nat Commun. 2014;5:4426.
108. Alvarez-Gonzalez R. 3'-Deoxy-NAD+ as a substrate for poly(ADP-ribose)polymerase and the reaction mechanism of poly(ADP-ribose) elongation. J Biol Chem. 1988;263(33):17690-6.
109. Aberle L, Krüger A, Reber JM, Lippmann M, Hufnagel M, Schmalz M, *et al.* PARP1 catalytic variants reveal branching and chain length-specific functions of poly(ADP-ribose) in cellular physiology and stress response. Nucleic Acids Res. 2020;48(18):10015-33.
110. Satoh MS, Lindahl T. Role of poly(ADP-ribose) formation in DNA repair. Nature. 1992;356(6367):356-8.
111. Yang G, Chen Y, Wu J, Chen SH, Liu X, Singh AK, *et al.* Poly(ADP-ribosyl)ation mediates early phase histone eviction at DNA lesions. Nucleic Acids Res. 2020;48(6):3001-13.
112. Ying S, Chen Z, Medhurst AL, Neal JA, Bao Z, Mortusewicz O, *et al.* DNA-PKcs and PARP1 Bind to Unresected Stalled DNA Replication Forks Where They Recruit XRCC1 to Mediate Repair. Cancer Res. 2016;76(5):1078-88.
113. Barkauskaite E, Brassington A, Tan ES, Warwicker J, Dunstan MS, Banos B, *et al.* Visualization of poly(ADP-ribose) bound to PARG reveals inherent balance between exo- and endo-glycohydrolase activities. Nat Commun. 2013;4:2164.

114. Wei L, Nakajima S, Hsieh CL, Kanno S, Masutani M, Levine AS, *et al.* Damage response of XRCC1 at sites of DNA single strand breaks is regulated by phosphorylation and ubiquitylation after degradation of poly(ADP-ribose). J Cell Sci. 2013;126(Pt 19):4414-23.
115. Fathers C, Drayton RM, Solovieva S, Bryant HE. Inhibition of poly(ADP-ribose) glycohydrolase (PARG) specifically kills BRCA2-deficient tumor cells. Cell Cycle. 2012;11(5):990-7.
116. Andrabi SA, Dawson TM, Dawson VL. Mitochondrial and nuclear cross talk in cell death: parthanatos. Ann N Y Acad Sci. 2008;1147:233-41.
117. Weinberg RA. The biology of cancer. Garland Science. 2014.
118. Markkanen E. Not breathing is not an option: How to deal with oxidative DNA damage. DNA Repair. 2017;59:82-105.
119. Krokan HE, Bjørås M. Base Excision Repair. Cold Spring Harbor Perspectives in Biology. 2013;5(4):a012583.
120. Nicolai MM, Weishaupt A-K, Baesler J, Brinkmann V, Wellenberg A, Winkelbeiner N, *et al.* Effects of Manganese on Genomic Integrity in the Multicellular Model Organism *Caenorhabditis elegans*. International Journal of Molecular Sciences. 2021;22(20):10905.
121. Wang Y, Dawson VL, Dawson TM. Poly(ADP-ribose) signals to mitochondrial AIF: a key event in parthanatos. Exp Neurol. 2009;218(2):193-202.
122. Sasaki Y, Vohra BPS, Lund FE, Milbrandt J. Nicotinamide mononucleotide adenylyl transferase-mediated axonal protection requires enzymatic activity but not increased levels of neuronal nicotinamide adenine dinucleotide. The Journal of neuroscience : the official journal of the Society for Neuroscience. 2009;29(17):5525-35.
123. Brochier C, Jones JI, Willis DE, Langley B. Poly(ADP-ribose) polymerase 1 is a novel target to promote axonal regeneration. Proceedings of the National Academy of Sciences of the United States of America. 2015;112(49):15220-5.
124. Sung YJ, Ambron RT. PolyADP-ribose polymerase-1 (PARP-1) and the evolution of learning and memory. Bioessays. 2004;26(12):1268-71.
125. Cohen-Armon M, Visochek L, Katzoff A, Levitan D, Susswein AJ, Klein R, *et al.* Long-term memory requires polyADP-ribosylation. Science. 2004;304(5678):1820-2.
126. Goldberg S, Visochek L, Giladi E, Gozes I, Cohen-Armon M. PolyADP-ribosylation is required for long-term memory formation in mammals. Journal of Neurochemistry. 2009;111(1):72-9.

127. Boiteux S, Guillet M. Abasic sites in DNA: repair and biological consequences in Saccharomyces cerevisiae. DNA Repair. 2004;3(1):1-12.
128. Allgayer J, Kitsera N, Bartelt S, Epe B, Khobta A. Widespread transcriptional gene inactivation initiated by a repair intermediate of 8-oxoguanine. Nucleic Acids Res. 2016;44(15):7267-80.
129. Sczepanski JT, Wong RS, McKnight JN, Bowman GD, Greenberg MM. Rapid DNA–protein cross-linking and strand scission by an abasic site in a nucleosome core particle. Proceedings of the National Academy of Sciences. 2010;107(52):22475-80.
130. Bravard A, Vacher M, Gouget B, Coutant A, de Boisferon FH, Marsin S, *et al.* Redox regulation of human OGG1 activity in response to cellular oxidative stress. Mol Cell Biol. 2006;26(20):7430-6.
131. Chen P, Bornhorst J, Aschner M. Manganese metabolism in humans. Front Biosci (Landmark Ed). 2018;23:1655-79.
132. Williams M, Todd GD, Roney N, Crawford J, Coles C, McClure PR, *et al.* Agency for Toxic Substances and Disease Registry (ATSDR) Toxicological Profiles. Toxicological Profile for Manganese. Atlanta (GA): Agency for Toxic Substances and Disease Registry (US); 2012.
133. Commission E. Opinion of the Scientific Committee on Food on the Tolerable Upper Intake Level of Manganese. Opinion of the Scientific Committee on Food. 2000.
134. Malcolm Williams GDT, NICKOLETTE RONEY. Toxicological Profile for Manganese. Agency for Toxci Substances and Disease Registry (US). 2012.
135. Santamaria A. Manganese exposure, essentiality & toxicity. Indian Journal of Medical Research. 2008;128(4):484-500.
136. Bock CW, Katz AK, Markham GD, Glusker JP. Manganese as a Replacement for Magnesium and Zinc: Functional Comparison of the Divalent Ions. Journal of the American Chemical Society. 1999;121(32):7360-72.
137. Nielsen FH. Ultratrace minerals. Modern nutrition in Health and Disease. 1999.
138. Martinez-Finley EJ, Gavin CE, Aschner M, Gunter TE. Manganese Neurotoxicity and the Role of Reactive Oxygen Species. Free radical biology & medicine. 2013;62:65-75.
139. IPCS I. Manganese and its compounds: environmenal aspects. 2004.
140. WHO. Manganese in Drinking Water. WHO Guidlines for Drinking-water Quality. 2011.
141. Rollin H, Nogueira C, editors. Manganese: Environmental Pollution and Health Effects2011.

142. Frisbie SH, Mitchell EJ, Roudeau S, Domart F, Carmona A, Ortega R. Manganese levels in infant formula and young child nutritional beverages in the United States and France: Comparison to breast milk and regulations. PloS one. 2019;14(11):e0223636-e.
143. Helmer PO, Nicolai MM, Schwantes V, Bornhorst J, Hayen H. Investigation of cardiolipin oxidation products as a new endpoint for oxidative stress in *C. elegans* by means of online two-dimensional liquid chromatography and high-resolution mass spectrometry. Free Radic Biol Med. 2021;162:216-24.
144. Bell JG, Keen CL, Lonnerdal B. Higher retention of manganese in suckling than in adult rats is not due to maturational differences in manganese uptake by rat small intestine. Journal of toxicology and environmental health. 1989;26(4):387-98.
145. Garcia-Aranda JA, Wapnir RA, Lifshitz F. In vivo intestinal absorption of manganese in the rat. The Journal of nutrition. 1983;113(12):2601-7.
146. Johnson PE, Lykken GI, Korynta ED. Absorption and biological half-life in humans of intrinsic and extrinsic 54Mn tracers from foods of plant origin. The Journal of nutrition. 1991;121(5):711-7.
147. Davidsson L, Cederblad A, Lonnerdal B, Sandstrom B. Manganese retention in man: a method for estimating manganese absorption in man. The American journal of clinical nutrition. 1989;49(1):170-9.
148. Trumbo P, Yates AA, Schlicker S, Poos M. Dietary reference intakes: vitamin A, vitamin K, arsenic, boron, chromium, copper, iodine, iron, manganese, molybdenum, nickel, silicon, vanadium, and zinc. Journal of the American Dietetic Association. 2001;101(3):294-301.
149. Roth JA. Homeostatic and toxic mechanisms regulating manganese uptake, retention, and elimination. Biological research. 2006;39(1):45-57.
150. Aschner JL, Aschner M. Nutritional aspects of manganese homeostasis. Mol Aspects Med. 2005;26(4-5):353-62.
151. Crossgrove RAYJS. Manganese toxicokinetics at the blood-brain-barrier. Phamaceutical Science Reports. 2004;1-2004.
152. Crossgrove JS, Allen DD, Bukaveckas BL, Rhineheimer SS, Yokel RA. Manganese Distribution Across the Blood–Brain Barrier: I. Evidence for Carrier-Mediated Influx of Manganese Citrate as Well as Manganese and Manganese Transferrin. NeuroToxicology. 2003;24(1):3-13.

153. Au C, Benedetto A, Aschner M. Manganese transport in eukaryotes: The role of DMT1. NeuroToxicology. 2008;29(4):569-76.
154. Aschner M, Aschner JL. Manganese transport across the blood-brain barrier: Relationship to iron homeostasis. Brain Research Bulletin. 1990;24(6):857-60.
155. Gunter TE, Gerstner B, Gunter KK, Malecki J, Gelein R, Valentine WM, *et al.* Manganese transport via the transferrin mechanism. NeuroToxicology. 2013;34:118-27.
156. Maynard LS, Cotzias GC. The partition of manganese among organs and intracellular organelles of the rat. The Journal of biological chemistry. 1955;214(1):489-95.
157. Erikson KM, Dobson AW, Dorman DC, Aschner M. Manganese exposure and induced oxidative stress in the rat brain. Sci Total Environ. 2004;334-335:409-16.
158. Michalke B, Berthele A, Venkataramani V. Simultaneous Quantification and Speciation of Trace Metals in Paired Serum and CSF Samples by Size Exclusion Chromatography-Inductively Coupled Plasma-Dynamic Reaction Cell-Mass Spectrometry (SEC-DRC-ICP-MS). Int J Mol Sci. 2021;22(16).
159. Rubin LL, Staddon JM. The cell biology of the blood-brain barrier. Annu Rev Neurosci. 1999;22:11-28.
160. Bowman AB, Aschner M. Considerations on manganese (Mn) treatments for in vitro studies. Neurotoxicology. 2014;41:141-2.
161. Prohaska JR. Functions of trace elements in brain metabolism. Physiol Rev. 1987;67(3):858-901.
162. Morello M, Canini A, Mattioli P, Sorge RP, Alimonti A, Bocca B, *et al.* Sub-cellular localization of manganese in the basal ganglia of normal and manganese-treated rats An electron spectroscopy imaging and electron energy-loss spectroscopy study. Neurotoxicology. 2008;29(1):60-72.
163. Finley JW. Manganese absorption and retention by young women is associated with serum ferritin concentration. The American journal of clinical nutrition. 1999;70(1):37-43.
164. Finley JW, Johnson PE, Johnson LK. Sex affects manganese absorption and retention by humans from a diet adequate in manganese. The American journal of clinical nutrition. 1994;60(6):949-55.
165. Keen CL, Ensunsa, J. L., Watson, M. H., Baly, D. K., Donovan, S. M., Monaco, M. H., & Clegg, M. S. Nutritional aspects of manganese from experimental studies. NeuroToxicology. 1999;20(2-3):213-24.

166. Howe PD, Malcolm HM, Dobson S, World Health O, International Programme on Chemical S. Manganese and its compounds : environmental aspects. Geneva: World Health Organization; 2004.
167. Finkelstein Y, Milatovic D, Aschner M. Modulation of cholinergic systems by manganese. NeuroToxicology. 2007;28(5):1003-14.
168. Calne DB, Chu NS, Huang CC, Lu CS, Olanow W. Manganism and idiopathic parkinsonism: similarities and differences. Neurology. 1994;44(9):1583-6.
169. Kim G, Lee HS, Seok Bang J, Kim B, Ko D, Yang M. A current review for biological monitoring of manganese with exposure, susceptibility, and response biomarkers. J Environ Sci Health C Environ Carcinog Ecotoxicol Rev. 2015;33(2):229-54.
170. Livingstone C. Manganese Provision in Parenteral Nutrition: An Update. Nutr Clin Pract. 2018;33(3):404-18.
171. Zheng YX, Chan P, Pan ZF, Shi NN, Wang ZX, Pan J, *et al.* Polymorphism of metabolic genes and susceptibility to occupational chronic manganism. Biomarkers. 2002;7(4):337-46.
172. Aboud AA, Tidball AM, Kumar KK, Neely MD, Ess KC, Erikson KM, *et al.* Genetic risk for Parkinson's disease correlates with alterations in neuronal manganese sensitivity between two human subjects. Neurotoxicology. 2012;33(6):1443-9.
173. Tan J, Zhang T, Jiang L, Chi J, Hu D, Pan Q, *et al.* Regulation of intracellular manganese homeostasis by Kufor-Rakeb syndrome-associated ATP13A2 protein. J Biol Chem. 2011;286(34):29654-62.
174. Bonifati V. Genetics of Parkinson's disease-state of the art, 2013. Parkinsonism Relat Disord. 2014;20 Suppl 1:S23-8.
175. Kalia K, Jiang W, Zheng W. Manganese accumulates primarily in nuclei of cultured brain cells. Neurotoxicology. 2008;29(3):466-70.
176. Sissoëff I, Grisvard J, Guillé E. Studies on metal ions-DNA interactions: specific behaviour of reiterative DNA sequences. Prog Biophys Mol Biol. 1976;31(2):165-99.
177. Granot J, Feigon J, Kearns DR. Interactions of DNA with divalent metal ions. I. 31P-NMR studies. Biopolymers. 1982;21(1):181-201.
178. Polyanichko AM, Andrushchenko VV, Chikhirzhina EV, Vorob'ev VI, Wieser H. The effect of manganese(II) on DNA structure: electronic and vibrational circular dichroism studies. Nucleic Acids Res. 2004;32(3):989-96.

179. Malecki EA. Manganese toxicity is associated with mitochondrial dysfunction and DNA fragmentation in rat primary striatal neurons. Brain Research Bulletin. 2001;55(2):225-8.
180. Galvani P, Fumagalli P, Santagostino A. Vulnerability of mitochondrial complex I in PC12 cells exposed to manganese. Eur J Pharmacol. 1995;293(4):377-83.
181. Gugnani KS, Vu N, Rondón-Ortiz AN, Böhlke M, Maher TJ, Pino-Figueroa AJ. Neuroprotective activity of macamides on manganese-induced mitochondrial disruption in U-87 MG glioblastoma cells. Toxicol Appl Pharmacol. 2018;340:67-76.
182. Liu Y, Barber DS, Zhang P, Liu B. Complex II of the mitochondrial respiratory chain is the key mediator of divalent manganese-induced hydrogen peroxide production in microglia. Toxicol Sci. 2013;132(2):298-306.
183. Dobson AW, Weber S, Dorman DC, Lash LK, Erikson KM, Aschner M. Oxidative stress is induced in the rat brain following repeated inhalation exposure to manganese sulfate. Biol Trace Elem Res. 2003;93(1-3):113-26.
184. Bornhorst J, Ebert F, Hartwig A, Michalke B, Schwerdtle T. Manganese inhibits poly(ADP-ribosyl)ation in human cells: a possible mechanism behind manganese-induced toxicity? J Environ Monit. 2010;12(11):2062-9.
185. Alnajjar KS, Sweasy JB. A new perspective on oxidation of DNA repair proteins and cancer. DNA repair. 2019;76:60-9.
186. Gunter KK, Aschner M, Miller LM, Eliseev R, Salter J, Anderson K, *et al.* Determining the oxidation states of manganese in PC12 and nerve growth factor-induced PC12 cells. Free Radic Biol Med. 2005;39(2):164-81.
187. Sengupta A, Mense SM, Lan C, Zhou M, Mauro RE, Kellerman L, *et al.* Gene expression profiling of human primary astrocytes exposed to manganese chloride indicates selective effects on several functions of the cells. Neurotoxicology. 2007;28(3):478-89.
188. Giordano G, Pizzurro D, VanDeMark K, Guizzetti M, Costa LG. Manganese inhibits the ability of astrocytes to promote neuronal differentiation. Toxicol Appl Pharmacol. 2009;240(2):226-35.
189. Roth JA. Correlation between the biochemical pathways altered by mutated parkinson-related genes and chronic exposure to manganese. Neurotoxicology. 2014;44:314-25.
190. A. K. Corsi BW, M. Chalfie. A Transparent window into biology: A primer on *Caenorhabditis elegans*. wormbookorg. 2015.

191. Riddle DL BT, Meyer BJ, *et al. C. elegans* II. 2nd edition. 1997.
192. Chalfie M, Tu Y, Euskirchen G, Ward WW, Prasher DC. Green fluorescent protein as a marker for gene expression. Science. 1994;263(5148):802-5.
193. Jorgensen EM, Mango SE. The art and design of genetic screens: *Caenorhabditis elegans*. Nature Reviews Genetics. 2002;3:356.
194. Sulston JE, Horvitz HR. Post-embryonic cell lineages of the nematode, *Caenorhabditis elegans*. Dev Biol. 1977;56(1):110-56.
195. White JG, Southgate E, Thomson JN, Brenner S. The structure of the nervous system of the nematode *Caenorhabditis elegans*. Philos Trans R Soc Lond B Biol Sci. 1986;314(1165):1-340.
196. Genome sequence of the nematode *C. elegans*: a platform for investigating biology. Science. 1998;282(5396):2012-8.
197. Frøkjær-Jensen C. Exciting prospects for precise engineering of *Caenorhabditis elegans* genomes with CRISPR/Cas9. Genetics. 2013;195(3):635-42.
198. Conte D, Jr., MacNeil LT, Walhout AJM, Mello CC. RNA Interference in *Caenorhabditis elegans*. Curr Protoc Mol Biol. 2015;109:26.3.1-.3.30.
199. Kaletta T, Hengartner MO. Finding function in novel targets: *C. elegans* as a model organism. Nat Rev Drug Discov. 2006;5(5):387-98.
200. Culetto E, Sattelle DB. A role for *Caenorhabditis elegans* in understanding the function and interactions of human disease genes. Hum Mol Genet. 2000;9(6):869-77.
201. Cassada RC, Russell RL. The dauerlarva, a post-embryonic developmental variant of the nematode *Caenorhabditis elegans*. Developmental biology. 1975;46(2):326-42.
202. Piñero González J, Carrillo Farnés O, Vasconcelos AT, González Pérez A. Conservation of key members in the course of the evolution of the insulin signaling pathway. Biosystems. 2009;95(1):7-16.
203. Blackwell TK, Steinbaugh MJ, Hourihan JM, Ewald CY, Isik M. SKN-1/Nrf, stress responses, and aging in *Caenorhabditis elegans*. Free radical biology & medicine. 2015;88(Pt B):290-301.
204. Sakaguchi A, Matsumoto K, Hisamoto N. Roles of MAP kinase cascades in *Caenorhabditis elegans*. J Biochem. 2004;136(1):7-11.
205. Leiers B, Kampkötter A, Grevelding CG, Link CD, Johnson TE, Henkle-Dührsen K. A stress-responsive glutathione S-transferase confers resistance to oxidative stress in *Caenorhabditis elegans*. Free Radical Biology and Medicine. 2003;34(11):1405-15.

206. Larsen PL. Aging and resistance to oxidative damage in *Caenorhabditis elegans*. Proc Natl Acad Sci U S A. 1993;90(19):8905-9.
207. Stergiou L, Hengartner MO. Death and more: DNA damage response pathways in the nematode *C. elegans*. Cell Death Differ. 2004;11(1):21-8.
208. O'Neil N, Rose A. DNA repair. WormBook. 2006:1-12.
209. Barreto S, Cadavid COM, Moura RAO, Silva GMM, Araújo SVF, Silva Filho J, *et al.* In Vitro and In Vivo Antioxidant Activity of Agave sisalana Agro-Industrial Residue. Biomolecules. 2020;10(10).
210. Zarkower D. Somatic sex determination. WormBook. 2006:1-12.
211. Hillier LW, Coulson A, Murray JI, Bao Z, Sulston JE, Waterston RH. Genomics in *C. elegans*: so many genes, such a little worm. Genome Res. 2005;15(12):1651-60.
212. Hammarlund M, Jin Y. Axon regeneration in *C. elegans*. Current Opinion in Neurobiology. 2014;27:199-207.
213. Driscoll M, Chalfie M. Developmental and abnormal cell death in *C. elegans*. Trends in Neurosciences. 1992;15(1):15-9.
214. Dong X, Liu OW, Howell AS, Shen K. An extracellular adhesion molecule complex patterns dendritic branching and morphogenesis. Cell. 2013;155(2):296-307.
215. Oikonomou G, Shaham S. The glia of *Caenorhabditis elegans*. Glia. 2011;59(9):1253-63.
216. Hobert O. Neurogenesis in the nematode *Caenorhabditis elegans*. WormBook. 2010:1-24.
217. Bargmann CI. Chemosensation in *C. elegans*. WormBook. 2006:1-29.
218. Iwanir S, Ruach R, Itskovits E, Pritz CO, Bokman E, Zaslaver A. Irrational behavior in *C. elegans* arises from asymmetric modulatory effects within single sensory neurons. Nature Communications. 2019;10(1):3202.
219. Gruninger TR, Gualberto DG, LeBoeuf B, Garcia LR. Integration of Male Mating and Feeding Behaviors in *Caenorhabditis elegans*. The Journal of Neuroscience. 2006;26(1):169-79.
220. Ardiel EL, Rankin CH. An elegant mind: learning and memory in *Caenorhabditis elegans*. Learn Mem. 2010;17(4):191-201.
221. Taylor CA, Tuschl K, Nicolai MM, Bornhorst J, Gubert P, Varão AM, *et al.* Maintaining Translational Relevance in Animal Models of Manganese Neurotoxicity. J Nutr. 2020;150(6):1360-9.

222. Au C, Benedetto A, Anderson J, Labrousse A, Erikson K, Ewbank JJ, *et al.* SMF-1, SMF-2 and SMF-3 DMT1 orthologues regulate and are regulated differentially by manganese levels in *C. elegans*. PLoS One. 2009;4(11):e7792.
223. Chakraborty S, Chen P, Bornhorst J, Schwerdtle T, Schumacher F, Kleuser B, *et al.* Loss of pdr-1/parkin influences Mn homeostasis through altered ferroportin expression in *C. elegans*. Metallomics. 2015;7(5):847-56.
224. Anderson CP, Leibold EA. Mechanisms of iron metabolism in *Caenorhabditis elegans*. Front Pharmacol. 2014;5:113.
225. Baesler J, Michaelis V, Stiboller M, Haase H, Aschner M, Schwerdtle T, *et al.* Nutritive Manganese and Zinc Overdosing in Aging *C. elegans* Result in a Metallothionein-Mediated Alteration in Metal Homeostasis. Mol Nutr Food Res. 2021;65(8):e2001176.
226. Van Pelt KM, Truttmann MC. *Caenorhabditis elegans* as a model system for studying aging-associated neurodegenerative diseases. Translational Medicine of Aging. 2020;4:60-72.
227. Johnson TE. Advantages and disadvantages of *Caenorhabditis elegans* for aging research. Exp Gerontol. 2003;38(11-12):1329-32.
228. Waterston RH, Sulston JE, Coulson AR. The Genome. In: Riddle DL, Blumenthal T, Meyer BJ, Priess JR, editors. C elegans II. Cold Spring Harbor (NY): Cold Spring Harbor Laboratory Press 1997.
229. Çelen İ, Doh JH, Sabanayagam CR. Genetic Adaptation of *C. elegans* to Environment Changes I: Multigenerational Analysis of the Transcriptome. bioRxiv. 2017:194506.
230. Stiernagle T. Maintenance of *C. elegans*. WormBook. 2006:1-11.
231. Lotharius J, Falsig J, van Beek J, Payne S, Dringen R, Brundin P, *et al.* Progressive degeneration of human mesencephalic neuron-derived cells triggered by dopamine-dependent oxidative stress is dependent on the mixed-lineage kinase pathway. J Neurosci. 2005;25(27):6329-42.
232. Zhang XM, Yin M, Zhang MH. Cell-based assays for Parkinson's disease using differentiated human LUHMES cells. Acta Pharmacol Sin. 2014;35(7):945-56.
233. Sayre LM, Smith MA, Perry G. Chemistry and biochemistry of oxidative stress in neurodegenerative disease. Curr Med Chem. 2001;8(7):721-38.

234. Sykora P, Wilson DM, 3rd, Bohr VA. Base excision repair in the mammalian brain: implication for age related neurodegeneration. Mech Ageing Dev. 2013;134(10):440-8.
235. Påhlman S, Mamaeva S, Meyerson G, Mattsson ME, Bjelfman C, Ortoft E, *et al.* Human neuroblastoma cells in culture: a model for neuronal cell differentiation and function. Acta Physiol Scand Suppl. 1990;592:25-37.
236. Grau CM, Greene LA. Use of PC12 cells and rat superior cervical ganglion sympathetic neurons as models for neuroprotective assays relevant to Parkinson's disease. Methods Mol Biol. 2012;846:201-11.
237. Schüle B, Pera RA, Langston JW. Can cellular models revolutionize drug discovery in Parkinson's disease? Biochim Biophys Acta. 2009;1792(11):1043-51.
238. Sulston J, Dew M, Brenner S. Dopaminergic neurons in the nematode *Caenorhabditis elegans*. J Comp Neurol. 1975;163(2):215-26.
239. Alexander AG, Marfil V, Li C. Use of *Caenorhabditis elegans* as a model to study Alzheimer's disease and other neurodegenerative diseases. Front Genet. 2014;5:279-.
240. Ray A, Martinez BA, Berkowitz LA, Caldwell GA, Caldwell KA. Mitochondrial dysfunction, oxidative stress, and neurodegeneration elicited by a bacterial metabolite in a *C. elegans* Parkinson's model. Cell Death Dis. 2014;5(1):e984-e.
241. Cioffi F, Adam RHI, Broersen K. Molecular Mechanisms and Genetics of Oxidative Stress in Alzheimer's Disease. Journal of Alzheimer's disease : JAD. 2019;72(4):981-1017.
242. Giasson BI, Duda JE, Murray IV, Chen Q, Souza JM, Hurtig HI, *et al.* Oxidative damage linked to neurodegeneration by selective alpha-synuclein nitration in synucleinopathy lesions. Science. 2000;290(5493):985-9.
243. Suthammarak W, Somerlot BH, Opheim E, Sedensky M, Morgan PG. Novel interactions between mitochondrial superoxide dismutases and the electron transport chain. Aging Cell. 2013;12(6):1132-40.
244. Copes N, Edwards C, Chaput D, Saifee M, Barjuca I, Nelson D, *et al.* Metabolome and proteome changes with aging in *Caenorhabditis elegans*. Exp Gerontol. 2015;72:67-84.
245. Imanikia S, Galea F, Nagy E, Phillips DH, Stürzenbaum SR, Arlt VM. The application of the comet assay to assess the genotoxicity of environmental pollutants in the nematode *Caenorhabditis elegans*. Environmental toxicology and pharmacology. 2016;45:356-61.

246. Montero-Bullon JF, Melo T, Rosário MDM, Domingues P. Liquid chromatography/tandem mass spectrometry characterization of nitroso, nitrated and nitroxidized cardiolipin products. Free Radic Biol Med. 2019;144:183-91.
247. Schlame M, Rua D, Greenberg ML. The biosynthesis and functional role of cardiolipin. Prog Lipid Res. 2000;39(3):257-88.
248. Kagan VE, Tyurin VA, Jiang J, Tyurina YY, Ritov VB, Amoscato AA, *et al.* Cytochrome c acts as a cardiolipin oxygenase required for release of proapoptotic factors. Nat Chem Biol. 2005;1(4):223-32.
249. Ostrander DB, Sparagna GC, Amoscato AA, McMillin JB, Dowhan W. Decreased cardiolipin synthesis corresponds with cytochrome c release in palmitate-induced cardiomyocyte apoptosis. J Biol Chem. 2001;276(41):38061-7.
250. Li XX, Tsoi B, Li YF, Kurihara H, He RR. Cardiolipin and its different properties in mitophagy and apoptosis. J Histochem Cytochem. 2015;63(5):301-11.
251. Yurkova I, Huster D, Arnhold J. Free radical fragmentation of cardiolipin by cytochrome c. Chem Phys Lipids. 2009;158(1):16-21.
252. Pope S, Land JM, Heales SJ. Oxidative stress and mitochondrial dysfunction in neurodegeneration; cardiolipin a critical target? Biochim Biophys Acta. 2008;1777(7-8):794-9.
253. Tyurina YY, Winnica DE, Kapralova VI, Kapralov AA, Tyurin VA, Kagan VE. LC/MS characterization of rotenone induced cardiolipin oxidation in human lymphocytes: implications for mitochondrial dysfunction associated with Parkinson's disease. Mol Nutr Food Res. 2013;57(8):1410-22.
254. Tyurina YY, Polimova AM, Maciel E, Tyurin VA, Kapralova VI, Winnica DE, *et al.* LC/MS analysis of cardiolipins in substantia nigra and plasma of rotenone-treated rats: Implication for mitochondrial dysfunction in Parkinson's disease. Free Radic Res. 2015;49(5):681-91.
255. Li L, Zhong S, Shen X, Li Q, Xu W, Tao Y, *et al.* Recent development on liquid chromatography-mass spectrometry analysis of oxidized lipids. Free Radic Biol Med. 2019;144:16-34.
256. Brenner S. The genetics of *Caenorhabditis elegans*. Genetics. 1974;77(1):71-94.
257. Rohn I, Raschke S, Aschner M, Tuck S, Kuehnelt D, Kipp A, *et al.* Treatment of *Caenorhabditis elegans* with Small Selenium Species Enhances Antioxidant Defense Systems. Molecular nutrition & food research. 2019;63(9):e1801304-e.

258. Matyash V, Liebisch G, Kurzchalia TV, Shevchenko A, Schwudke D. Lipid extraction by methyl-tert-butyl ether for high-throughput lipidomics. Journal of lipid research. 2008;49(5):1137-46.
259. Helmer PO, Wienken CM, Korf A, Hayen H. Mass spectrometric investigation of cardiolipins and their oxidation products after two-dimensional heart-cut liquid chromatography. J Chromatogr A. 2020;1619:460918.
260. Myers OD, Sumner SJ, Li S, Barnes S, Du X. One Step Forward for Reducing False Positive and False Negative Compound Identifications from Mass Spectrometry Metabolomics Data: New Algorithms for Constructing Extracted Ion Chromatograms and Detecting Chromatographic Peaks. Anal Chem. 2017;89(17):8696-703.
261. Helmer PO, Korf A, Hayen H. Analysis of artificially oxidized cardiolipins and monolyso-cardiolipins via liquid chromatography/high-resolution mass spectrometry and Kendrick mass defect plots after hydrophilic interaction liquid chromatography based sample preparation. Rapid Communications in Mass Spectrometry. 2020;34(1):e8566.
262. Korf A, Jeck V, Schmid R, Helmer PO, Hayen H. Lipid Species Annotation at Double Bond Position Level with Custom Databases by Extension of the MZmine 2 Open-Source Software Package. Anal Chem. 2019;91(8):5098-105.
263. Liebisch G, Vizcaino JA, Kofeler H, Trotzmuller M, Griffiths WJ, Schmitz G, *et al.* Shorthand notation for lipid structures derived from mass spectrometry. J Lipid Res. 2013;54(6):1523-30.
264. Leung MC, Williams PL, Benedetto A, Au C, Helmcke KJ, Aschner M, *et al.* *Caenorhabditis elegans*: an emerging model in biomedical and environmental toxicology. Toxicol Sci. 2008;106(1):5-28.
265. Witting M, Schmitt-Kopplin P. The *Caenorhabditis elegans* lipidome: A primer for lipid analysis in *Caenorhabditis elegans*. Arch Biochem Biophys. 2016;589:27-37.
266. Watts JL, Ristow M. Lipid and Carbohydrate Metabolism in *Caenorhabditis elegans*. Genetics. 2017;207(2):413-46.
267. Kudryavtseva AV, Krasnov GS, Dmitriev AA, Alekseev BY, Kardymon OL, Sadritdinova AF, *et al.* Mitochondrial dysfunction and oxidative stress in aging and cancer. Oncotarget. 2016;7(29):44879-905.
268. Hauck AK, Bernlohr DA. Oxidative stress and lipotoxicity. J Lipid Res. 2016;57(11):1976-86.

269. Zhong H, Xiao M, Zarkovic K, Zhu M, Sa R, Lu J, *et al.* Mitochondrial control of apoptosis through modulation of cardiolipin oxidation in hepatocellular carcinoma: A novel link between oxidative stress and cancer. Free Radic Biol Med. 2017;102:67-76.
270. Hou NS, Gutschmidt A, Choi DY, Pather K, Shi X, Watts JL, *et al.* Activation of the endoplasmic reticulum unfolded protein response by lipid disequilibrium without disturbed proteostasis in vivo. Proc Natl Acad Sci U S A. 2014;111(22):E2271-80.
271. Gao AW, Chatzispyrou IA, Kamble R, Liu YJ, Herzog K, Smith RL, *et al.* A sensitive mass spectrometry platform identifies metabolic changes of life history traits in *C. elegans*. Scientific Reports. 2017;7(1):2408.
272. Colombo S, Criscuolo A, Zeller M, Fedorova M, Domingues MR, Domingues P. Analysis of oxidised and glycated aminophospholipids: Complete structural characterisation by C30 liquid chromatography-high resolution tandem mass spectrometry. Free Radic Biol Med. 2019;144:144-55.
273. Hsu FF, Turk J, Rhoades ER, Russell DG, Shi Y, Groisman EA. Structural characterization of cardiolipin by tandem quadrupole and multiple-stage quadrupole ion-trap mass spectrometry with electrospray ionization. J Am Soc Mass Spectrom. 2005;16(4):491-504.
274. Jussupow A, Di Luca A, Kaila VRI. How cardiolipin modulates the dynamics of respiratory complex I. Sci Adv. 2019;5(3):eaav1850-eaav.
275. Paradies G, Paradies V, Ruggiero FM, Petrosillo G. Oxidative stress, cardiolipin and mitochondrial dysfunction in nonalcoholic fatty liver disease. World J Gastroenterol. 2014;20(39):14205-18.
276. Mersch-Sundermann V, Knasmüller S, Wu XJ, Darroudi F, Kassie F. Use of a human-derived liver cell line for the detection of cytoprotective, antigenotoxic and cogenotoxic agents. Toxicology. 2004;198(1-3):329-40.
277. Xie Y, Zhang Y, Zhang L-T, Zeng S-X, Guo Z-B, Zheng B-D. Protective effects of alkaloid compounds from Nelumbinis Plumula on tert-butyl hydroperoxide-induced oxidative stress. Molecules (Basel, Switzerland). 2013;18(9):10285-300.
278. Zhao W, Feng H, Sun W, Liu K, Lu J-J, Chen X. Tert-butyl hydroperoxide (t-BHP) induced apoptosis and necroptosis in endothelial cells: Roles of NOX4 and mitochondrion. Redox Biol. 2017;11:524-34.

279. Yeh Y-C, Liu T-J, Lai H-C. Pathobiological Mechanisms of Endothelial Dysfunction Induced by tert-Butyl Hydroperoxide via Apoptosis, Necrosis and Senescence in a Rat Model. Int J Med Sci. 2020;17(3):368-82.
280. Desjardins D, Cacho-Valadez B, Liu J-L, Wang Y, Yee C, Bernard K, *et al.* Antioxidants reveal an inverted U-shaped dose-response relationship between reactive oxygen species levels and the rate of aging in *Caenorhabditis elegans*. Aging Cell. 2017;16(1):104-12.
281. Tyurin VA, Tyurina YY, Jung M-Y, Tungekar MA, Wasserloos KJ, Bayir H, *et al.* Mass-spectrometric analysis of hydroperoxy- and hydroxy-derivatives of cardiolipin and phosphatidylserine in cells and tissues induced by pro-apoptotic and pro-inflammatory stimuli. Journal of chromatography B, Analytical technologies in the biomedical and life sciences. 2009;877(26):2863-72.
282. Tyurina YY, Domingues RM, Tyurin VA, Maciel E, Domingues P, Amoscato AA, *et al.* Characterization of cardiolipins and their oxidation products by LC-MS analysis. Chemistry and physics of lipids. 2014;179:3-10.
283. Chen Z, Wu Y, Ma YS, Kobayashi Y, Zhao YY, Miura Y, *et al.* Profiling of cardiolipins and their hydroperoxides in HepG2 cells by LC/MS. Anal Bioanal Chem. 2017;409(24):5735-45.
284. Mao G, Qu F, St Croix CM, Tyurina YY, Planas-Iglesias J, Jiang J, *et al.* Mitochondrial Redox Opto-Lipidomics Reveals Mono-Oxygenated Cardiolipins as Pro-Apoptotic Death Signals. ACS Chem Biol. 2016;11(2):530-40.
285. Ischiropoulos H, Beckman JS. Oxidative stress and nitration in neurodegeneration: cause, effect, or association? J Clin Invest. 2003;111(2):163-9.
286. Zuryn S, Kuang J, Tuck A, Ebert PR. Mitochondrial dysfunction in *Caenorhabditis elegans* causes metabolic restructuring, but this is not linked to longevity. Mech Ageing Dev. 2010;131(9):554-61.
287. Sharma M, Pandey R, Saluja D. ROS is the major player in regulating altered autophagy and lifespan in sin-3 mutants of *C. elegans*. Autophagy. 2018;14(7):1239-55.
288. Kosztelnik M, Kurucz A, Papp D, Jones E, Sigmond T, Barna J, *et al.* Suppression of AMPK/aak-2 by NRF2/SKN-1 down-regulates autophagy during prolonged oxidative stress. FASEB J. 2019;33(2):2372-87.
289. Dues DJ, Schaar CE, Johnson BK, Bowman MJ, Winn ME, Senchuk MM, *et al.* Uncoupling of oxidative stress resistance and lifespan in long-lived isp-1

mitochondrial mutants in *Caenorhabditis elegans*. Free radical biology & medicine. 2017;108:362-73.

290. Pohl F, Teixeira-Castro A, Costa MD, Lindsay V, Fiúza-Fernandes J, Goua M, *et al.* GST-4-Dependent Suppression of Neurodegeneration in *C. elegans* Models of Parkinson's and Machado-Joseph Disease by Rapeseed Pomace Extract Supplementation. Front Neurosci. 2019;13:1091-.
291. Yasui M, Fukuda T, Ukai A, Maniwa J, Imamura T, Hashizume T, *et al.* Weight of evidence approach using a TK gene mutation assay with human TK6 cells for follow-up of positive results in Ames tests: a collaborative study by MMS/JEMS. Genes and Environment. 2021;43(1):7.
292. Doke SK, Dhawale SC. Alternatives to animal testing: A review. Saudi Pharmaceutical Journal. 2015;23(3):223-9.
293. Freires IA, Sardi JC, de Castro RD, Rosalen PL. Alternative Animal and Non-Animal Models for Drug Discovery and Development: Bonus or Burden? Pharm Res. 2017;34(4):681-6.
294. Hartwig A, Klyszcz-Nasko H, Schlepegrell R, Beyersmann D. Cellular damage by ferric nitrilotriacetate and ferric citrate in V79 cells: interrelationship between lipid peroxidation, DNA strand breaks and sister chromatid exchanges. Carcinogenesis. 1993;14(1):107-12.
295. Daniel FB, Haas DL, Pyle SM. Quantitation of chemically induced DNA strand breaks in human cells via an alkaline unwinding assay. Anal Biochem. 1985;144(2):390-402.
296. Garberg P, Akerblom EL, Bolcsfoldi G. Evaluation of a genotoxicity test measuring DNA-strand breaks in mouse lymphoma cells by alkaline unwinding and hydroxyapatite elution. Mutat Res. 1988;203(3):155-76.
297. Moore SM, Hess SM, Jorgenson JW. Extraction, Enrichment, Solubilization, and Digestion Techniques for Membrane Proteomics. J Proteome Res. 2016;15(4):1243-52.
298. Vagasi AS, Rahman MM, Chaudhari SN, Kipreos ET. Primary Culture System for Germ Cells from *Caenorhabditis elegans* Tumorous Germline Mutants. Bio Protoc. 2017;7(15):e2424.
299. Xiong H, Pears C, Woollard A. An enhanced *C. elegans* based platform for toxicity assessment. Sci Rep. 2017;7(1):9839-.
300. Park S, Choi S, Ahn B. DNA Strand Breaks in Mitotic Germ Cells of *Caenorhabditis elegans* Evaluated by Comet Assay. Mol Cells. 2016;39(3):204-10.

301. Kruszewski M, Iwaneńko T, Bartłomiejczyk T, Woliński J, Starzyński RR, Gralak MA, *et al.* Hepatic iron content corresponds with the susceptibility of lymphocytes to oxidative stress in neonatal pigs. Mutat Res. 2008;657(2):146-9.
302. H. R. Barton D, N. Le Gloahec Vr, Patin H. Radical chemistry of tert-butyl hydroperoxide (TBHP). Part 2. Studies of the FeII–TBHP mechanism. New Journal of Chemistry. 1998;22(6):565-8.
303. Martín C, Martínez R, Navarro R, Ruiz-Sanz JI, Lacort M, Ruiz-Larrea MB. tert-Butyl hydroperoxide-induced lipid signaling in hepatocytes: involvement of glutathione and free radicals11Abbreviations: [14C]-AA, [14C]-arachidonic acid; DCF, 2′,7′-dichlorofluorescein; DCFDA, 2′,7′-dichlorofluorescin diacetate; DTT, 1,4-dithiothreitol; MDA, malondialdehyde; PLA2, phospholipase A2; ROS, reactive oxygen species; TBARS, thiobarbituric acid reactive substances; and TBHP, tert-butyl hydroperoxide. Biochemical Pharmacology. 2001;62(6):705-12.
304. Müller WE, Zahn RK. Effect of bleomycin on DNA, RNA, protein, chromatin and on cell transformation by oncogenic RNA viruses. Prog Biochem Pharmacol. 1976;11:28-47.
305. Hsieh CJ, Sun M, Osborne G, Ricker K, Tsai FC, Li K, *et al.* Cancer Hazard Identification Integrating Human Variability: The Case of Coumarin. Int J Toxicol. 2019;38(6):501-52.
306. Toraason E, Adler VL, Kurhanewicz NA, DiNardo A, Saunders AM, Cahoon CK, *et al.* Automated and customizable quantitative image analysis of whole *Caenorhabditis elegans* germlines. Genetics. 2021;217(3):iyab010.
307. OECD. Test No. 471: Bacterial Reverse Mutation Test2020.
308. Nigon VM, Félix MA. History of research on *C. elegans* and other free-living nematodes as model organisms. WormBook. 2017;2017:1-84.
309. Corsi AK, Wightman B, Chalfie M. A Transparent Window into Biology: A Primer on *Caenorhabditis elegans*. Genetics. 2015;200(2):387-407.
310. Gupta S, You P, SenGupta T, Nilsen H, Sharma K. Crosstalk between Different DNA Repair Pathways Contributes to Neurodegenerative Diseases. Biology. 2021;10(2):163.
311. Elsakrmy N, Zhang-Akiyama QM, Ramotar D. The Base Excision Repair Pathway in the Nematode *Caenorhabditis elegans*. Front Cell Dev Biol. 2020;8:598860.
312. Arlt VM, Poirier MC, Sykes SE, John K, Moserova M, Stiborova M, *et al.* Exposure to benzo[a]pyrene of Hepatic Cytochrome P450 Reductase Null (HRN) and P450

Reductase Conditional Null (RCN) mice: Detection of benzo[a]pyrene diol epoxide-DNA adducts by immunohistochemistry and 32P-postlabelling. Toxicology Letters. 2012;213(2):160-6.

313. Anttila S, Raunio H, Hakkola J. Cytochrome P450-mediated pulmonary metabolism of carcinogens: regulation and cross-talk in lung carcinogenesis. Am J Respir Cell Mol Biol. 2011;44(5):583-90.
314. Bodhicharla R, Ryde IT, Prasad GL, Meyer JN. The tobacco-specific nitrosamine 4-(methylnitrosamino)-1-(3-pyridyl)-1-butanone (NNK) induces mitochondrial and nuclear DNA damage in *Caenorhabditis elegans*. Environ Mol Mutagen. 2014;55(1):43-50.
315. Hunt PR. The *C. elegans* model in toxicity testing. J Appl Toxicol. 2017;37(1):50-9.
316. Menzel R, Bogaert T, Achazi R. A systematic gene expression screen of *Caenorhabditis elegans* cytochrome P450 genes reveals CYP35 as strongly xenobiotic inducible. Arch Biochem Biophys. 2001;395(2):158-68.
317. Hartman JH, Widmayer SJ, Bergemann CM, King DE, Morton KS, Romersi RF, *et al.* Xenobiotic metabolism and transport in *Caenorhabditis elegans*. J Toxicol Environ Health B Crit Rev. 2021;24(2):51-94.
318. Abbass M, Chen Y, Arlt VM, Stürzenbaum SR. Benzo[a]pyrene and *Caenorhabditis elegans*: defining the genotoxic potential in an organism lacking the classical CYP1A1 pathway. Arch Toxicol. 2021;95(3):1055-69.
319. EFSA SCoF, Scientific Panel on Dietetic Products, Nutrition and Allergies. Tolerable upper intake levels for vitamins and minerals. Opinion of the Scientific Committee on Food. 2006.
320. Mattison DR, Milton B, Krewski D, Levy L, Dorman DC, Aggett PJ, *et al.* Severity scoring of manganese health effects for categorical regression. Neurotoxicology. 2017;58:203-16.
321. O'Neal SL, Zheng W. Manganese Toxicity Upon Overexposure: a Decade in Review. Current environmental health reports. 2015;2(3):315-28.
322. Fitzgerald K, Mikalunas V, Rubin H, McCarthy R, Vanagunas A, Craig RM. Hypermanganesemia in Patients Receiving Total Parenteral Nutrition. Journal of Parenteral and Enteral Nutrition. 1999;23(6):333-6.
323. Abdalian R, Saqui O, Fernandes G, Allard JP. Effects of manganese from a commercial multi-trace element supplement in a population sample of Canadian patients on long-term parenteral nutrition. JPEN J Parenter Enteral Nutr. 2013;37(4):538-43.

324. Scher DP, Goeden HM, Klos KS. Potential for Manganese-Induced Neurologic Harm to Formula-Fed Infants: A Risk Assessment of Total Oral Exposure. Environmental health perspectives. 2021;129(4):47011-.
325. Dorman DC, Struve MF, Marshall MW, Parkinson CU, James RA, Wong BA. Tissue manganese concentrations in young male rhesus monkeys following subchronic manganese sulfate inhalation. Toxicol Sci. 2006;92(1):201-10.
326. Erikson KM, Dorman DC, Lash LH, Aschner M. Manganese inhalation by rhesus monkeys is associated with brain regional changes in biomarkers of neurotoxicity. Toxicol Sci. 2007;97(2):459-66.
327. Lai CH, Chou CY, Ch'ang LY, Liu CS, Lin W. Identification of novel human genes evolutionarily conserved in *Caenorhabditis elegans* by comparative proteomics. Genome Res. 2000;10(5):703-13.
328. Volkova NV, Meier B, González-Huici V, Bertolini S, Gonzalez S, Vöhringer H, *et al.* Mutational signatures are jointly shaped by DNA damage and repair. Nat Commun. 2020;11(1):2169.
329. Guérard M, Baum M, Bitsch A, Eisenbrand G, Elhajouji A, Epe B, *et al.* Assessment of mechanisms driving non-linear dose-response relationships in genotoxicity testing. Mutat Res Rev Mutat Res. 2015;763:181-201.
330. Vock EH, Lutz WK, Hormes P, Hoffmann HD, Vamvakas S. Discrimination between genotoxicity and cytotoxicity in the induction of DNA double-strand breaks in cells treated with etoposide, melphalan, cisplatin, potassium cyanide, Triton X-100, and gamma-irradiation. Mutat Res. 1998;413(1):83-94.
331. Bornhorst J, Chakraborty S, Meyer S, Lohren H, Brinkhaus SG, Knight AL, *et al.* The effects of pdr1, djr1.1 and pink1 loss in manganese-induced toxicity and the role of α-synuclein in *C. elegans*. Metallomics. 2014;6(3):476-90.
332. Milatovic D, Zaja-Milatovic S, Gupta RC, Yu Y, Aschner M. Oxidative damage and neurodegeneration in manganese-induced neurotoxicity. Toxicol Appl Pharmacol. 2009;240(2):219-25.
333. Lindahl T. Instability and decay of the primary structure of DNA. Nature. 1993;362(6422):709-15.
334. Meier B, Volkova NV, Hong Y, Bertolini S, González-Huici V, Petrova T, *et al.* Protection of the *C. elegans* germ cell genome depends on diverse DNA repair pathways during normal proliferation. PLoS One. 2021;16(4):e0250291.

335. Wu Y, Li M, Yang M. Post-Translational Modifications in Oocyte Maturation and Embryo Development. Front Cell Dev Biol. 2021;9:645318-.
336. Hubbard EJ, Greenstein D. Introduction to the germ line. WormBook. 2005:1-4.
337. Fortini P, Dogliotti E. Mechanisms of dealing with DNA damage in terminally differentiated cells. Mutat Res. 2010;685(1-2):38-44.
338. Wandt VK, Winkelbeiner N, Bornhorst J, Witt B, Raschke S, Simon L, *et al.* A matter of concern - Trace element dyshomeostasis and genomic stability in neurons. Redox Biol. 2021;41:101877.
339. Papaluca A, Wagner JR, Saragovi HU, Ramotar D. UNG-1 and APN-1 are the major enzymes to efficiently repair 5-hydroxymethyluracil DNA lesions in *C. elegans*. Sci Rep. 2018;8(1):6860.
340. Dizdaroglu M, Coskun E, Jaruga P. Repair of oxidatively induced DNA damage by DNA glycosylases: Mechanisms of action, substrate specificities and excision kinetics. Mutation research. 2017;771:99-127.
341. Di Mascio P, Martinez GR, Miyamoto S, Ronsein GE, Medeiros MHG, Cadet J. Singlet Molecular Oxygen Reactions with Nucleic Acids, Lipids, and Proteins. Chemical Reviews. 2019;119(3):2043-86.
342. Valavanidis A, Vlachogianni T, Fiotakis C. 8-hydroxy-2' -deoxyguanosine (8-OHdG): A critical biomarker of oxidative stress and carcinogenesis. J Environ Sci Health C Environ Carcinog Ecotoxicol Rev. 2009;27(2):120-39.
343. Ramon O, Sauvaigo S, Gasparutto D, Faure P, Favier A, Cadet J. Effects of 8-oxo-7,8-dihydro-2′-deoxyguanosine on the binding of the transcription factor Sp1 to its cognate target DNA sequence (GC box). Free Radical Research. 1999;31(3):217-29.
344. Graham MK, Meeker A. Telomeres and telomerase in prostate cancer development and therapy. Nature Reviews Urology. 2017;14(10):607-19.
345. Ahn JM, Eom HJ, Yang X, Meyer JN, Choi J. Comparative toxicity of silver nanoparticles on oxidative stress and DNA damage in the nematode, *Caenorhabditis elegans*. Chemosphere. 2014;108:343-52.
346. Yang X, Yang H, Wu F, Qi Z, Li J, Xu B, *et al.* Mn Inhibits GSH Synthesis via Downregulation of Neuronal EAAC1 and Astrocytic xCT to Cause Oxidative Damage in the Striatum of Mice. Oxid Med Cell Longev. 2018;2018:4235695-.
347. Sava V, Mosquera D, Song S, Cardozo-Pelaez F, Sánchez-Ramos JR. Effects of melanin and manganese on DNA damage and repair in PC12-derived neurons. Free Radic Biol Med. 2004;36(9):1144-54.

348. Zakharcheva KA, Gening LV, Kazachenko KY, Tarantul VZ. Cells Resistant to Toxic Concentrations of Manganese Have Increased Ability to Repair DNA. Biochemistry (Mosc). 2017;82(1):38-45.
349. Whitaker AM, Schaich MA, Smith MR, Flynn TS, Freudenthal BD. Base excision repair of oxidative DNA damage: from mechanism to disease. Front Biosci (Landmark Ed). 2017;22:1493-522.
350. Morinaga H, Yonekura S, Nakamura N, Sugiyama H, Yonei S, Zhang-Akiyama QM. Purification and characterization of *Caenorhabditis elegans* NTH, a homolog of human endonuclease III: essential role of N-terminal region. DNA Repair (Amst). 2009;8(7):844-51.
351. Sanada Y, Zhang-Akiyama Q-M. An increase of oxidised nucleotides activates DNA damage checkpoint pathway that regulates post-embryonic development in *Caenorhabditis elegans*. Mutagenesis. 2014;29(2):107-14.
352. Winkelbeiner N, Wandt VK, Ebert F, Lossow K, Bankoglu EE, Martin M, *et al.* A Multi-Endpoint Approach to Base Excision Repair Incision Activity Augmented by PARylation and DNA Damage Levels in Mice: Impact of Sex and Age. International Journal of Molecular Sciences. 2020;21(18):6600.
353. Stephenson AP, Mazu TK, Miles JS, Freeman MD, Reams RR, Flores-Rozas H. Defects in base excision repair sensitize cells to manganese in S. cerevisiae. Biomed Res Int. 2013;2013:295635-.
354. Miyaji M, Hayashi Y, Funakoshi M, Tanaka A, Zhang-Akiyama Q-M. AP endonuclease EXO-3 deficiency causes developmental delay and abnormal vulval organogenesis, Pvl, through DNA glycosylase-initiated checkpoint activation in *Caenorhabditis elegans*. Scientific reports. 2018;8(1):16736-.
355. Whitehouse CJ, Taylor RM, Thistlethwaite A, Zhang H, Karimi-Busheri F, Lasko DD, *et al.* XRCC1 Stimulates Human Polynucleotide Kinase Activity at Damaged DNA Termini and Accelerates DNA Single-Strand Break Repair. Cell. 2001;104(1):107-17.
356. St-Laurent JF, Gagnon SN, Dequen F, Hardy I, Desnoyers S. Altered DNA damage response in *Caenorhabditis elegans* with impaired poly(ADP-ribose) glycohydrolases genes expression. DNA Repair (Amst). 2007;6(3):329-43.
357. Bae W, Park JH, Lee MH, Park HW, Koo HS. Hypersensitivity to DNA double-strand breaks associated with PARG deficiency is suppressed by exo-1 and polq-1 mutations in *Caenorhabditis elegans*. Febs j. 2020;287(6):1101-15.

358. Janisiw E, Raices M, Balmir F, Paulin LF, Baudrimont A, von Haeseler A, *et al.* Poly(ADP-ribose) glycohydrolase coordinates meiotic DNA double-strand break induction and repair independent of its catalytic activity. Nat Commun. 2020;11(1):4869.
359. Nicolai MM, Witt B, Hartwig A, Schwerdtle T, Bornhorst J. A fast and reliable method for monitoring genomic instability in the model organism *Caenorhabditis elegans*. Archives of Toxicology. 2021.
360. Finke H, Winkelbeiner N, Lossow K, Hertel B, Wandt VK, Schwarz M, *et al.* Effects of a Cumulative, Suboptimal Supply of Multiple Trace Elements in Mice: Trace Element Status, Genomic Stability, Inflammation, and Epigenetics. Mol Nutr Food Res. 2020;64(16):e2000325.
361. Gartner A, MacQueen AJ, Villeneuve AM. Methods for analyzing checkpoint responses in *Caenorhabditis elegans*. Methods Mol Biol. 2004;280:257-74.
362. Zubel T, Martello R, Bürkle A, Mangerich A. Quantitation of Poly(ADP-Ribose) by Isotope Dilution Mass Spectrometry. Methods Mol Biol. 2017;1608:3-18.
363. Martins AC, Jr., Gubert P, Villas Boas GR, Meirelles Paes M, Santamaría A, Lee E, *et al.* Manganese-induced neurodegenerative diseases and possible therapeutic approaches. Expert Rev Neurother. 2020;20(11):1109-21.
364. Aschner M, Guilarte TR, Schneider JS, Zheng W. Manganese: recent advances in understanding its transport and neurotoxicity. Toxicol Appl Pharmacol. 2007;221(2):131-47.
365. Zhang S, Zhou Z, Fu J. Effect of manganese chloride exposure on liver and brain mitochondria function in rats. Environ Res. 2003;93(2):149-57.
366. Bornhorst J, Meyer S, Weber T, Böker C, Marschall T, Mangerich A, *et al.* Molecular mechanisms of Mn induced neurotoxicity: RONS generation, genotoxicity, and DNA-damage response. Mol Nutr Food Res. 2013;57(7):1255-69.
367. Piloni NE, Fermandez V, Videla LA, Puntarulo S. Acute iron overload and oxidative stress in brain. Toxicology. 2013;314(1):174-82.
368. Lohren H, Blagojevic L, Fitkau R, Ebert F, Schildknecht S, Leist M, *et al.* Toxicity of organic and inorganic mercury species in differentiated human neurons and human astrocytes. J Trace Elem Med Biol. 2015;32:200-8.
369. Schildknecht S, Pöltl D, Nagel DM, Matt F, Scholz D, Lotharius J, *et al.* Requirement of a dopaminergic neuronal phenotype for toxicity of low concentrations of 1-

methyl-4-phenylpyridinium to human cells. Toxicol Appl Pharmacol. 2009;241(1):23-35.

370. Chazotte B. Labeling mitochondria with MitoTracker dyes. Cold Spring Harb Protoc. 2011;2011(8):990-2.
371. Perry SW, Norman JP, Barbieri J, Brown EB, Gelbard HA. Mitochondrial membrane potential probes and the proton gradient: a practical usage guide. Biotechniques. 2011;50(2):98-115.
372. Brunk CF, Johnes KC, James TW. Assay for Nanogram Quantities of DNA in Cellular Homogenates. Analytical Biochemistry. 1979;92(2):497-500.
373. Greer EL, Blanco MA, Gu L, Sendinc E, Liu J, Aristizábal-Corrales D, *et al.* DNA Methylation on N6-Adenine in *C. elegans*. Cell. 2015;161(4):868-78.
374. Schwerdtle T, Hamann I, Jahnke G, Walter I, Richter C, Parsons JL, *et al.* Impact of copper on the induction and repair of oxidative DNA damage, poly(ADP-ribosyl)ation and PARP-1 activity. Mol Nutr Food Res. 2007;51(2):201-10.
375. Hartwig A, Groblinghoff UD, Beyersmann D, Natarajan AT, Filon R, Mullenders LH. Interaction of arsenic(III) with nucleotide excision repair in UV-irradiated human fibroblasts. Carcinogenesis. 1997;18(2):399-405.
376. Martello R, Mangerich A, Sass S, Dedon PC, Burkle A. Quantification of cellular poly(ADP-ribosyl)ation by stable isotope dilution mass spectrometry reveals tissue- and drug-dependent stress response dynamics. ACS Chem Biol. 2013;8(7):1567-75.
377. Ebert F, Thomann M, Witt B, Müller SM, Meyer S, Weber T, *et al.* Evaluating long-term cellular effects of the arsenic species thio-DMAV: qPCR-based gene expression as screening tool. Journal of Trace Elements in Medicine and Biology. 2016;37:78-84.
378. Witt B, Ebert F, Meyer S, Francesconi KA, Schwerdtle T. Assessing neurodevelopmental effects of arsenolipids in pre-differentiated human neurons. Mol Nutr Food Res. 2017;61(11).
379. Bornhorst J, Ebert F, Lohren H, Humpf HU, Karst U, Schwerdtle T. Effects of manganese and arsenic species on the level of energy related nucleotides in human cells. Metallomics. 2012;4(3):297-306.
380. Witt B, Stiboller M, Raschke S, Friese S, Ebert F, Schwerdtle T. Characterizing effects of excess copper levels in a human astrocytic cell line with focus on oxidative stress markers. J Trace Elem Med Biol. 2021;65:126711.

381. Bonke E, Zwicker K, Dröse S. Manganese ions induce H2O2 generation at the ubiquinone binding site of mitochondrial complex II. Arch Biochem Biophys. 2015;580:75-83.
382. Fishel ML, Vasko MR, Kelley MR. DNA repair in neurons: so if they don't divide what's to repair? Mutat Res. 2007;614(1-2):24-36.
383. Brooks PJ. DNA repair in neural cells: basic science and clinical implications. Mutat Res. 2002;509(1-2):93-108.
384. Lu T, Pan Y, Kao SY, Li C, Kohane I, Chan J, *et al.* Gene regulation and DNA damage in the ageing human brain. Nature. 2004;429(6994):883-91.
385. Kino K, Hirao-Suzuki M, Morikawa M, Sakaga A, Miyazawa H. Generation, repair and replication of guanine oxidation products. Genes Environ. 2017;39:21-.
386. Hegde ML, Hazra TK, Mitra S. Early steps in the DNA base excision/single-strand interruption repair pathway in mammalian cells. Cell Research. 2008;18(1):27-47.
387. Pilié PG, Tang C, Mills GB, Yap TA. State-of-the-art strategies for targeting the DNA damage response in cancer. Nature Reviews Clinical Oncology. 2019;16(2):81-104.
388. Smith R, Lebeaupin T, Juhász S, Chapuis C, D'Augustin O, Dutertre S, *et al.* Poly(ADP-ribose)-dependent chromatin unfolding facilitates the association of DNA-binding proteins with DNA at sites of damage. Nucleic acids research. 2019;47(21):11250-67.
389. Liu C, Vyas A, Kassab MA, Singh AK, Yu X. The role of poly ADP-ribosylation in the first wave of DNA damage response. Nucleic Acids Res. 2017;45(14):8129-41.
390. Ohgushi H, Yoshihara K, Kamiya T. Bovine thymus poly(adenosine diphosphate ribose) polymerase. Physical properties and binding to DNA. J Biol Chem. 1980;255(13):6205-11.
391. Langelier MF, Planck JL, Roy S, Pascal JM. Structural basis for DNA damage-dependent poly(ADP-ribosyl)ation by human PARP-1. Science. 2012;336(6082):728-32.
392. Gibbs-Seymour I, Fontana P, Rack JGM, Ahel I. HPF1/C4orf27 Is a PARP-1-Interacting Protein that Regulates PARP-1 ADP-Ribosylation Activity. Mol Cell. 2016;62(3):432-42.
393. Kim I-K, Stegeman RA, Brosey CA, Ellenberger T. A quantitative assay reveals ligand specificity of the DNA scaffold repair protein XRCC1 and efficient disassembly of complexes of XRCC1 and the poly(ADP-ribose) polymerase 1 by poly(ADP-ribose) glycohydrolase. The Journal of biological chemistry. 2015;290(6):3775-83.

394. Hazra TK, Hill JW, Izumi T, Mitra S. Multiple DNA glycosylases for repair of 8-oxoguanine and their potential in vivo functions. Prog Nucleic Acid Res Mol Biol. 2001;68:193-205.
395. Fukae J, Takanashi M, Kubo S, Nishioka K, Nakabeppu Y, Mori H, *et al.* Expression of 8-oxoguanine DNA glycosylase (OGG1) in Parkinson's disease and related neurodegenerative disorders. Acta Neuropathol. 2005;109(3):256-62.
396. Chu CT, Plowey ED, Dagda RK, Hickey RW, Cherra SJ, 3rd, Clark RSB. Autophagy in neurite injury and neurodegeneration: in vitro and in vivo models. Methods Enzymol. 2009;453:217-49.
397. Machado-Salas J, Ibarra O, Martinez Fong D, Cornejo A, Aceves J, Kuri J. Degenerative ultrastructural changes observed in the neuropil of caudate nuclei from Parkinson's disease patients. Stereotact Funct Neurosurg. 1990;54-55:297-305.
398. Lach B, Grimes D, Benoit B, Minkiewicz-Janda A. Caudate nucleus pathology in Parkinson's disease: ultrastructural and biochemical findings in biopsy material. Acta Neuropathol. 1992;83(4):352-60.
399. Stanwood GD, Leitch DB, Savchenko V, Wu J, Fitsanakis VA, Anderson DJ, *et al.* Manganese exposure is cytotoxic and alters dopaminergic and GABAergic neurons within the basal ganglia. Journal of Neurochemistry. 2009;110(1):378-89.
400. Pham-Huy LA, He H, Pham-Huy C. Free radicals, antioxidants in disease and health. Int J Biomed Sci. 2008;4(2):89-96.
401. Mason RP. Imaging free radicals in organelles, cells, tissue, and in vivo with immuno-spin trapping. Redox Biol. 2016;8:422-9.
402. Dey S, Sidor A, O'Rourke B. Compartment-specific Control of Reactive Oxygen Species Scavenging by Antioxidant Pathway Enzymes. The Journal of biological chemistry. 2016;291(21):11185-97.
403. Panieri E, Gogvadze V, Norberg E, Venkatesh R, Orrenius S, Zhivotovsky B. Reactive oxygen species generated in different compartments induce cell death, survival, or senescence. Free Radic Biol Med. 2013;57:176-87.
404. Ho E, Karimi Galougahi K, Liu C-C, Bhindi R, Figtree GA. Biological markers of oxidative stress: Applications to cardiovascular research and practice. Redox Biol. 2013;1(1):483-91.
405. Paradies G, Paradies V, Ruggiero FM, Petrosillo G. Role of Cardiolipin in Mitochondrial Function and Dynamics in Health and Disease: Molecular and Pharmacological Aspects. Cells. 2019;8(7).

406. Cheng A, Hou Y, Mattson MP. Mitochondria and neuroplasticity. ASN Neuro. 2010;2(5):e00045.
407. Scholz J, Helmer PO, Nicolai MM, Bornhorst J, Hayen H. Profiling of sphingolipids in *Caenorhabditis elegans* by two-dimensional multiple heart-cut liquid chromatography - mass spectrometry. J Chromatogr A. 2021;1655:462481.
408. Bartke N, Hannun YA. Bioactive sphingolipids: metabolism and function. Journal of Lipid Research. 2009;50:S91-S6.
409. Lee Y-J, Huang X, Kropat J, Henras A, Merchant SS, Dickson RC, *et al.* Sphingolipid signaling mediates iron toxicity. Cell Metab. 2012;16(1):90-6.
410. Sarasija S, Norman KR. Analysis of Mitochondrial Structure in the Body Wall Muscle of *Caenorhabditis elegans*. Bio Protoc. 2018;8(7):e2801.
411. Wittkowski P, Marx-Stoelting P, Violet N, Fetz V, Schwarz F, Oelgeschläger M, *et al.* *Caenorhabditis elegans* As a Promising Alternative Model for Environmental Chemical Mixture Effect Assessment-A Comparative Study. Environ Sci Technol. 2019;53(21):12725-33.
412. Honnen S. *Caenorhabditis elegans* as a powerful alternative model organism to promote research in genetic toxicology and biomedicine. Arch Toxicol. 2017;91(5):2029-44.
413. Walmsley RM, Billinton N. How accurate is in vitro prediction of carcinogenicity? Br J Pharmacol. 2011;162(6):1250-8.
414. Yasuhara S, Zhu Y, Matsui T, Tipirneni N, Yasuhara Y, Kaneki M, *et al.* Comparison of comet assay, electron microscopy, and flow cytometry for detection of apoptosis. J Histochem Cytochem. 2003;51(7):873-85.
415. Ostling O, Johanson KJ. Microelectrophoretic study of radiation-induced DNA damages in individual mammalian cells. Biochem Biophys Res Commun. 1984;123(1):291-8.
416. Schumacher B, Hanazawa M, Lee M-H, Nayak S, Volkmann K, Hofmann R, *et al.* Translational Repression of *C. elegans* p53 by GLD-1 Regulates DNA Damage-Induced Apoptosis. Cell. 2005;120(3):357-68.
417. Rieckher M, Bujarrabal A, Doll MA, Soltanmohammadi N, Schumacher B. A simple answer to complex questions: *Caenorhabditis elegans* as an experimental model for examining the DNA damage response and disease genes. J Cell Physiol. 2018;233(4):2781-90.

418. Hartwig A, Dally H, Schlepegrell R. Sensitive analysis of oxidative DNA damage in mammalian cells: use of the bacterial Fpg protein in combination with alkaline unwinding. Toxicol Lett. 1996;88(1-3):85-90.
419. Collins AR. The use of bacterial repair endonucleases in the comet assay. Methods Mol Biol. 2011;691:137-47.
420. Craig AL, Moser SC, Bailly AP, Gartner A. Methods for studying the DNA damage response in the Caenorhabdatis elegans germ line. Methods Cell Biol. 2012;107:321-52.
421. Derks KWJ, Hoeijmakers JHJ, Pothof J. The DNA damage response: the omics era and its impact. DNA repair. 2014;19:214-20.
422. Dicks N, Gutierrez K, Michalak M, Bordignon V, Agellon LB. Endoplasmic reticulum stress, genome damage, and cancer. Front Oncol. 2015;5:11-.
423. Kamaletdinova T, Fanaei-Kahrani Z, Wang Z-Q. The Enigmatic Function of PARP1: From PARylation Activity to PAR Readers. Cells. 2019;8(12):1625.
424. Cooper JF, Van Raamsdonk JM. Modeling Parkinson's Disease in *C. elegans*. J Parkinsons Dis. 2018;8(1):17-32.
425. Ge P, Dawson VL, Dawson TM. PINK1 and Parkin mitochondrial quality control: a source of regional vulnerability in Parkinson's disease. Molecular Neurodegeneration. 2020;15(1):20.
426. Kausar S, Wang F, Cui H. The Role of Mitochondria in Reactive Oxygen Species Generation and Its Implications for Neurodegenerative Diseases. Cells. 2018;7(12):274.
427. Fleck SC, Sauter F, Pfeiffer E, Metzler M, Hartwig A, Köberle B. DNA damage and repair kinetics of the Alternaria mycotoxins alternariol, altertoxin II and stemphyltoxin III in cultured cells. Mutat Res Genet Toxicol Environ Mutagen. 2016;798-799:27-34.
428. Byrne AB, McWhirter RD, Sekine Y, Strittmatter SM, Miller DM, Hammarlund M. Inhibiting poly(ADP-ribosylation) improves axon regeneration. Elife. 2016;5:e12734.
429. Qian H-R, Yang Y. Neuron differentiation and neuritogenesis stimulated by N-acetylcysteine (NAC). Acta pharmacologica Sinica. 2009;30(7):907-12.
430. Coles LD, Tuite PJ, Öz G, Mishra UR, Kartha RV, Sullivan KM, *et al.* Repeated-Dose Oral N-Acetylcysteine in Parkinson's Disease: Pharmacokinetics and Effect on Brain Glutathione and Oxidative Stress. J Clin Pharmacol. 2018;58(2):158-67.

431. Monti DA, Zabrecky G, Kremens D, Liang TW, Wintering NA, Bazzan AJ, *et al.* N-Acetyl Cysteine Is Associated With Dopaminergic Improvement in Parkinson's Disease. Clin Pharmacol Ther. 2019;106(4):884-90.

Curriculum Vitae

Due to data protection, the curriculum vitae is not included in the online version of this dissertation.

List of Publications and Presentations

Publications in Peer-Review Journals Used in this Thesis:

Submitted to Food and Chemical Toxicology: **Nicolai MM**, Witt B, Friese S, Michaelis V, Hölz-Armstrong L, Martin M, Ebert F, Schwerdtle T, Bornhorst J, *Mechanistic studies on the adverse effects of manganese overexposure in differentiated LUHMES cells.*

Nicolai MM, Weishaupt AK, Baesler J, Brinkmann V, Wellenberg A, Winkelbeiner N, Gremme A, Aschner M, Fritz G, Schwerdtle T, Bornhorst J, Int. J. Mol. Sci (2021). 22(20) 10905 *Effects of Manganese on Genomic Integrity in the Multicellular Model Organism Caenorhabditis elegans*

Nicolai MM, Witt B, Hartwig A, Schwerdtle T, Bornhorst J, Arch Toxicol (2021) 3417-3424. *A fast and reliable method for monitoring genomic instability in the model organism Caenorhabditis elegans*

Helmer PO*, **Nicolai MM***, Schwantes V, Bornhorst J, Hayen H, Free Radic Biol Med (2021) 216-224. *Investigation of cardiolipin oxidation products as a new endpoint for oxidative stress in C. elegans by means of online two-dimensional liquid chromatography and high-resolution mass spectrometry* *these authors contributed equally

Additional Publications in Peer-Review Journals:

Scholz J, Helmer PO, **Nicolai MM**, Bornhorst J, Hayen H, J Chromatogr A (2021) 1655. *Profiling of sphingolipids in Caenorhabditis elegans by two-dimensional multiple heart-cut liquid chromatography - mass spectrometry*

Wandt VK, Winkelbeiner N, Lossow K, Kopp JF, Schwarz M, Alker W, **Nicolai MM**, Simon L, Dietzel C, Hertel B, Pohl G, Ebert F, Schomburg L, Bornhorst J, Haase H, Kipp AP, Schwerdtle T, Redox Biol (2021) 102083. *Ageing-associated effects of a long-term dietary modulation of four trace elements in mice*

Taylor CA, Tuschl K, **Nicolai MM**, Bornhorst J, Gubert P, Varão AM, Aschner M, Smith DR, Mukhopadhyay S, J. Nutr. (2020) 1360-1369. *Maintaining Translational Relevance in Animal Models of Manganese Neurotoxicity*

Neumann C, Baesler J, Steffen G, **Nicolai MM**, Zubel T, Aschner M, Bürkle A, Mangerich A, Schwerdtle T, Bornhorst J, J Trace Elm Med Biol. (2020) 21-27. *The role of poly(ADP-ribose) polymerase in manganese exposed Caenorhabditis elegans*

Oral Presentations

March 2020	**Nicolai MM**, Baesler J, Aschner M, Schwerdtle T, Bornhorst J, 5th German Pharm-Tox Summit, Leibzig, Germany, *Consequences of manganese overload in C. elegans: oxidative stress and DNA damage*
September 2019	**Nicolai MM**, Wandt VK, Winkelbeiner N, Baesler J, Ebert F, Aschner M, Schwerdtle T, Bornhorst J, GUM 2019 Young Scientist Workshop, Basel, Switzerland, *Investigations on manganese-induced oxidative stress and its impact on DNA repair in C. elegans*
March 2019	**Nicolai MM**, Baesler J, Aschner M, Schwerdtle T, Bornhorst J, Regionalverbandstagung LChG NRW, Wuppertal, Switzerland, *Investigations on manganese-induced oxidative stress and its impact on DNA repair in C. elegans*

Poster Presentations

June 2021	**Nicolai MM**, Winkelbeiner N, Weishaupt AK, Reimer A, Schwerdtle T, Bornhorst J, New Investigators session at the EEMGS Annual General Meeting, online, *Genotoxicity and C. elegans – using the worm for assessment of Mn-induced DNA damage and DNA damage response*
June 2021	**Nicolai MM**, Brinkmann V, Weishaupt AK, Fritz G, Schwerdtle T, Bornhorst J, 23rd International *C. elegans* conference, online, *Genotoxicity and C. elegans – using the worm for DNA damage and DNA repair/ damage response research*
September 2019	**Nicolai MM**, Wandt VK, Winkelbeiner N, Baesler J, Aschner M, Ebert F, Schwerdtle T, Bornhorst J, 31st GUM Meeting, Basel, Switzerland, *Establishing quantitative and qualitative methods for investigations on Mn-induced DNA damage and DNA repair in C. elegans*
June 2019	**Nicolai MM**, Baesler J, Aschner M, Schwerdtle T, Bornhorst J, 22nd International *C. elegans* conference, LA, USA, *Investigations on manganese-induced oxidative stress and its impact on DNA repair in C. elegans*

Acknowledgement

In the course of my doctorate, many amazing people have supported me on this journey, without whom this work would not have been possible. I would therefore like to take this opportunity to thank everyone who has supported me in one way or another.

A very special thanks goes to my PhD supervisor Prof. Dr. Julia Bornhorst. Thank you for the extraordinarily wonderful time I was able to spend with you and the working group - both in Potsdam and in Wuppertal. Mit dem Umzug, dem Aufbau der Labore und dem Wachstum der Arbeitsgruppe war es eine unglaublich abenteuerreiche und manchmal wohl auch ungewöhnliche Zeit. Ich danke dir für den Spaß an der Wissenschaft, dem Vertrauen, dass du mir entgegengebracht hast, die fachlichen Diskussionen, deinen Optimismus und vor allem die geteilte Begeisterungsfähigkeit für (absurde) Wissenschaft und Methoden. Ich habe sehr viel gelernt und schätze meine Promotionszeit sehr. Zusätzlich möchte ich dir dafür danken, dass du mir die Möglichkeit gegeben hast unsere Forschungsergebnisse auf nationalen und internationalen Tagungen vorzustellen, zu Netzwerken und mir die Freiheit gegeben hast, immer mehr in die Genotox einzutauchen – ein Forschungsgebiet, dass ich so sehr lieben gelernt habe.

Furthermore I would like to thank Prof. Dr. Tanja Schwerdtle who has become a dear mentor of mine and who was the most important collaboration partner for the work presented here. Vielen Dank, dass ich immer in deinen Laboren willkommen war. Ich danke dir für all den Rat und die Unterstützung, die du mir schon als Studentin entgegengebracht hast und die schöne Zeit, die ich in deiner Arbeitsgruppe in Potsdam hatte. Viele Möglichkeiten hätte ich ohne dich nicht gehabt und dafür bin ich sehr dankbar.

Many other collaborators have helped me on a wide variety of projects. Special thanks goes to Dr. Patrick O. Helmer and Prof. Dr. Heiko Hayen from the University of Münster for working with me on the joint project of cardiolipins. Danke Patrick, dass ich von dir so viel mehr über LC-Kopplungen lernen durfte und dass der Schreibprozess mit dir so unglaublich angenehm war.

I also thank Dr. Vanessa Brinkmann, (Dr.) Anna Wellenberg, and Prof. Dr. Gerhard Fritz for always welcoming me at the University of Düsseldorf for my irradiation experiments and conducting the acridine orange staining for me. Vanessa und Anna, ich danke euch sehr, dass ihr mir so geholfen habt und freue mich schon auf meinen nächsten Besuch bei euch.

A huge thanks goes to Dr. Nicola Winkelbeiner und Dr. Barbara Witt from the Schwerdtle lab in Potsdam for making the incision activity and LUHMES experiments work. Ich bin euch beiden sehr dankbar, dass ihr mir zu so unterschiedlichen Zeiten in meiner Promotion so viel geholfen habt. Ohne eure Unterstützung im Labor und beim Schreiben der Publikationen wäre ich nicht so weit gekommen. Noch viel mehr als den wissenschaftlichen Input bedanke ich mich aber für die schöne Zeit in Potsdam und später auch virtuell.

Moving labs wasn´t easy, but the upside of it was that I was able to work within two fantastic working groups. I would like to thank all (former) members of the AKS in Potsdam for the great time during my master thesis and the beginning of my doctorate.

Ich habe so viel von euch gelernt und vermisse die Zeit des Bescheids. Ganz besonders froh bin ich, mit Nici, Viki und Jessi zusammen gearbeitet zu haben – es war mir ein Fest.

Describing working in the AGB in Wuppertal as eventful is an understatement, but I have no better words. I am very thankful for every member of the group, former students that helped on my projects and former students that then became PhD-students here. Ich danke euch sehr für die verrückten Zeiten, das gemeinsame Durchstehen von nervigen Situationen, Bastelaktionen, Essenbestellen, Dinokostümen, Lemikaner und strukturierte Herangehensweisen ☺

A huge thanks goes to Vivien Michaelis with whom I have spent more time with in the last 2.5 years than with anyone else. I owe you (and not just gum). Ich danke dir, dass du es mit mir für die ganze Zeit im Büro und Labor ausgehalten hast, für deine Begeisterungsfähigkeit, deine Motivation und Zuverlässigkeit. Ich danke dir für all die verrückten Lieder, Zeiten, Schnäpse, Putzaktionen, Feiertags-Labor-Partys und und und. Die Promotionszeit war wirklich nicht immer einfach, danke, dass du auch die schwierigen Zeiten mit mir durchlebt hast. Und falls du mal einen Schnaps brauchst: ¾ Becher Tomatensaft, 1 Becher Sangrita, ¾ Becher Korn, etwas Zitronensaft, Tabasco, und Pfeffer ergeben einen wunderbaren Lemikaner.

Thanks to the people from the 11th floor - the Didactics of Chemistry and the people of the Delaittre and Schebb labs. I look back on a time full of teaching fun, game nights, popcorn, carnivals, ouzo, and weekend-work-coffee-breaks. Thank you for keeping me sane.

I would also like to thank the AG Simon and PTC for allowing me to use your labs and for the pleasant atmospheres there. Ich freue mich schon auf die weitere Zusammenarbeit. Ganz besonders möchte ich mich auch bei den Leuten des Büros V.08.074 bedanken, dafür, dass ihr mich bei euch im Kreis aufgenommen habt, für die Boulder- und Kletter-Aktionen, Snickers-Eis und Flens.

Meinen Berliner Mädels möchte ich dafür danken, dass ihr immer für mich da wart und für all die schönen Ablenkungen zur Arbeit. Ihr helft mir, die wirklich wichtigen Dinge im Leben zu sehen. Ich danke euch fürs da sein.

Alex, ich danke dir, dass du mir die schönen Orte Wuppertals gezeigt und dass du meine Zeit hier so viel liebenswerter gemacht hast. Vielen Dank für deine Unterstützung, die Motivation, dein Verständnis und ganz besonders die geteilte Begeisterung für Wissenschaft.

Mein größter Dank gilt meinen Eltern, meinem Bruder und Svenja, die mich immer Unterstützt haben. Ich bin euch so dankbar, dafür, dass ihr stets an mich geglaubt und mich motiviert habt, fürs Erden und Perspektiven zeigen. Ohne euch wäre ich jetzt nicht an diesem Punkt. Danke für Alles!

Declaration

The here presented semi-cumulatively constituted doctoral thesis comprises four independent research articles, which were published (chapter 4, 5 and 6) or are currently in the publishing process (chapter 7) of international peer-reviews scientific journals. These articles include suggestions of co-authors, reviewers, and editors as an outcome of the peer-review process.

As the leading author of these articles (or co-leading author for chapter 4), I compiled the studies´ concept together with my supervisor Prof. Dr Julia Bornhorst (chapter 4: plus Dr Patrick O. Helmer and Prof. Dr Heiko Hayen), carried out the majority of the experiments, conducted the data analysis and interpretation, and wrote the main manuscript. All work by the co-authors has been described at the end of each publication.

When referring to published data and methods or when citing statements and results provided by others, it is indicated by the appropriate references in the respective articles, as well as in all other chapters of this thesis.

_____

Merle Marie Nicolai

(Doctoral candidate)